

Ultrathin Ionic Liquid Films on Metal Surfaces: Growth, Stability and Exchange Phenomena

Ultradünne Filme Ionischer Flüssigkeiten auf Metalloberflächen:
Wachstum, Stabilität und Austauschphänomene

Der Naturwissenschaftlichen Fakultät der
Friedrich-Alexander-Universität Erlangen-Nürnberg
zur Erlangung des Doktorgrades

Dr. rer. nat.

vorgelegt von
Matthias Lexow
aus Berlin

Als Dissertation genehmigt von der Naturwissenschaftlichen Fakultät
der Friedrich-Alexander-Universität Erlangen-Nürnberg

Tag der mündlichen Prüfung: 13.03.2020

Vorsitzender des Promotionsorgans: Prof. Dr. Georg Kreimer

Gutachter: Prof. Dr. Hans-Peter Steinrück
Prof. Dr. Peter Wasserscheid

Für Maryam.

Table of Contents

1.	Introduction	1
2.	Materials and Methods	5
2.1	Materials	5
2.1.1	Chemicals	5
2.1.2	Metal Single Crystals	9
2.2	Angle-Resolved X-Ray Photoelectron Spectroscopy (ARXPS)	9
2.3	Physical Vapor Deposition of ILs and Porphyrins	13
2.4	Monitoring Thin Film Growth with XPS	15
2.5	Estimation of the IL Monolayer Height	16
3.	Results	19
3.1	Ionic Liquid Thin Film Growth on Metal Surfaces [P1, P2, P3, P4]	19
3.2	Time-Dependent Changes in the Growth of IL Films [P1]	24
3.3	Growth and Desorption of 2H-TPP on Ag(111) and Au(111) [P4]	27
3.4	Desorption of ILs from Metal Surfaces [P2, P3, P4].....	28
3.5	Ion Exchange at the IL/Solid Interface [P2, P3].....	34
3.5.1	Anion Exchange	34
3.5.2	Cation Exchange.....	36
3.6	Replacement of IL by Porphyrins at Metal Interfaces [P4]	38
4.	Summary.....	43
5.	Kurzfassung der Arbeit.....	47
6.	References	51
7.	Acknowledgements	69
8.	Appendix	71
8.1	Atomic Sensitivity Factors for XPS	71
8.2	Calculated IL Monolayer Heights	71
8.3	Variation of X-Ray Gun Power During Time-Dependent XPS	72

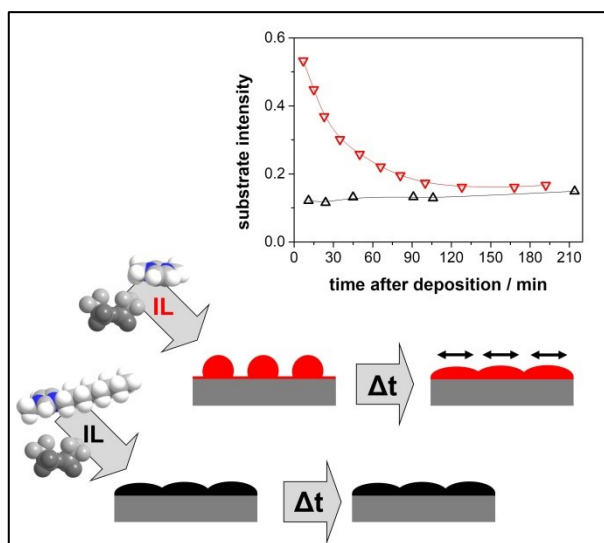
8.4	Technical Drawings of the IL Evaporator Parts	75
8.5	Technical Drawing of the Single Crystals	80
8.6	Publications [P1-P4]	81

List of Papers [P1-P4] in the Appendix

[P1] M. Lexow, T. Talwar, B.S.J. Heller, B. May, R.G. Bhui, F. Maier, H.-P. Steinrück:

Time-dependent changes in the growth of ultrathin ionic liquid films on Ag(111)

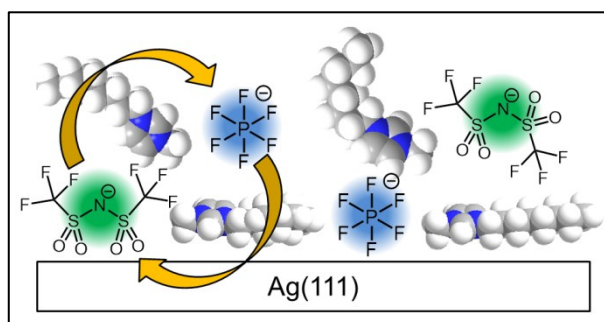
Physical Chemistry Chemical Physics, 20, 12929-12938 (2018), 10.1039/C8CP01411F.



[P2] M. Lexow, B.S.J. Heller, F. Maier, H.-P. Steinrück:

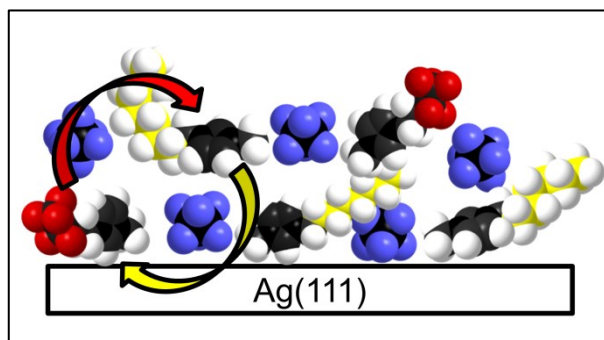
Anion exchange in ultrathin ionic liquid films on Ag(111)

ChemPhysChem, 19, 2978-2984 (2018), 10.1002/cphc.201800773.



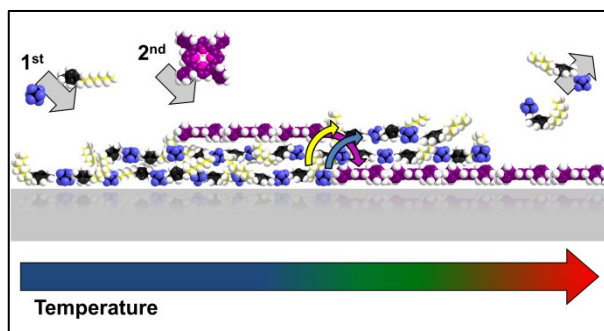
[P3] M. Lexow, B.S.J. Heller, G. Partl, R.G. Bhui, F. Maier, H.-P. Steinrück:
Cation Exchange at the Interfaces of Ultrathin Films of Fluorous Ionic Liquids on Ag(111)

Langmuir, 35, 398-405 (2019), 10.1021/acs.langmuir.8b03517.



[P4] M. Lexow, S. Massicot, F. Maier, H.-P. Steinrück:
Stability and Exchange Processes in Ionic Liquid/Porphyrin Composite Films on Metal Surfaces

The Journal of Physical Chemistry C, 123, 29708-29721 (2019), 10.1021/acs.jpcc.9b08531.



Beitrag von Matthias Lexow zu den Publikationen [P1-P4]:

Matthias Lexow hat die untersuchten Systeme im Ultrahochvakuum präpariert, die Messungen durchgeführt, die Daten analysiert und in Form der Abbildungen aufbereitet. In Abstimmung mit den Koautoren hat Matthias Lexow als Erstautor die Manuskripte zu den Publikationen [P1-P4] verfasst. Die Koautoren sind mit der Verwendung der Publikationen [P1-P4] als Grundlage der Dissertation von Matthias Lexow einverstanden.

Matthias Lexow, 11.12.2019

Teile dieser Dissertation sind gegenwärtig als Bestandteil einer weiteren Publikation mit dem Titel „Ultrathin Ionic Liquid Films on Metal Surfaces: Adsorption, Growth, Stability and Exchange Phenomena“ im Journal *Advances in Physics: X* zur Begutachtung.

Matthias Lexow, 23.03.2020

1. Introduction

Ionic liquids (ILs) are a diverse and fascinating class of materials. As salts with comparably low melting points – often even below room temperature (RT) – they combine typically very low vapor pressures with a large number of tunable chemical and physicochemical properties, depending on the numerous possible pairings of cations and anions.¹⁻¹³ One of the most successful applications involving bulk amounts of ILs is the BASILTM process for the production of alkoxyphenylphosphines.¹⁴⁻¹⁵ The continuously growing interest in interfaces of IL systems goes in line with increasing realization of the incredible potential of task-specific ILs. The importance of IL interfaces becomes even more apparent for interface-controlled applications as *e.g.* in sensors,^{4, 16-19} lubrication,²⁰⁻²² separation,^{4, 19, 23-29} electrochemistry^{4, 19, 30-46} and electronics⁴⁷⁻⁴⁹ technologies. ILs further stimulated completely new concepts for catalysis. Thin IL films on high surface area solid supports are the key ingredient to highly effective SCILL⁵⁰ (Solid Catalyst with Ionic Liquid Layer) and SILP^{23, 51-52} (Supported Ionic Liquid Phase) catalysis.^{1, 4, 50-64} The groundbreaking discovery in SCILL, for example, was the ability of the IL phase to make the reactive sites of a heterogeneous catalyst more resistant towards poisoning while simultaneously increasing the reactivity and selectivity.^{50, 65-66} The examples of pioneering work and substantial reviews in Figure 1 highlight the fundamental interest in liquid/solid and liquid/gas interfaces and how for all of the applications mentioned above, the function, performance and stability of the respective system is very sensitive towards the interface properties of the IL films.^{11, 64, 67-71} The low vapor pressure and excellent thermal stability of many ILs enable not only their use under extreme conditions, but also their investigation in ultra-high vacuum (UHV) under well-defined conditions with atomic level accuracy,^{11, 72} coining the term “Ionic Liquid Surface Science” as a pivotal sub-discipline of IL research¹¹ and initiating a new age for the spectroscopic investigation of liquid surfaces in general.^{11, 69, 73}

Porphyrins are an equally diverse and fascinating class of materials. Mimicking their vital role in numerous biological catalytic reactions and transport mechanisms,⁷⁴⁻⁷⁵ porphyrins also stimulated particular interest for technical applications.⁷⁶⁻⁸³ They offer great functional diversity through a vast degree of freedom concerning the variation of the substituents at the periphery of the tetrapyrrole core of the molecule.⁸⁴ Knowledge and control of the formation and structure of self-assembled porphyrin adlayers on the surfaces of solid supports are essential for the synthesis of custom-tailored environments and catalysts.^{76-77, 82, 85-87} Prototypical porphyrin/IL composite systems offer synergies between the two molecular

classes in, for example, catalysis⁸⁶ and dye-sensitized solar cell⁴⁷⁻⁴⁸ technologies. So far, the potential of these pioneering works has only been touched at the surface.⁸⁴ In such applications, again, the function, performance and stability of the organic thin films are strongly determined by the properties of the interface to the support.^{11, 64, 67-71, 84}

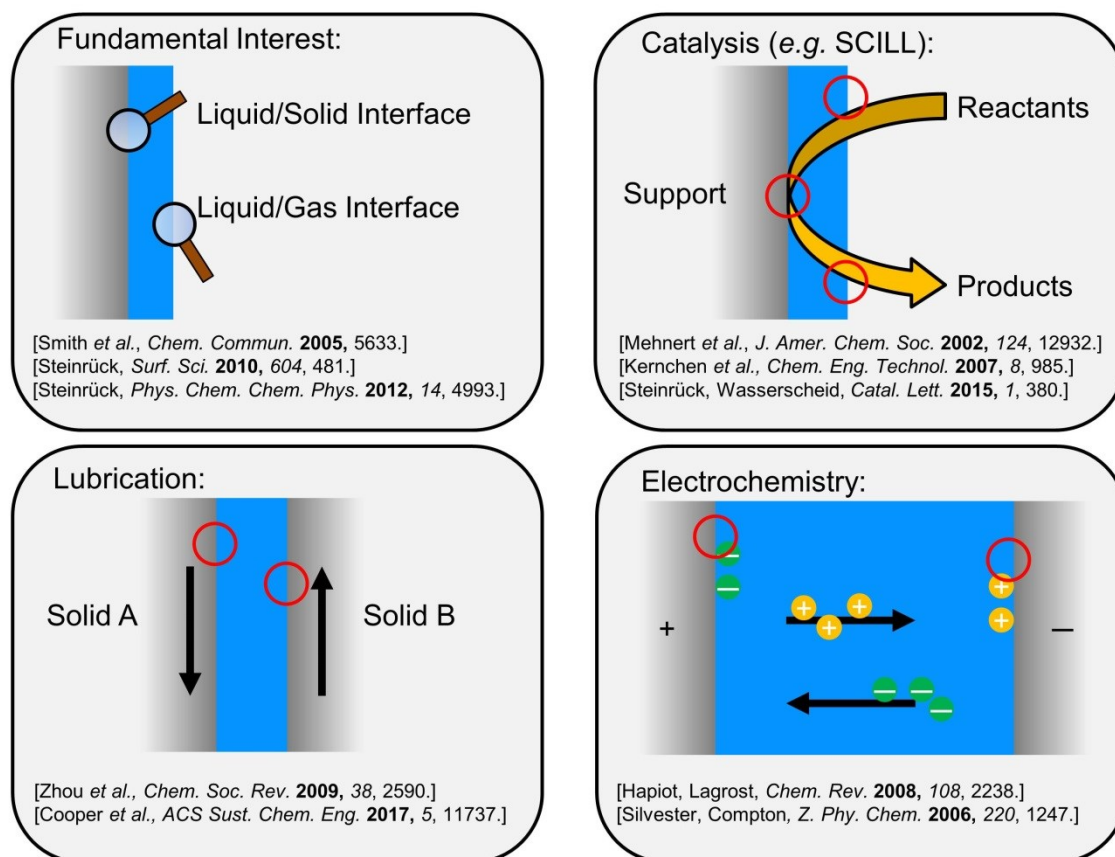


Figure 1: Examples of pioneering work and substantial reviews, highlighting the fundamental interest in liquid/solid and liquid/gas interfaces in general^{69, 72-73} and the relevance of IL interfaces for applications.^{11, 20-21, 32, 50, 88-90} The function, performance and stability of the applied systems strongly rely on the interface properties.^{11, 64, 67-71}

IL/solid interfaces buried under macroscopically thick IL films are generally not accessible by most of the sophisticated UHV surface science methods.¹¹ After the first report of the successful distillation of ILs at reduced pressure without decomposition,⁹¹ the first use of physical vapor deposition (PVD) of ILs in 2008⁹²⁻⁹³ combined with angle-resolved X-ray photoelectron spectroscopy (ARXPS) led the way to establishing powerful new methods for the investigation of the properties of IL/solid and IL/vacuum interfaces like wetting behavior and IL film growth with molecular resolution under well-controlled and clean conditions for coverages ranging from less than a monolayer to several multilayers.^{11, 69, 93-102} Within this thickness range, the limited information depth of highly surface sensitive methods – as for example XPS – is large enough for a detailed characterization of IL/solid interfaces.¹¹

Based on previous studies of ultrathin IL films on metal surfaces, this thesis systematically looks to answer how the IL/solid interface forms, how the ions arrange at the interfaces, what the initial stages of thin film growth are, whether the film morphology can change over time and how stable the ultrathin IL films are at elevated temperatures.^{84, 103-105} Further extending the scope by looking at mixtures of ILs – instead of using one IL comprised of one type of cation and anion – on metal surfaces promises an even larger parameter space for targeted applications of ultrathin IL films¹⁰⁴ and raises a whole new set of fundamental questions specifically for mixed thin films: Are there effects of preferential adsorption, segregation and enrichment? What is the structure and composition at the IL/support and IL/vacuum interfaces? How do these phenomena relate to varying combinations of ions and how do they evolve with temperature?¹⁰⁴⁻¹⁰⁵

This thesis sheds light on the questions raised above, on the example of a set of selected ILs (Table 1) and single-crystalline Ag(111) and Au(111) surfaces. For the first time, mixed ultrathin IL films were prepared by sequential PVD of two different ILs on the metal surfaces – the evaporators were built in the course of the experiments and optimized specifically for the evaporation of ILs. The films were analyzed by ARXPS with Al K α radiation at emission angles of 0° and 80°. The information depth at 0° is 7–9 nm (depending on the kinetic energy) and only 1–1.5 nm at 80°. Thus, in the latter case, the experiment is about six times more surface sensitive and mainly the topmost surface layer is probed (for details see Chapter 2.2).

As the experimental results blend very well into recent and potential future studies, the presentation of IL thin film growth in Chapter 3.1 involves a thorough discussion of complimentary results from literature. Chapter 3.2 deals with a special case of time-dependent behavior of IL film morphology immediately after PVD. The growth and desorption behavior of the porphyrin 2H-TPP (see Table 1) is the topic of Chapter 3.3. Just as in Chapter 3.1, the results of thermal stability of ultrathin IL films in Chapter 3.4 find close correlation to previous studies, however extending the scope by examples of selective desorption from mixed thin films. In Chapter 3.5, the exchange of anions and cations at the IL/Ag(111) interface of mixed thin films and the resulting interface compositions will be discussed, before a detailed analysis of the interaction of co-adsorbed porphyrins with ILs on metal surfaces in Chapter 3.6 sets the ground for potential future studies of porphyrins at the interfaces of thin IL films.

2. Materials and Methods

2.1 Materials

2.1.1 Chemicals

The compounds used in this thesis are summarized in Table 1 along with selected properties that are essential to this work. 3-Methyl-1-octylimidazolium hexafluorophosphate, $[C_8C_1Im][PF_6]$, was purchased from Sigma-Aldrich (purity > 95%). 1,3-Dimethylimidazolium bis[(trifluoromethyl)sulfonyl]imide, $[C_1C_1Im][Tf_2N]$, and 1-methyl-3-octylimidazolium bis[(trifluoromethyl)sulfonyl]imide, $[C_8C_1Im][Tf_2N]$, were synthesized under ultrapure conditions by Dr. Nicola Taccardi according to previous publications.¹⁰⁶ 3-Methyl-1-(3,3,4,4,4-pentafluorobutyl)imidazolium hexafluorophosphate, $[PFBMIm][PF_6]$, was prepared by Dr. Gabriel Partl as described in the corresponding publication.¹⁰⁵ 5,10,15,20-Tetraphenylporphyrin, 2H-TPP, was purchased from Porphyrin Systems (purity 98%). The ILs and 2H-TPP were carefully degassed in UHV at elevated temperature prior to the deposition experiments. Table 1 also shows a selection of other ILs that were not studied here, but will be mentioned in the discussion.

For comparing the thin film results with bulk mixtures, bulk amounts of IL mixtures were prepared with varying composition using acetonitrile (Sigma-Aldrich, purity 99.8%) as co-solvent to ensure proper mixing of the respective ILs.^{104-105, 107} The IL mixtures were spread as macroscopic films (about 0.1 mm thickness) on polycrystalline Ag foil. For ARXPS, each sample was only introduced into the vacuum chamber after careful degassing of the liquid film in the chamber's load lock.¹⁰⁴⁻¹⁰⁵

Table 1: Names, molecular structures and further details of the compounds discussed in this thesis. The compounds shaded in gray were used for the experimental part.

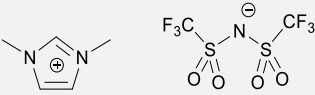
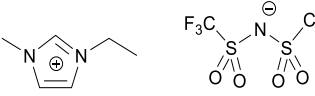
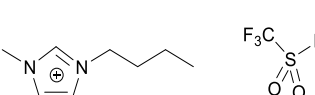
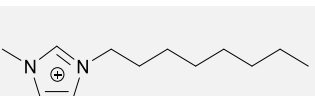
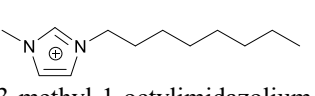
Short name	Molecular structure and IUPAC name	Glass transition ^a T_g / K	Melting point ^a T_m / K	Surface tension σ / mN/m	Density ρ / g/cm ³	Molecular volume V_m / nm ³	Monolayer height ^b h / nm
[C ₁ C ₁ Im][Tf ₂ N]	 1,3-dimethylimidazolium bis[(trifluoromethyl)sulfonyl]imide	-	295 ¹⁰⁸ 299 ¹⁰⁹	36.3 ^{f,8}	1.554 ^{f,109} 1.567 ^{f,8}	0.400 ^{f,8}	0.73 ^{94, 99, 103, 110}
[C ₂ C ₁ Im][Tf ₂ N]	 1-ethyl-3-methylimidazolium bis[(trifluoromethyl)sulfonyl]imide	178 ¹¹¹ 180 ¹¹² 181 ¹¹³ 186 ¹⁰⁹ 195 ¹¹⁴	252 ¹¹⁴ 254 ¹¹⁵ 255 ^{109, 112} 256 ¹¹³ 257 ¹¹¹ 263 ¹¹⁶ 270 ¹⁰⁸ 257–271 ¹¹⁷	32.6 ^{f,118} 35.1 ^{f,119} 35.2 ^{f,120-121} 41.6 ^{f,122}	1.516 ¹²³ 1.518 ^{f,119} 1.519 ^{f,114} 1.522 ^{f,109} 1.524 ^{g,116}	0.428 ^{f,8, 119}	0.75
[C ₄ C ₁ Im][Tf ₂ N]	 1-butyl-3-methylimidazolium bis[(trifluoromethyl)sulfonyl]imide	169 ² 181 ¹²⁴ 182 ¹²⁵ 186 ^{109, 111, 114, 126} 187 ¹¹³	248 ² 267 ¹¹⁴ 268 ¹¹⁵ 269 ^{108, 125} 270 ^{109, 126} 271 ¹¹³ 272 ¹¹¹	30.7 ^{f,8} 30.8 ^{f,118} 37.5 ^{f,2}	1.43 ^{f,2, 118} 1.435 ^{f,8} 1.436 ^{f,114} 1.437 ¹²³ 1.44 ^{f,109, 113}	0.485 ^{f,8}	0.79 ⁹⁸
[C ₈ C ₁ Im][Tf ₂ N]	 3-methyl-1-octylimidazolium bis[(trifluoromethyl)sulfonyl]imide	171 ¹¹⁷ 187 ^{125, 127} 189 ¹¹⁴ 193 ¹⁰⁹	250–264 ¹¹⁷	29.5 ^{f,8} 30.2 ^{f,128} 30.4 ¹²¹	1.31 ^{f,8, 125, 129} 1.32 ^{f,114, 128} 1.322 ^{f,109} 1.325 ¹²³	0.598 ^d 0.603 ^{f,8} 0.62 ⁶	0.84 ^{94, 103-104}
[C ₈ C ₁ Im]Cl	 3-methyl-1-octylimidazolium chloride	186 ²	191 ¹³⁰	30.9 ^{f,8} 33.8 ^{f,2}	1.00 ^{f,2, 131} 1.009 ^{f,8} 1.01 ⁶	0.380 ^{f,6, 8}	0.72 ¹³²

Table 1 continued.

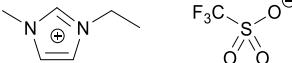
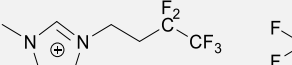
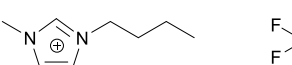
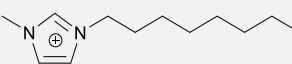
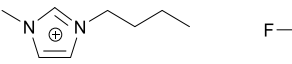
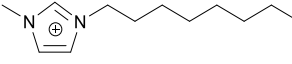
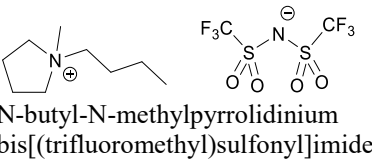
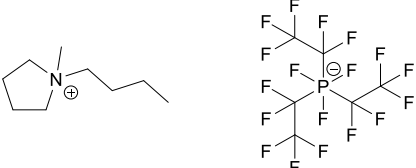
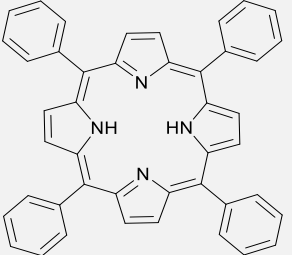
Short name	Molecular structure and IUPAC name	Glass transition ^a T_g / K	Melting point ^a T_m / K	Surface tension σ / mN/m	Density ρ / g/cm ³	Molecular volume V_m / nm ³	Monolayer height ^b h / nm
[C ₂ C ₁ Im][TfO]	 1-ethyl-3-methylimidazolium trifluoromethanesulfonate	175 ¹¹²	258 ¹¹² 264 ¹⁰⁸	37.8 ^{f,118} 44.4 ^{f,122}	1.388 ^{g,133} 1.39 ^{f,118}	0.311 ^{g,133}	0.68 ¹⁰¹
[PFBMIm][PF ₆]	 3-methyl-1-(3,3,4,4,4-pentafluorobutyl)imidazolium hexafluorophosphate	-	339 ¹⁰⁵			0.360 ^{b,105}	0.71 ¹⁰⁵
[C ₄ C ₁ Im][PF ₆]	 1-butyl-3-methylimidazolium hexafluorophosphate	189 ¹²⁴ 193 ² 196 ^{114, 126} 197 ¹¹³ 212 ¹³⁴	212 ¹³⁰ 284 ¹¹³ 282 ¹¹⁵ 283 ^{2, 126}	47.9 ^{f,122} 48.8 ^{f,2}	1.31 ^{f,131} 1.360 ^{f,2, 135} 1.368 ^{f,114}	0.345 ^e 0.347 ^{f,135}	0.70
[C ₈ C ₁ Im][PF ₆]	 3-methyl-1-octylimidazolium hexafluorophosphate	191 ² 194 ¹²⁴ 202 ¹¹⁴	203 ¹³⁰	32.5 ^{f,8} 36.5 ^{f,2}	1.19 ^{f,131} 1.22 ^{f,2, 123, 135} 1.235 ^{f,8} 1.237 ^{f,114}	0.458 ^{f,8} 0.46 ⁶ 0.461 ^{f,135}	0.77 ^{84, 104-105}
[C ₄ C ₁ Im][BF ₄]	 1-butyl-3-methylimidazolium tetrafluoroborate	176 ² 178 ¹³⁶ 182 ¹²⁴ 188 ¹¹³ 190 ¹²⁶ 192 ¹³⁴	192 ¹³⁰⁻¹³¹	46.6 ^{f,2}	1.12 ^{f,2} 1.205 ¹¹³ 1.26 ^{f,131}	0.312 ¹³⁷	0.68
[C ₈ C ₁ Im][BF ₄]	 3-methyl-1-octylimidazolium tetrafluoroborate	190 ¹³⁶ 193 ¹³¹	193 ¹³⁰	30.8 ^{f,8}	1.08 ^{f,6, 131} 1.091 ¹³⁵ 1.099 ^{f,8} 1.104 ^{f,138} 1.105 ^{f,123, 139}	0.424 ^{f,138} 0.426 ^{f,8} 0.43 ^{f,6, 135}	0.75 0.6 ^{c,138}

Table 1 continued.

Short name	Molecular structure and IUPAC name	Glass transition ^a T_g / K	Melting point ^a T_m / K	Surface tension σ / mN/m	Density ρ / g/cm ³	Molecular volume V_m / nm ³	Monolayer height ^b h / nm
[C ₄ C ₁ Pyrr][Tf ₂ N]	 N-butyl-N-methylpyrrolidinium bis[(trifluoromethyl)sulfonyl]imide	181 ¹⁴⁰ 186 ^{111, 140}	252 ¹⁴⁰ 255 ¹¹¹ 262 ¹⁴⁰ 264 ¹¹⁵ 267 ¹¹⁶	32.3 ^{f,8}	1.39 ¹²³ 1.394 ^{f,8} 1.399 ^{g,116}	0.503 ^{f,8}	0.80
[C ₄ C ₁ Pyrr][FAP]	 N-butyl-N-methylpyrrolidinium tris(pentafluoroethyl)trifluorophosphate	157 ¹⁴¹	277 ¹⁴¹	38 ^{g,141}	1.59 ¹²³	0.613 ¹²³	0.85
2H-TPP	 5,10,15,20-tetraphenylporphyrin	-	-		1.273 ¹⁴²⁻¹⁴³	0.34 ^{c,84}	

a: Can depend strongly on heating rate, thermal history (*e.g.* cooling rate) or water content.^{2, 109, 117, 119, 127, 129, 140} Some studies suggest different temperatures for melting of organized domains at and below monolayer coverage on metal surfaces^{96, 144-146} and even for multilayers;^{92, 138}

b: For details on the calculation of h , see Chapter 2.5;

c: Value determined experimentally;

d: Based on literature data;¹²⁸

e: Based on literature data;¹⁴⁷

f: At 298 K;

g: At 293 K.

2.1.2 Metal Single Crystals

The round Ag(111) and Au(111) single crystals with a diameter of 15 mm and a thickness of 2 mm were purchased from MaTecK with a purity of 99.999 % and one side polished and aligned to the (111) plane with an accuracy better than 0.1° . The crystals were mounted to Mo sample holders and fixed with Ta wire, see Figure 2. For temperature measurement, type K thermocouples were contacted and stuck into a pinhole ($\varnothing = 0.3$ mm) at the side of the crystal (see also technical drawing in the Appendix). Surface preparation was done in UHV by sputtering with 600 eV Ar^+ ions followed by annealing at 800 K. The sample cleanliness and long range order were checked by XPS and low energy electron diffraction (LEED), respectively.¹⁰³⁻¹⁰⁵

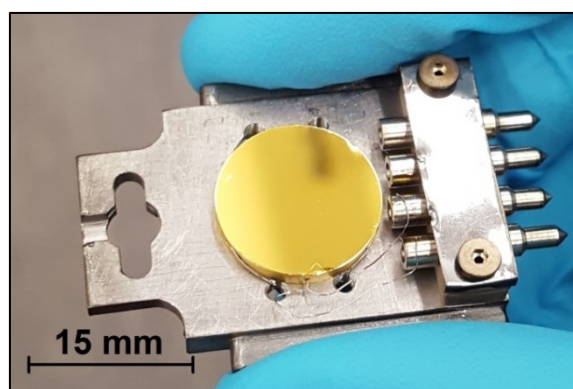


Figure 2: Photograph of the Au(111) single crystal mounted on a Mo sample plate. A technical drawing of the Ag(111) and Au(111) crystals is provided in the Appendix.

Ag(111) and Au(111) show low reactivity towards the ILs and 2H-TPP, and no changes in the atomic structure of these surfaces were reported upon deposition.^{85, 103, 148} In addition to the excellent suitability as model systems, Ag and Au in the form of Ag/Au alloys could be relevant for future applications in SCILL¹⁰³ where Ag activates molecular oxygen in oxygen-assisted coupling reactions.¹⁴⁹⁻¹⁵⁰

2.2 Angle-Resolved X-Ray Photoelectron Spectroscopy (ARXPS)

X-ray photoelectron spectroscopy (XPS) is the main method applied throughout this thesis. As sketched in Figure 3, XPS is based on the photoelectric effect,¹⁵¹⁻¹⁵³ that is, the emission of electrons from matter upon interaction with electromagnetic radiation. These so-called photoelectrons have kinetic energies E_{kin} that correlate directly to the energy ($h\nu$) of the incident photons and the binding energy E_b of the electrons occupying the various core levels of the elements present in a given sample:

$$E_{kin} = h\nu - (E_b + \Phi_{sp}) \quad (1)$$

The work function Φ_{sp} of the spectrometer is typically considered by calibrating the spectrometer to the Fermi level of the sample.⁹⁵ An analyzer collects the emitted photoelectrons and separates them by E_{kin} , providing counts per second for discrete energy intervals upon scanning the spectrum. Figure 4a shows the XP spectrum of a clean Ag(111) single crystal under Al $K\alpha$ radiation ($h\nu = 1486.6$ eV). Note the characteristic set of core levels distributed across the spectrum, all related to the electronic structure of Ag, which allows for a clear identification of this element. The XP spectrum of the IL $[C_1C_1Im][Tf_2N]$ in Figure 4b shows a spread of lines which as indicated in the graph are related to the different elements (C, F, N, O, S) present in the IL sample.

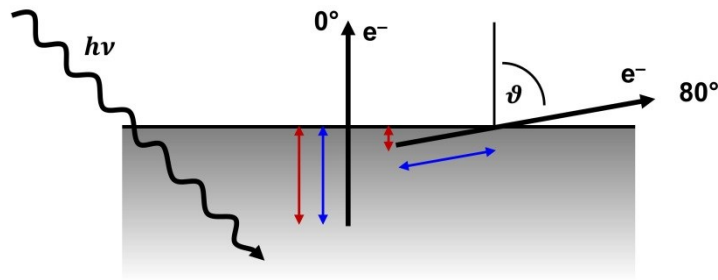


Figure 3: Angle-resolved X-ray photoelectron spectroscopy (ARXPS). Photoelectrons are emitted from the sample upon X-ray irradiation. The blue arrows correspond to 3λ . The red arrows indicate the information depth ID and how it varies for a change in the detection (or emission) angle ϑ from normal emission (0° , bulk sensitive: $ID = 7$ to 9 nm) to grazing emission (80° , surface sensitive: $ID = 1$ to 1.5 nm).

The inelastic mean free path λ of electrons in condensed matter is generally very short (1 to 3 nm,¹⁵⁴ see also Chapter 2.4), that means, XPS inherently is a highly surface sensitive technique. In angle-resolved XPS (ARXPS), a variation of the angle ϑ between the sample's surface normal and the electron analyzer (commonly by rotation of the sample) can lead to considerable changes in ID :

$$ID(\vartheta) = 3\lambda \cdot \cos \vartheta \quad (2)$$

Changing the detection (or emission) angle from normal emission (0° , bulk sensitive) to grazing emission (80° , surface sensitive) causes a decrease in ID from typically 7 to 9 nm for $\vartheta = 0^\circ$ to about 1 to 1.5 nm for $\vartheta = 80^\circ$, that is, the experiment at 80° emission is about six times more surface sensitive, and mainly the topmost surface layer is probed.

As the count of photoelectrons is directly proportional to the intensity of the incident photon beam, a quantitative analysis of a sample's chemical composition is possible.¹⁵⁵ In ad-

dition to the identification of elements present within the sample (as shown in Figure 4), it is also possible to obtain information on the chemical and physical environment of an element by looking at relative chemical shifts of E_b . Figure 5 shows the spectrum of F 1s photoelectrons of a mixed thin film of two ILs, $[\text{C}_8\text{C}_1\text{Im}][\text{Tf}_2\text{N}]$ and $[\text{C}_8\text{C}_1\text{Im}][\text{PF}_6]$.¹⁰⁴ Within this film, the different chemical environments of the F atoms in the two different anions result in distinct binding energies of the respective F 1s core levels. This allows for a direct quantitative analysis of the relative amount of the respective anion. By variation of the detection angle of the photoelectrons (and thus ID) it is further possible to quantify and compare for example the relative amount of $[\text{Tf}_2\text{N}]^-$ and $[\text{PF}_6]^-$ anions in the bulk (0° emission) and at the vacuum interface (80°) of the IL film.

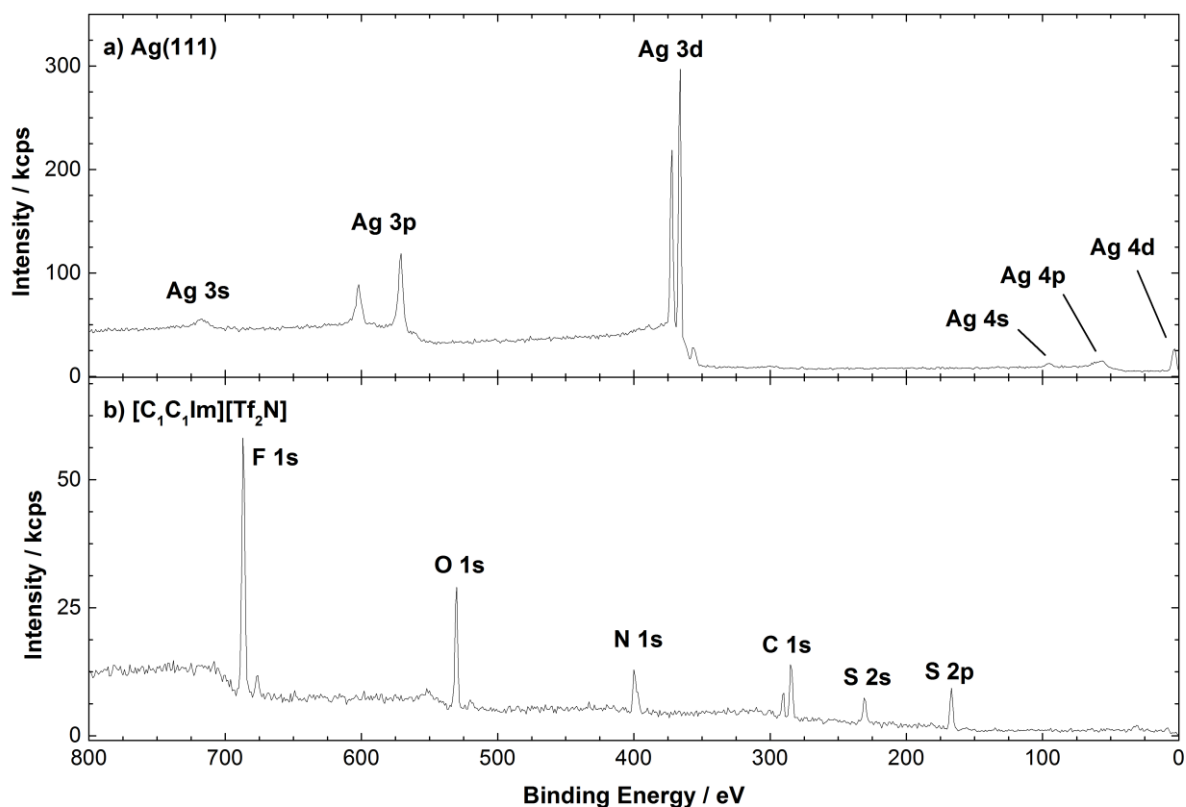


Figure 4: XPS spectra of a) Ag(111) and b) $[\text{C}_1\text{C}_1\text{Im}][\text{Tf}_2\text{N}]$.

The experiments in this thesis were performed using a two-chamber UHV system for preparation (sputtering, annealing, PVD of ILs and 2H-TTP, LEED, QMS) and analysis (ARXPS), with a base pressure of about 5×10^{-11} mbar. The ARXP spectra were acquired with a non-monochromated Al $K\alpha$ X-ray source (SPECS XR 50, 1486.6 eV, 240 W) and a hemispherical electron analyzer (VG SCIENTA R3000). All spectra were measured with a pass energy of 100 eV, which resulted in an overall energy resolution of ~ 0.9 eV. For more

details, see Refs.^{95, 100, 103, 156} Peak fitting and background subtraction were done using CasaXPS V2.3.16Dev6. For the Ag 3d and Au 4f peaks, a Shirley background was subtracted,¹⁵⁷ for N 1s on Au(111), F 1s and P 2p a two-point linear background, and for the C 1s region a three-point linear background. For the N 1s spectra on Ag(111), an additional background was subtracted to account for overlapping shake-up and plasmon satellites, and inelastically scattered electrons of the Ag 3d core levels;¹⁵⁸⁻¹⁶¹ for further details, see Figure 6.¹⁰³ The IL spectra were fitted with a Voigt profile (30% Lorentzian contribution). For fitting of the IL C 1s peaks, a constraint of $\text{FWHM}(C_{\text{hetero}}) = 1.11 \times \text{FWHM}(C_{\text{alkyl}})$ was applied.^{96, 106} The atomic sensitivity factors (ASF) for the quantitative analysis are supplied in the Appendix. All binding energies were referenced to the Fermi edge, yielding 368.20 eV for the Ag 3d_{5/2} line and 83.85 eV for Au 4f_{7/2}. The XP spectra of the macroscopic IL films were referenced to the binding energy of either C_{alkyl} at 285.0 eV or of C_{hetero} at 287.0 eV if the IL did not contain any C_{alkyl}.¹⁰³⁻¹⁰⁵

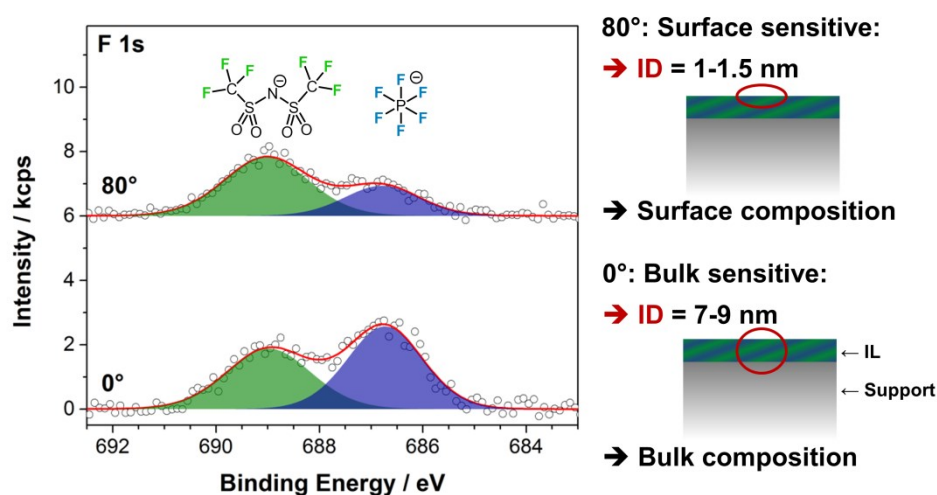


Figure 5: F 1s core level spectra from ARXPS at 0° (bulk sensitive) and 80° (surface sensitive) emission angles of a mixed thin film of two ILs, [C₈C₁Im][Tf₂N] and [C₈C₁Im][PF₆]. By quantification of the peak areas it is possible to determine the ratio of [Tf₂N]⁻ anions to [PF₆]⁻ anions in the bulk and at the vacuum interface. Spectra adapted from Ref¹⁰⁴ under license CC BY 4.0.

Time-dependent ARXPS measurements for the investigation of temporal changes of film morphology were started immediately after the deposition of the respective IL. Because the sample needed to be transferred from the preparation chamber to the analysis chamber of our UHV system between IL deposition and XPS measurement, the first data point could be obtained approximately 4 min after ending the IL deposition. The acquisition time for the Ag 3d region was approximately 2 min. The time values given in the corresponding figures represent the start of each measurement.¹⁰³

For temperature-programmed XPS (TP-XPS), the sample was heated continuously during the measurements at a rate of 2 K/min. The acquisition time for F 1s spectra ranged from 2 to 5 min, for C 1s spectra from 5 to 10 min and for Ag 3d spectra from 1 to 2 min.⁸⁴
104-105

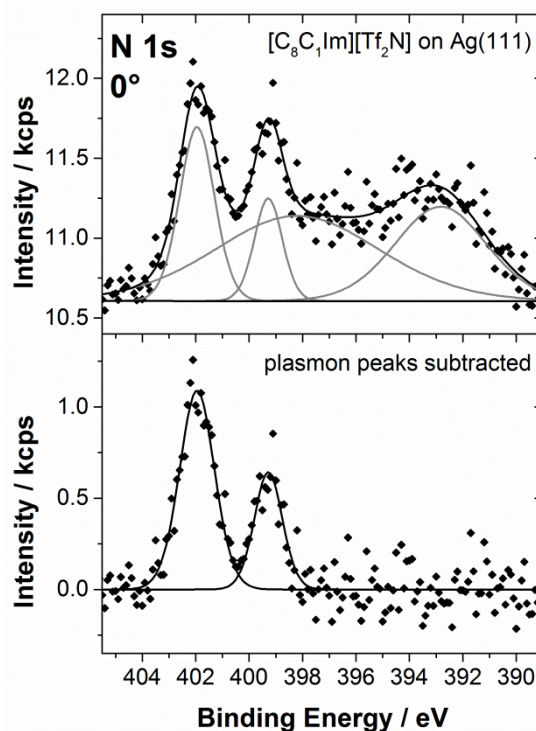


Figure 6: N 1s signal in 0° emission of 2.8 nm of [C₈C₁Im][Tf₂N] on Ag(111). The peak at higher binding energy corresponds to the two N atoms in the cationic imidazolium ring and the peak at lower binding energy to the single N atom in the anion. The peaks overlap strongly with satellites of the Ag 3d line of the substrate. A least-squares fit of the N 1s peaks together with the satellites was used to deal with the complicated background. The lower spectrum shows the IL-related N 1s spectrum after subtraction of the substrate contributions of the spectra. Reproduced from¹⁰³ under license CC BY-NC 3.0 – Published by the PCCP Owner Societies.

2.3 Physical Vapor Deposition of ILs and Porphyrins

Since 2008,⁹³ *in vacuo* physical vapor deposition (PVD) of ultrathin IL films combined with ARXPS was gradually established as a potent method for molecular-level investigations of IL/solid interactions, wetting behavior and IL film growth in the coverage range from less than a monolayer to several multilayers.^{10, 39, 44, 84, 93-98, 100, 102-105, 110, 144, 162-163} By deposition of ultra-thin films of only a few molecular layers (and less), it is possible to monitor the IL/solid interface with XPS through the IL film, despite the highly surface sensitive nature of XPS.¹¹

For the measurements on the ultrathin layers, well-defined amounts of the different ILs were deposited via PVD using two effusion cells dedicated to IL deposition.¹⁰⁴ Figure 7

shows a sketch of the effusion cell which was developed and optimized in this work. The complete technical drawings are provided in the Appendix. This evaporator setup was used for ILs as well as for 2H-TPP. The flux was checked using a quartz crystal microbalance (QCM) to ensure stable and reproducible evaporation rates. This QCM can be rotated in and out between the sample and the effusion cells. To remove volatile impurities, the compounds were thoroughly degassed in UHV for more than 24 hours at evaporator temperatures between 370 and 500 K. The evaporation temperatures ranged from 370 to 460 K for the ILs and from 570 to 600 K for 2H-TPP. During deposition, the chamber background pressure was typically around 1×10^{-9} mbar. With the exception of dialkylimidazolium halides,¹⁶⁴⁻¹⁶⁵ most other alkyylimidazolium ILs evaporate intact in the form of neutral ion pairs.^{93-94, 102-105, 110, 145-146, 165-170} In the present work, the XP spectra of the thin films from PVD were compared to spectra of macroscopically thick IL films prepared *ex-situ*, and no indications of decomposition were observed for the films prepared by PVD.^{84, 103-105}

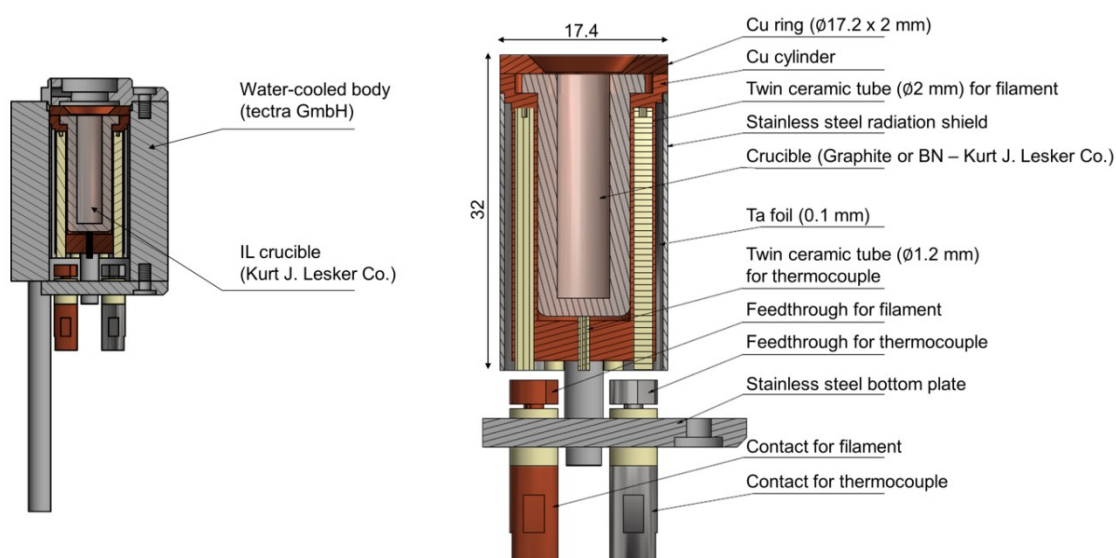


Figure 7: Sketch of the heating cartridge for the effusion cell developed by our group specifically for the evaporation of ILs in UHV. The water-cooled body was acquired from tectra GmbH. A graphite or boron nitride crucible (purchased from Kurt J. Lesker Co.) sits in a copper cylinder which is heated by a tantalum filament ($\varnothing = 0.25$ mm). This filament winds through six ceramic twin tubes ($\varnothing = 2$ mm) which are distributed equidistantly in wall bores of the copper cylinder. A copper ring holds the crucible in place. A type K thermocouple ($\varnothing = 0.125$ mm) is contacted to the bottom of the crucible to ensure a stable and accurate temperature reading. Note that the wall bores for the filaments do not go all the way through. In this way, the setup quite effectively prevents ILs (which tend to creep out of the crucible) from direct contact with the hot filaments, which would cause decomposition of the ions and possible contaminations on the target. Adapted from ¹⁰⁵ under license CC BY-NC 3.0 – Published by the PCCP Owner Societies. The complete technical drawings are provided in the Appendix.

For the study of ultrathin IL films, X-ray beam damage can play a crucial role.^{84, 94} In order to avoid undesired effects due to high X-ray doses, each film for one deposition experiment was prepared on a freshly cleaned Ag(111) surface after completely removing the previous film by sputtering and annealing.^{84, 103-105}

2.4 Monitoring Thin Film Growth with XPS

The coverage and growth of IL and porphyrin films on Ag(111) and Au(111) was monitored through the changes in the XPS signal (Ag 3d and Au 4f, respectively) intensity of the crystal at emission angles of $\vartheta = 0^\circ$ and 80° relative to the surface normal. For homogeneous two-dimensional (2D) growth, the Ag 3d signal at an angle ϑ decreases from I_0 , for the clean surface, to I_d , when a film of thickness d is covering the surface, according to:^{94, 103-105, 110, 171}

$$\frac{I_d}{I_0} = e^{-\frac{d}{\lambda \cdot \cos \vartheta}} \quad (3)$$

ϑ is the detection angle relative to the surface normal and λ the inelastic mean free path of the electrons, which depends on the kinetic energy of the respective core level electrons and the composition of the IL film.¹⁵⁵ In the work presented here, values for λ were obtained by linear interpolation of λ values of previous studies of similar ILs on gold, graphene, mica, nickel and silicon oxide substrates at kinetic energies of the respective core levels between 630 and 1400 eV, see Figure 8.^{93-94, 96, 98-99, 110} Studies by Tanuma *et al.*¹⁷² show that within this energy range λ indeed scales linearly with the kinetic energy. For Ag 3d electrons with a kinetic energy of around 1110 eV, λ is in that way approximated to 2.5 nm in IL films.^{84, 103-105} For Au 4f electrons (1400 eV) $\lambda = 3.0$ nm is used in agreement with literature.^{84, 94, 101, 132, 173-174} Because of the similarities in chemical composition and density, similar λ values are assumed for 2H-TPP.⁸⁴

For the sake of clarity, it should be noted that for ideal layer-by-layer growth (that means the full completion of a layer is achieved before a new layer starts to grow on top) the substrate signal should decrease in a section-wise linear fashion for each layer.^{94, 103, 110, 171, 173} The statistics of the data presented here are, however, not good enough to unequivocally resolve such slope changes between adjacent straight sections. In order to detect deviations from 2D film growth, the mean film thickness d for a given deposition experiment was calculated from the experimental I_d/I_0 ratios at $\vartheta = 0^\circ$, that is, in the bulk-sensitive emission geometry, according to Eq. (3).^{84, 94, 103-105} With the obtained d value, the expected attenuation at $\vartheta = 80^\circ$, that is, in the surface-sensitive emission, was then calculated using the same equation. While agreement between the experimental data at 80° and the calculation at 80° in-

dicates 2D growth, I_d/I_0 ratios above the calculated curve indicate a three-dimensional (3D) morphology of the IL film;¹⁷¹ such behavior was observed for a number of systems.^{84, 98-99, 101, 103-105, 110}

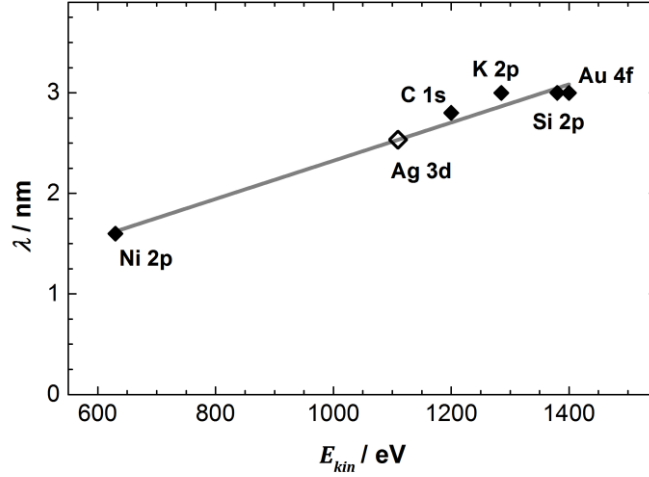


Figure 8: Literature values for λ of various core levels (kinetic energies, E_{kin} , between 630 and 1400 eV) in IL films^{93-94, 96, 98-99, 110} and interpolated value for Ag 3d electrons¹⁰³ with a kinetic energy of around 1110 eV.

Notably, in the present study the IL films of $[C_1C_1Im][Tf_2N]$ were found to change their morphology from an initial pronounced 3D topology towards 2D over time, as evidenced by a change of the I_d/I_0 ratio after IL deposition was stopped, see Chapter 3.2.¹⁰³ Therefore, all values for mean film thickness d of $[C_1C_1Im][Tf_2N]$ denoted in this work were derived only after these changes leveled off, that is, when maximum attenuation of the support signals – and thus, a sort of final state – was reached; this was typically the case between 30 min and 2 h after ending the IL deposition.

2.5 Estimation of the IL Monolayer Height

For the discussion of the growth behavior of the ILs, coverage is given in ML, where 1 ML is defined as a closed double layer of ions irrespective of their relative arrangement.^{84, 93, 103-105, 169} The monolayer height h is approximated as the cubic root of the molecular volume V_m based on mass density ρ values of the IL from literature:^{94, 103-105, 110}

$$h = \sqrt[3]{V_m} = \sqrt[3]{\frac{M/N_A}{\rho}} \quad (4)$$

with M molar mass and N_A Avogadro constant.⁸ According to this relation, h is 0.73 nm for $[C_1C_1Im][Tf_2N]$, 0.84 nm for $[C_8C_1Im][Tf_2N]$ and 0.77 nm for $[C_8C_1Im][PF_6]$ using values for V_m from literature.^{8, 103-104}

Due to the ability to freely change substituents at the imidazolium head group, it is quite likely to come across an IL with a so far unexplored mass density. This is for example the case for [PFBMIm][PF₆]. Additionally, this IL is solid at RT,¹⁰⁵ meaning, that ρ can be highly dependent on the conditions of solidification (cooling rate, crystallinity), which could make a reliable value for ρ fairly difficult to achieve. The monolayer height h of [PFBMIm][PF₆] can, however, be estimated by comparison to the values for the non-fluorinated [C_nC₁Im][PF₆] ILs (calculated from known mass densities), considering the increase of V_m upon exchange of hydrogen by fluorine.¹⁷⁵ This estimation is based on a study by Morgado *et al.*, who determined the molar volume v_m of n-alkanes and n-perfluoroalkanes as a function of the number of carbon atoms in the molecule. According to their data, v_m of the molecules increases in a nearly linear fashion by ≈ 16 cm³/mol per CH₂ and upon insertion of CF₂ by ≈ 24 cm³/mol.¹⁷⁵ In good agreement to the alkanes, v_m of [C_nC₁Im][PF₆] and [C_nC₁Im][Tf₂N] ILs, shown in Figure 9a, increases almost linearly by ≈ 17 cm³/mol for every CH₂ unit added to the linear carbon chain substituent. Due to the good agreement, v_m for [PFBMIm][PF₆] can be estimated from this data. Starting from the v_m of [C₂C₁Im][PF₆] of 169 cm³/mol, we extend the alkyl chain by two CF₂ units adding 48 cm³/mol, which yields a v_m for [PFBMIm][PF₆] of 217 cm³/mol. From this value, h of [PFBMIm][PF₆] is calculated to 0.71 nm, which is, as expected, only slightly larger than h of [C₄C₁Im][PF₆] of 0.70 nm¹⁰⁵ (Figure 9b) because the side chain is only a part of the larger ion pair.

Porphyrin coverages are given in this work by the number of complete layers. This means, one monolayer corresponds to one saturated layer with all porphyrin molecules lying flat in direct contact with the metal surface.⁸⁴ In some previous publications, the porphyrin coverage in ML was also defined as the number of porphyrin molecules per metal atom of the substrate. For 2H-TPP on Ag(111) and Au(111), one monolayer corresponds by this definition to a coverage of 0.037 ML.¹⁷⁶ To avoid any confusion, the unit ML will not be used to denote porphyrin coverages in this work. Monolayer coverage of 2H-TPP on Ag(111) and Au(111) can be prepared by heating to 500 K (above the temperature of multilayer desorption,^{84, 177} see Chapter 3.3) after the deposition of multilayers of the porphyrin on the metal crystal. From the attenuation of the substrate XPS signal in 0° emission, the height of the monolayer of flat lying 2H-TPP molecules was calculated to 0.34 nm using $\lambda = 2.5$ nm on Ag(111) and $\lambda = 3.0$ nm on Au(111), respectively, as stated above.⁸⁴

Upon heating above 525 K, signs of dehydrogenation at the phenyl groups were reported for 2H-TPP molecules in contact with the Ag(111) surface.¹⁷⁸ In this work, the

porphyrin layers were only heated to 500 K to avoid dehydrogenation at the molecule's periphery. Di Santo *et al.* reported a shift to lower binding energy of the N 1s and C 1s signals and a change in the C 1s peak shape after heating to 550 K. Both were attributed to a change in the orientation of the phenyl groups of the 2H-TPP molecule relative to the metal surface upon dehydrogenation at the molecules periphery.¹⁷⁸ In the present study, the spectra of monolayer 2H-TPP films showed no difference after heating to 500 K compared to films of similar thickness prepared by direct deposition.⁸⁴

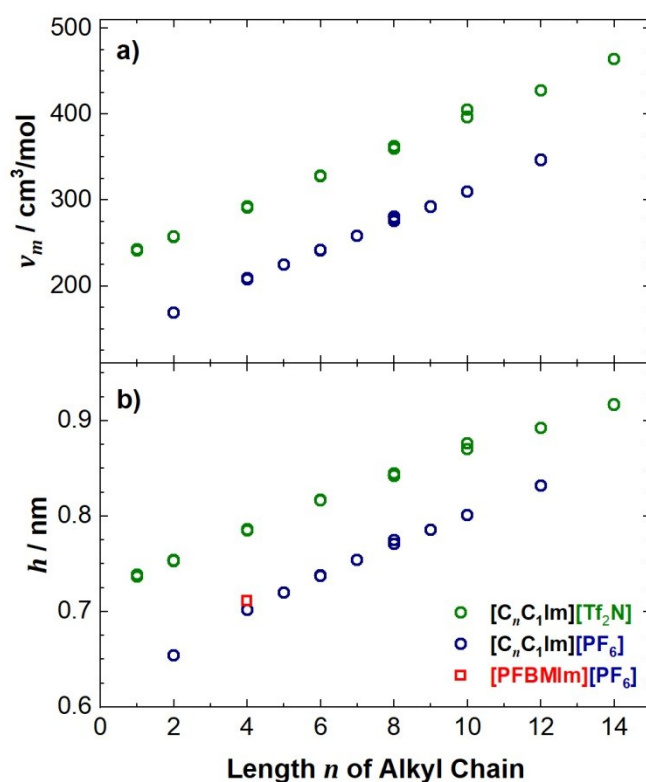


Figure 9: Molar volumes v_m (a) and corresponding estimates of monolayer height h (b) of $[\text{C}_n\text{C}_1\text{Im}][\text{Tf}_2\text{N}]$ and $[\text{C}_n\text{C}_1\text{Im}][\text{PF}_6]$ ILs calculated from the ILs' respective mass densities ρ . ρ of $[\text{Tf}_2\text{N}]^-$ ILs from Refs;^{8, 109, 128, 147} ρ of $[\text{PF}_6]^-$ ILs from Refs.^{8, 128, 135, 147, 179-182} For the estimation of h of $[\text{PFBMIm}][\text{PF}_6]$, see the text. The values of h are also provided in a table in the Appendix.

3. Results

The main part of the results accumulated in this dissertation is published in a series of peer-reviewed journal articles [P1-P4]. This chapter provides a summary of the individual results, finding common ground through the topical connections between all four studies and by further support of so far unpublished findings. For the detailed description of the individual results and the specific systems under investigation, the reader is referred to the corresponding publications [P1-P4] in the Appendix.

3.1 Ionic Liquid Thin Film Growth on Metal Surfaces [P1, P2, P3, P4]

Studying the interaction of ILs with solid supports was one major focus of this thesis, with the aim to understand fundamental aspects relevant for thin film applications such as SILP or SCILL catalysis.¹¹ These aspects are in particular the structure and arrangement at the liquid/solid interface, the initial stages of thin film growth and ultimately the wetting behavior of thin IL films on the solid supports at room temperature (RT).^{11, 64, 69, 73, 103} Aside from the specific interaction of the molecules with the support, a good wettability of the IL film is a crucial requirement for the performance of the composite systems.^{11, 28, 64} While wetting of ILs has been studied quite extensively on the macroscopic and mesoscopic scale, mostly by contact angle measurements and atomic force microscopy (AFM),^{10, 64, 118, 183-195} only a few studies are available on the molecular scale.^{10, 93-94, 96, 98-99, 101, 110, 132, 138, 146, 196-197}

The growth was characterized by measuring the attenuation of the core level intensity of the supporting crystal upon varying the coverage of the IL. Four model ILs, [C₁C₁Im][Tf₂N], [C₈C₁Im][Tf₂N], [C₈C₁Im][PF₆] and [PFBMIm][PF₆] (see Table 1) were studied on the Ag(111) and Au(111) surfaces by quantitative ARXPS. The main differences between the selected ILs are the different length and chemical composition of the alkyl chain at the imidazolium head group and the nature of the counter ion.

Figure 10 shows the attenuation of the Ag 3d signal of the supporting Ag(111) crystal as a function of IL film thickness for [C₈C₁Im][Tf₂N]. Up to 0.5 ML, the good agreement of the 80° data to the corresponding curve calculated for 2D growth (dashed line) indicates the formation of a closed molecular layer at the IL/Ag(111) interface where both, cations and anions, adsorb in a checkerboard arrangement, that is, within this wetting layer (WL), both ions are in contact with the metal surface.¹⁰³ Upon increasing the film thickness, the 80° data systematically falls above the 2D curve, indicating the formation of 3D islands on top of the WL.¹⁰³

For coverages of $[\text{C}_8\text{C}_1\text{Im}][\text{Tf}_2\text{N}]$ below 0.5 ML (which is less than the WL), the $[\text{C}_8\text{C}_1\text{Im}]^+$ cation was found to adsorb in a flat geometry on Ag(111) at RT, with both, the imidazolium head group as well as the octyl chain, in contact with the metal surface. Approaching 0.5 ML, *i.e.* one closed molecular layer, the octyl chains gradually detach from the metal surface and orient towards the vacuum.¹⁰³ This behavior was previously observed by Cremer *et al.* for $[\text{C}_8\text{C}_1\text{Im}][\text{Tf}_2\text{N}]$ on Au(111),⁹⁴ and it also occurs for $[\text{C}_8\text{C}_1\text{Im}][\text{PF}_6]$ on Ag(111) and Au(111).⁸⁴ The driving force behind this molecular rearrangement approaching 0.5 ML coverage is most likely related to the fact that it allows for a tighter packing of the ions within the WL at the interface.^{94, 103} Although it implies that the cations' individual adsorption energy is lowered by the (missing) contribution of attractive van der Waals interactions of the alkyl chains with the metal surface, it likely creates an energetic net benefit by reducing the average lateral distance between the adsorbed ionic head groups and further by freeing up more adsorption sites at the interface to adsorb further IL ion pairs in direct contact with the metal.⁸⁴

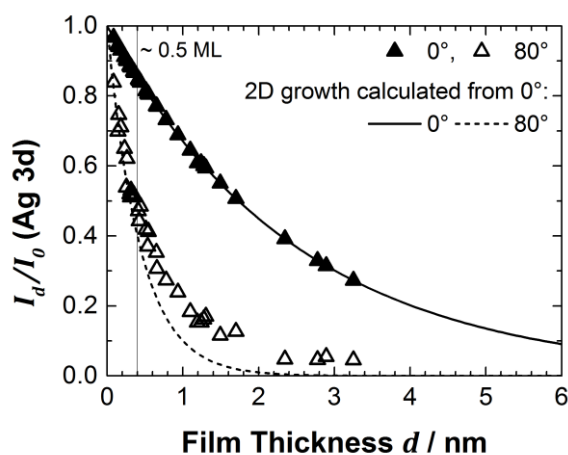


Figure 10: Attenuation of the Ag 3d intensity in 0° and 80° emission as a function of the film thickness d of the IL $[\text{C}_8\text{C}_1\text{Im}][\text{Tf}_2\text{N}]$ on Ag(111) at RT. The curves for 2D growth are calculated from Eq. (3) with an inelastic mean free path λ of 2.5 nm and the corresponding detection angles. Adapted from ¹⁰³ under license CC BY-NC 3.0 – Published by the PCCP Owner Societies.

Independent of the length of the alkyl substituents at the imidazolium cation, the $[\text{Tf}_2\text{N}]^-$ anion was found to adsorb on Ag(111) in a *cis* conformation with an upright orientation, that is, with the oxygen atoms pointing towards the metal and the CF_3 groups away from the surface.¹⁰³⁻¹⁰⁴ This geometry of the $[\text{Tf}_2\text{N}]^-$ anion was observed previously for several ILs with $[\text{Tf}_2\text{N}]^-$ as anion by ARXPS on Au(111)^{94, 96} and by scanning tunneling microscopy (STM) on Ag(111)^{145, 198} and Au(111),^{96, 145, 198} and other surfaces.^{97, 99, 162, 199-201} Notably, this preferential orientation of the $[\text{Tf}_2\text{N}]^-$ anion is found at RT^{94, 96, 99, 103-104, 199-201}

and also at temperatures around 100 K.^{94, 96, 104, 145, 162} Preferential orientation of the anion at the IL/metal interface was also reported for [C₂C₁Im][TfO] on Pd(111)²⁰²⁻²⁰⁴ and on Co-covered Pd(111),²⁰⁵ such that the SO₃ group points towards the metal and the CF₃ group away from the surface.

Table 2 provides an overview over a range of molecular-level studies that deal with the initial stages of thin film growth and the structure at IL/metal interfaces. The formation of a 2D WL with a checkerboard arrangement of (on average) alternating anions and cations is with overwhelming consistency the result of the majority of the molecular-level studies of IL/solid interfaces.^{84, 92-94, 96-99, 101, 103-105, 132, 144-145, 174, 186, 198, 202-203, 206-207} One exception is the growth of [C₁C₁Im][Tf₂N] on Ni(111) at 220 K, where for coverages below 0.5 ML the ions were reported to adsorb in a sandwich-type arrangement, where initially only the [C₁C₁Im]⁺ cation is in contact with the Ni(111) surface and the [Tf₂N]⁻ anion sitting on top of the cation.¹¹⁰

Table 2: Overview over selected molecular-level studies of IL thin film growth and structure at IL/metal interfaces. The entries shaded in gray were studied in this work.

Ionic Liquid	Surface	WL	Multilayer	Remarks ^a	Ref.
[C ₁ C ₁ Im][Tf ₂ N]	Ag(111)	Yes	3D	ARXPS for sub-monolayer to multilayers at RT. Time-dependent changes of film morphology at RT.	103
	Au(111)	Yes	2D	ARXPS for sub-monolayer to multilayers at RT.	94
	Ni(111)	Yes	3D	ARXPS for sub-monolayer to multilayers at 220 K. Sandwich arrangement of ion pairs in WL.	110
[C ₂ C ₁ Im][Tf ₂ N]	Ag(111), Au(111)	Yes	-	STM for sub-monolayer coverage at < 120 K.	145
	Au(110)	Yes	3D	STM at 128 K, LEED and UPS at RT, surface reconstruction upon IL adsorption. Time-dependent changes of film morphology at RT.	146
	Ni(111)	Yes	-	TOF-SIMS at 150 to 280 K.	92
[C ₄ C ₁ Im][Tf ₂ N]	Au film on mica	Yes	3D	Pulsed-valve deposition. XPS and <i>ex-situ</i> AFM at RT.	207
[C ₈ C ₁ Im][Tf ₂ N]	Ag(111)	Yes	3D	STM for sub-monolayer coverage at < 120 K, ARXPS for sub-monolayer to multilayers at RT. Interaction with co-adsorbed [C ₈ C ₁ Im][PF ₆].	103, 145
	Au(111)	Yes	2D	STM for sub-monolayer coverage at < 120 K and RT. ARXPS for sub-monolayer to multilayers at RT, study of beam damage.	94, 102, 132, 145
	Cu(100)	Yes	-	STM for WL coverage and XPS for sub-monolayer to multilayers at RT. STM showed no clear order in the WL at RT.	102

Table 2 continued.

Ionic Liquid	Surface	WL	Multilayer	Remarks ^a	Ref.
[C ₈ C ₁ Im]Cl	Au(111)	Yes	3D	ESI deposition. ARXPS for sub-monolayer to multilayers and ex-situ AFM on multilayers at RT.	132
[C ₈ C ₁ Im][PF ₆]	Ag(111), Au(111)	Yes	3D	ARXPS for sub-monolayer to multilayers at RT and < 90 K. Interaction with co-adsorbed porphyrin layer, [C ₈ C ₁ Im][Tf ₂ N] and [PFBMIm][PF ₆].	84, 104-105
[C ₄ C ₁ Im][BF ₄]	Pt on Al ₂ O ₃	Yes	2D	Nano-inkjet printing. AFM at RT indicates 2D growth up to 4 nm.	208
[C ₈ C ₁ Im][BF ₄]	Cu(111)	Yes	3D	XPS and UPS at 120 K and RT. The film morphology changes upon heating to RT after deposition at 120 K.	138
[PFBMIm][PF ₆]	Ag(111)	Yes	3D	ARXPS for sub-monolayer to multilayers at RT. Interaction with co-adsorbed [C ₈ C ₁ Im][PF ₆].	105
[C ₂ C ₁ Im][TfO]	Au(111)	Yes	3D	ARXPS for sub-monolayer to multilayers at RT. Growth is closer to 2D on partially Pd-covered Au(111).	101
	Pd(111)	Yes	-	IRAS on WL and multilayers. At 220 K, checkerboard arrangement in first layer. Strong interaction of the anion with the metal influences multilayer structure.	202-203
[C ₄ C ₁ Pyrr][Tf ₂ N]	Ag(111)	Yes	-	STM for sub-monolayer coverage at < 120 K.	198
	Au(111)	Yes	2D	STM for sub-monolayer coverage at < 120 K. ARXPS for sub-monolayer to multilayers at RT.	96, 198
	Cu(111)	Yes	-	STM for sub-monolayer coverage at 100 K and RT.	97
[C ₄ C ₁ Pyrr][FAP]	Au(111)	Yes	-	STM for sub-monolayer coverage at 210 K and RT. Not clear, whether checkerboard or sandwich arrangement in WL.	206

a: IL films prepared by PVD, if not indicated otherwise.

On top of the initially formed homogeneous WL, *i.e.* for coverages above 0.5 ML, all ILs studied within this thesis show more or less pronounced island growth on Ag(111) and Au(111),^{84, 103-105} as schematically depicted in Figure 11. This Stranski-Krastanov-like growth²⁰⁹ (or pseudo partial wetting²¹⁰) again appears to be a quite common observation for molecular level studies of ILs on metals,^{84, 101, 103-105, 110, 132, 138, 174, 207} see Table 2, and also on various other surfaces.^{89, 93, 98-99, 110, 186, 196, 199} Studies on the mesoscopic scale also commonly report the formation of a 2D WL and subsequent droplet formation of ILs on a wide range of surfaces.^{184-185, 187-193, 211}

For $[\text{C}_8\text{C}_1\text{Im}][\text{PF}_6]$, the initial stages of film growth were studied on the bare $\text{Ag}(111)^{84, 105}$ and $\text{Au}(111)^{84}$ surfaces, and also after pre-adsorption of one closed layer of 2H-TPP on these two surfaces.⁸⁴ Just as on pristine $\text{Ag}(111)^{84, 104}$ and $\text{Au}(111),^{84}$ $[\text{C}_8\text{C}_1\text{Im}][\text{PF}_6]$ forms a closed WL on top of the porphyrin layer. At IL coverages above 0.5 ML, again the formation of 3D islands on top of the WL is observed. The 3D island growth appears more pronounced on the 2H-TPP layer as compared to the pristine metal surfaces.⁸⁴

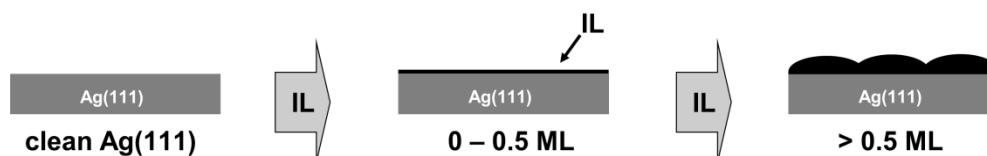


Figure 11: Scheme of the initial stages of IL film growth observed on $\text{Ag}(111).$ ¹⁰³⁻¹⁰⁵ Initially, formation of a 2D WL, followed by 3D droplets on top. Adapted from¹⁰³ under license CC BY-NC 3.0 – Published by the PCCP Owner Societies.

On the molecular scale, the occurrence of 3D growth on top of the initial WL hints at two things. For one, the adsorption of the ions at the metal interface is stronger than the interaction of the ions within the IL film, and two, the structure that is forced on the IL within a 2D film arrangement could be energetically less favored compared to the more relaxed structure within the IL droplets that form on top of the WL – despite imposing a higher surface area. Terms like “structure” and “strain” commonly used for the description of nucleation and growth of thin films,²¹²⁻²¹⁶ however, appear somewhat unsuitable for the description of IL thin film growth at RT because of the highly mobile, liquid nature of the IL systems (see also Chapters 3.2 and 3.5). A more suitable concept could focus on the ionic nature of these films, that is, the precise structure within the multilayers is less important compared to the energetic benefits that can arise from a higher average coordination of ions with counter ions within a 3D island as compared to a 2D layered film. In the system of 3D IL droplets in equilibrium with a 2D molecular film wetting the entire metal surface, the IL WL forms due to a strongly stabilizing interaction of the metal surface (as deduced from higher desorption temperatures of the WL compared to multilayers, see Chapter 3.4), by formation of image dipoles within the metal and possible (partial) charge transfer.^{169, 217} This point of view is in overall agreement with more conventional molecular scale interpretations of growth behavior in metal-organic heteroepitaxy.²¹⁸⁻²¹⁹

On the mesoscale, the concept of pseudo partial wetting for nonvolatile liquids is well known. Already in 1991, de Gennes *et al.*²¹⁰ published a model based on the liquid’s surface tension, able to explain this wetting behavior for certain values of two parameters: Hamaker

constant A and spreading coefficient S . It remains to be shown, however, whether this model can be applied to ILs due to the limitations of this model considering long-range interactions²¹⁰ and the obvious Coulomb contributions to the intermolecular forces of ILs.

In conclusion, the entirety of data currently available already allows for the derivation of certain structure-property relationships. And while the formation of a closed WL on metal surfaces appears to be one general similarity for ILs, the intermolecular structure and molecular orientation at the interfaces seems to be determined predominantly by the composition of the IL and less by the nature of the substrate. In the present state, there is still need of further data on a wider range of systems to allow for a clear correlation of film morphologies in the later stages of thin film growth.

3.2 Time-Dependent Changes in the Growth of IL Films [P1]

Upon deposition of multilayers of $[C_1C_1Im][Tf_2N]$ on Ag(111) at RT, a time-dependent behavior of the IL film is observed.¹⁰³ Figure 12 shows the temporal evolution of the XPS signal intensity of the Ag support after IL deposition. The intensity ratio I_d/I_0 of the Ag 3d signals is plotted versus the time after ending the deposition of IL, for nominal (that means final) film thicknesses of a) 1.5 nm and b) 3.2 nm. On the timescale of several tens of minutes, a considerable decrease in intensity occurs, which is interpreted as a time-dependent change of the film morphology (schematically shown in Figure 13a) before a plateau is reached.

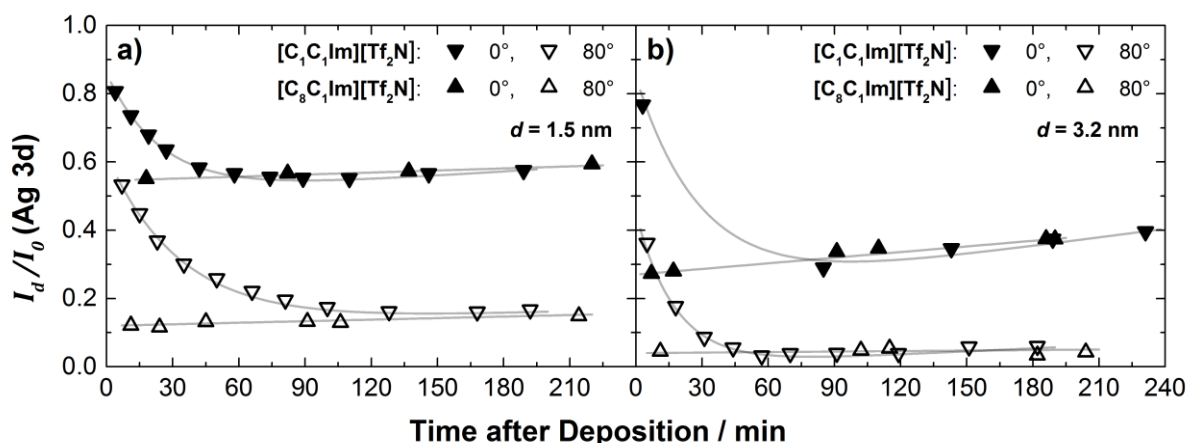


Figure 12: Temporal evolution of the Ag 3d signal intensity in 0° and 80° emission from time-dependent ARXPS of films of $[C_1C_1Im][Tf_2N]$ and $[C_8C_1Im][Tf_2N]$, respectively, after ending the IL deposition of equivalents of a) 1.5 nm and b) 3.2 nm on Ag(111) at RT. Adapted from¹⁰³ under license CC BY-NC 3.0 – Published by the PCCP Owner Societies.

The time-dependent measurements of $[\text{C}_1\text{C}_1\text{Im}][\text{Tf}_2\text{N}]$ in Figure 12 indicate that initially large 3D IL islands (droplets) form on a very fast timescale, that is, much faster than the time needed for an XPS scan (which takes typically several minutes). These droplets then spread over time into a nearly 2D film on a much slower timescale in the order of hours. Complementary time-dependent measurements in the C 1s and N 1s regions after the deposition of $[\text{C}_1\text{C}_1\text{Im}][\text{Tf}_2\text{N}]$ ¹⁰³ (not shown here) show an increase in the intensity of the IL-related peaks, which goes along with the decrease of the Ag 3d intensity as the IL droplets spread, further supporting the proposed morphology changes.¹⁰³

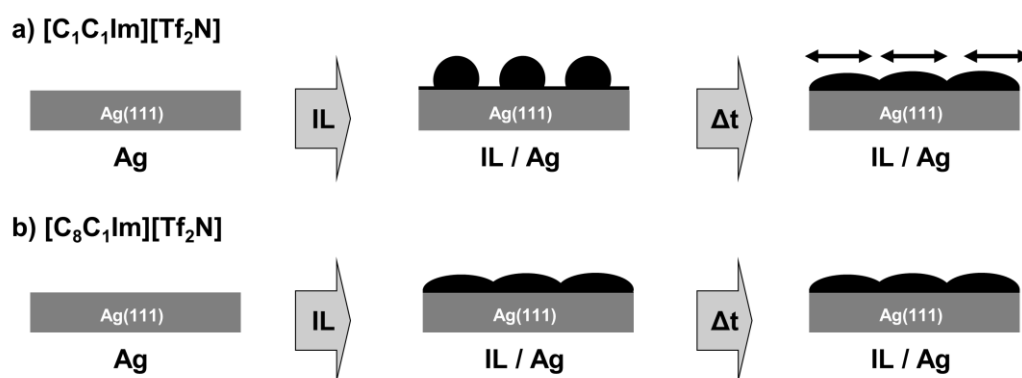


Figure 13: Scheme of the time-dependent behavior after the deposition of multilayers of a) $[\text{C}_1\text{C}_1\text{Im}][\text{Tf}_2\text{N}]$ and b) $[\text{C}_8\text{C}_1\text{Im}][\text{Tf}_2\text{N}]$ on Ag(111) at RT. Adapted in part from ¹⁰³ under license CC BY-NC 3.0 – Published by the PCCP Owner Societies.

Figure 12 also shows the temporal evolution of the Ag 3d signal after the deposition of $[\text{C}_8\text{C}_1\text{Im}][\text{Tf}_2\text{N}]$ films of similar thickness on Ag(111), that is, an IL structurally similar to $[\text{C}_1\text{C}_1\text{Im}][\text{Tf}_2\text{N}]$, but with an octyl chain instead of one of the methyl groups, see Table 1. As depicted schematically in Figure 13b, no changes in the morphology of the $[\text{C}_8\text{C}_1\text{Im}][\text{Tf}_2\text{N}]$ films are derived from the fairly constant course of the support intensity over time in Figure 12. Similar values for the intensity ratio I_d/I_0 in 0° and 80° emission near the end of the experiments indicate that the final structure of the $[\text{C}_1\text{C}_1\text{Im}][\text{Tf}_2\text{N}]$ films is very similar to the one formed for $[\text{C}_8\text{C}_1\text{Im}][\text{Tf}_2\text{N}]$ from the very beginning.^{94, 103}

The initial formation of comparably high 3D $[\text{C}_1\text{C}_1\text{Im}][\text{Tf}_2\text{N}]$ islands on top of the closed wetting layer and the subsequent time-dependent transformation to nearly flat films indicate the existence of two very different timescales. The formation of stable 2D islands on the WL from individual ion pairs obviously does not occur on the same time scale as 3D growth. Otherwise, the nearly flat film morphology as final state should evolve from the very beginning.¹⁰³ A general observation is that individual IL ion pairs are very mobile on metal

surfaces at RT.^{96-97, 102-103, 145-146, 198} We assume that statistically formed small 2D islands very quickly disintegrate due to the lack of stabilization by neighboring ions, leading to a low density of stable 2D islands, which would promote further 2D growth. At the same time, existing larger islands appear more stable and quickly grow into large 3D droplets. Within these droplets, the ions could benefit from a higher average coordination with counter ions compared to a 2D layer. After ending the deposition, the slow transformation (on the timescale of hours) towards a flat morphology is observed experimentally, as ripening and coalescence seem to occur. This behavior indicates that extended regions of rather flat layer-by-layer arrangements are thermodynamically more stable than pronounced 3D islands. The initial formation of the 3D islands is thus understood as a kinetic stabilization. Possible reasons for the slow timescale of the transformation towards a less 3D morphology could be a high activation barrier for the emission of an ion pair from the 3D island to the uncovered WL or successive flat layers, or the above mentioned low probability for forming stable 2D nuclei.¹⁰³ In contrast to previous assumptions,¹⁰³ more recent measurements indicated also an influence of the X-ray exposure during measurement on the time-dependent behavior of [C₁C₁Im][Tf₂N] on Ag(111). For details see the Appendix.

As time-dependent changes have previously also been found for [C₂C₁Im][Tf₂N] on Au(110),¹⁴⁶ it is proposed as a general conclusion that the observed behavior strongly depends on the molecular structure, which concerns in this case the alkyl substituents at the cationic imidazolium head group.¹⁰³ The different behavior observed for [C₈C₁Im][Tf₂N] is attributed to a stabilization of IL ion pairs on the WL (or successive flat layers) by the octyl chains; it has been reported that the dispersive attraction between the alkyl chains of [C₈C₁Im][Tf₂N] can be as large as 20 % of the Coulomb interaction between the ionic components.^{128, 166} A similar interaction is also expected with the underlying IL layers. This stabilization could on the one hand make the initial formation of 3D islands less favorable and on the other hand lead to a higher probability for the formation of 2D islands from IL ion pairs that are emitted from 3D islands; in addition, the octyl chain might also lead to a lower activation barrier for the detachment of IL ion pairs from 3D islands.¹⁰³ The fact that the same slow IL-spreading behavior is found for Ag(111)¹⁰³ and for the reconstructed Au(110)¹⁴⁶ surface is taken as strong indication that a pronounced influence of metal surface reconstruction on this process can be excluded.¹⁰³

3.3 Growth and Desorption of 2H-TPP on Ag(111) and Au(111) [P4]

In this chapter, we take a closer look on the growth behavior of 2H-TPP on Ag(111) and Au(111). The structure of multilayer porphyrins is of utmost importance for applications in organic electronic devices,²²⁰⁻²²¹ as parameters like charge carrier mobility and device efficiency strongly depend on the molecular arrangement and orientation.²²¹⁻²²⁵ Up to a coverage of a monolayer, the growth and structure of 2H-TPP on Ag(111)^{176, 219, 226-227} and Au(111)²²⁷⁻²²⁹ is well-studied. Information on porphyrin multilayers on metal substrates – in general – is, however, scarce.^{221, 230-235} To investigate the growth of 2H-TPP from sub-monolayer to multilayer coverages, increasing amounts of 2H-TPP were deposited on Ag(111) and Au(111). By monitoring the attenuation of the ARXPS signal intensity of the supporting metals (Ag 3d and Au 4f) as a function of the porphyrin coverage, we observe a very similar behavior on the two surfaces, for deposition at RT (between 295 and 315 K) and at low temperature (between 80 and 85 K). In each case, the experimental data exactly follows the prediction for 2D growth up to two monolayers, that is, an average thickness of ~ 0.68 nm, which indicates the formation of two homogeneous closed layers of flat lying porphyrin molecules as sketched in Figure 14. Up to monolayer coverage, self-assembly of 2H-TPP into extended, ordered 2D networks on Ag(111) and Au(111) has been reported previously at RT and also below 100 K.^{148, 219, 226-229, 236} While isolated 2H-TPP molecules are considered highly mobile on both metal surfaces at 300 K,²²⁷ the formation of ordered 2D networks is driven by a relatively strong molecule-molecule interaction.^{85, 148, 177-178, 219, 227-229, 236-242}



Figure 14: Scheme of the initial stages of 2H-TPP film growth on Ag(111) at temperatures between 80 and 315 K. The growth behavior on Au(111) is identical.⁸⁴

For coverages above two monolayers, the 80° data of the support signal from ARXPS falls systematically above the prediction for 2D growth, which is indicative of 3D island growth.⁸⁴ Pronounced 3D growth on top of two closed molecular layers is denoted as Stranski-Krastanov-like growth.^{171, 209, 243} Similar growth was observed previously for Cu-Pc on Cu(111)²³⁴ and for other large π -conjugated molecules on Ag(111) and Au(111).²⁴⁴⁻²⁴⁷ The formation of relaxed 3D crystallites on top of initial adlayers is likely thermodynamically favored, because it lowers the contact area to the strained initial 2D adlayers below,²⁴⁵ which

benefit from a strong adsorption of the molecules on the metal. Comparing bulk structures of 2H-TPP from crystallography¹⁴²⁻¹⁴³ to the structure of a 2H-TPP monolayer at the Ag(111) and Au(111) interfaces^{229, 236-237, 239} reveals not only different molecular conformations, but generally very different supermolecular arrangements^{84, 221} which in turn determine the intermolecular interactions.^{84, 142-143, 229, 236-237, 239}

The thermal stability of 2H-TPP multilayers on the two metal surfaces was monitored through the thermal evolution of the porphyrin-related C 1s signal and the respective core level (Ag 3d or Au 4f) of the supporting metal at 0° emission during heating of 2H-TPP multilayer films from RT to 540 K. On both surfaces, multilayer desorption of 2H-TPP occurs at 450 K.⁸⁴ From a Leading-Edge type analysis^{169, 248} of the data, we obtain an activation energy E_A for multilayer desorption of 193 kJ/mol (± 22 kJ/mol).⁸⁴ In agreement with a previous temperature-programmed desorption (TPD) study of 2H-TPP on Ag(111),¹⁷⁷ no further changes in the C 1s signal intensity are observed upon heating to 540 K after the desorption of the multilayers.⁸⁴

Contrasting earlier assumptions,^{82, 177-178, 221} it was reported later on that partial dehydrogenation of porphyrin monolayers on Ag(111) can occur upon heating to temperatures above 525 K.^{82, 177-178} In the case of 2H-TPP on Ag(111), heating to 550 K causes a shift of the porphyrin-related N 1s and C 1s signals to lower binding energy and a change in the C 1s peak shape, as result of a change in the orientation of the phenyl groups of 2H-TPP relative to the metal surface upon dehydrogenation at the molecule's periphery.¹⁷⁸ The spectra of monolayer 2H-TPP films prepared in the present work showed no difference after heating to 500 K compared to films of similar thickness prepared by direct deposition. The residual C 1s intensity and the remaining attenuation of the support signals (Ag 3d or Au 4f, respectively) after multilayer desorption further indicate that the remaining closed layer of 2H-TPP remains intact.⁸⁴

3.4 Desorption of ILs from Metal Surfaces [P2, P3, P4]

While many ILs exhibit high thermal stability and despite their commonly very low vapor pressures at RT, desorption can play a pivotal role for thin film applications at high temperature. Due to the finite thickness of the IL film, maximum reaction temperatures of SCILL systems, for example, are thus understandably limited *i.a.* by the stability of the IL film.¹¹ Within this work, the desorption of ILs from Ag(111) and Au(111) was studied by means of TP-XPS.^{84, 104-105} The results of these experiments are summarized in Table 3, supported by further information from literature. The plot of signal intensities from TP-XPS

in Figure 15 shows on the example of $[C_1C_1Im][Tf_2N]$, $[C_8C_1Im][Tf_2N]$ ¹⁰⁴ and $[C_8C_1Im][PF_6]$ on $Ag(111)$ ¹⁰⁴⁻¹⁰⁵ how IL films desorb in two steps. The multilayers desorb first, followed by the desorption of the WL, which indicates that the ions in contact with the metal surface are bound more strongly than in the multilayer.

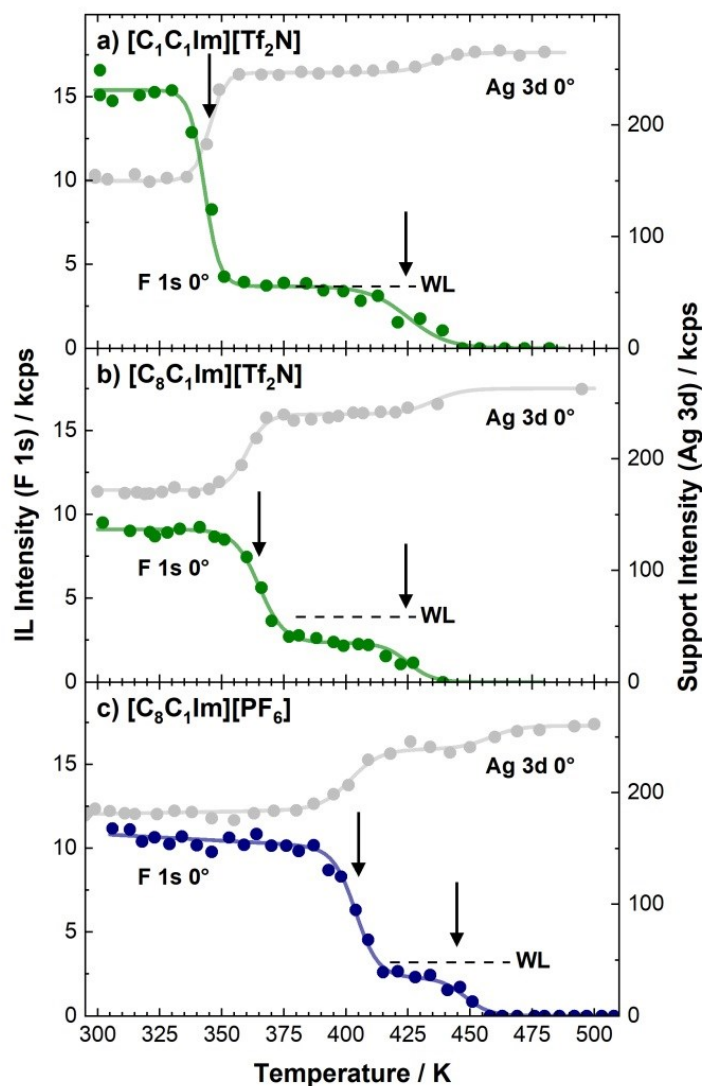


Figure 15: Thermal evolution of F 1s (F_{Tf_2N} (green), F_{PF_6} (blue)) and Ag 3d signal intensities at 0° emission from TP-XPS upon heating films of a) $[C_1C_1Im][Tf_2N]$, b) $[C_8C_1Im][Tf_2N]$,¹⁰⁴ and c) $[C_8C_1Im][PF_6]$ ¹⁰⁴⁻¹⁰⁵ on $Ag(111)$. Heating rate: 2 K/min. The vertical arrows indicate the rate maxima of multilayer and WL desorption, respectively. The horizontal dashed lines indicate the intensity of the WL as obtained upon adsorption at RT (for details see text).

Comparing the desorption temperatures of the ILs $[C_8C_1Im][Tf_2N]$ ¹⁰⁴ and $[C_8C_1Im][PF_6]$ ^{84, 104-105} on $Ag(111)$ in Figure 15b and 15c, we note differences in the thermal stability based on the differences in the molecular composition of the IL, more specifically, the nature of the anion, such that both, multilayers as well as the WL of $[C_8C_1Im][PF_6]$ on $Ag(111)$, desorb at higher temperatures than for $[C_8C_1Im][Tf_2N]$ on $Ag(111)$.¹⁰⁴ The higher

temperature for multilayer desorption, where the interaction with the underlying metal plays a negligible role, agrees well with literature values for enthalpy of vaporization ΔH_{vap} and vapor pressure p_{sat} , see Table 3, as $[C_8C_1Im][PF_6]$ has a higher ΔH_{vap} ¹⁶⁶ and accordingly also a lower p_{sat} ²⁴⁹ than $[C_8C_1Im][Tf_2N]$. For the WL on Ag(111), the lower desorption temperature of $[C_8C_1Im][Tf_2N]$ compared to $[C_8C_1Im][PF_6]$ indicates a stronger adsorption of the latter on the metal surface which likely results from the smaller size of the anion and thus a more localized charge which might induce a stronger image dipole within the metal.

Multilayers and the WL of $[C_8C_1Im][PF_6]$, respectively, desorb at similar temperatures on Ag(111) as on Au(111). The similar desorption temperatures of the WL indicate similar adsorption energies of this IL on both metals.⁸⁴

It was established previously that ΔH_{vap} of homologues of imidazolium-based $[C_nC_1Im]X$ ILs (with X: $[Tf_2N]$, $[TfO]$, $[BF_4]$) increases linearly with the number of C atoms in the alkyl chain (for $n = 2$ to 10).²⁴⁹⁻²⁵¹ While for short lengths of the alkyl chain (below four C atoms), the vapor pressure does not appear to follow this trend exactly,^{249, 251-252} and although no literature data is available for $n = 1$, it seems therefore reasonable that multilayers of $[C_1C_1Im][Tf_2N]$ desorb at a lower temperature of 345 K than multilayers of $[C_8C_1Im][Tf_2N]$, which desorb at 365 K, as shown in Figure 15. Similar desorption temperatures of the respective WL of the two ILs on Ag(111) indicate that the length of the side chain at the cationic imidazolium headgroup has a relatively small influence on the adsorption energy of the IL.

Notably, the residual F 1s intensity of the $[C_8C_1Im][Tf_2N]$ WL on Ag(111) after multilayer desorption at 405 K in Figure 15 is about 30% lower than for a WL obtained from direct deposition at RT (as indicated by the horizontal dashed line). This indicates a lower coverage. A similar behavior is also observed for $[C_8C_1Im][PF_6]$ on Ag(111) and Au(111). For $[C_1C_1Im][Tf_2N]$ on Ag(111), in contrast, the residual F 1s intensity of the WL after multilayer desorption matches exactly that of a WL from direct deposition. As described in Chapter 3.1, the alkyl chains gradually detach and point away from the surface upon approaching WL coverage during the initial stages of film growth. It seems possible that the alkyl chains in the (high temperature) WL assume a flat lying geometry on the Ag(111) surface after multilayer desorption. A lower coverage could then be the consequence of the larger spatial requirement of the $[C_8C_1Im]^+$ cation in this adsorption geometry. This would also explain why $[C_1C_1Im][Tf_2N]$ shows identical F 1s intensities in the WL after multilayer desorption and after direct WL deposition, because it lacks such an alkyl chain substituent.

Table 3: Desorption temperatures T_{des} of selected ILs on metal surfaces in comparison to values for activation energy of multilayer desorption E_a , enthalpy of vaporization ΔH_{vap} at 298 K and vapor pressure p_{sat} at 423 K (errors in the least significant figure in round brackets). β : Heating rate of the desorption experiment. The entries shaded in gray were subject of the experimental part of this thesis.

Ionic Liquid	Surface	T_{des} / K (WL)	T_{des} / K (Multilayer)	β / K/min	E_a / kJ/mol (Multilayer)	ΔH_{vap} / kJ/mol	p_{sat} / μ Pa	Remarks	Ref.
[C ₁ C ₁ Im][Tf ₂ N]	Ag(111)	425	345	2	118 ^b	-	-	TP-XPS.	a
	Ni(111)	< 400	< 400	-				IL desorbs entirely upon heating to 400 K.	110
[C ₂ C ₁ Im][Tf ₂ N]	Au(111)	380-500	380	30	118(2) ¹⁶⁶	134(2) ¹⁶⁶	1280 ²⁴⁹	TPD; broad range for WL desorption.	169
	Au(110)	> 520	~370	10	126 ¹⁶⁹	137(5) ¹⁶⁹		TP-UPS; IL covered Au(110) surface undergoes reconstruction from 1x1 to 1x3 upon heating > 490 K.	146
[C ₈ C ₁ Im][Tf ₂ N]	Ag(111)	425	365	2				TP-XPS; WL desorption shifts to < 370 K after replacement by [C ₈ C ₁ Im][PF ₆] at Ag(111) surface.	104
	Au(111)	> 400	< 400	-	126 ^b 131(2) ¹⁶⁶	149(2) ¹⁶⁶	380 ²⁴⁹	Multilayers desorb upon heating to 400 K for 10 min while the WL remains.	102
	Cu(100)	> 400	< 400	-				Multilayers desorb upon heating to 400 K for 10 min while the WL remains. XPS indicates stronger interaction of IL WL with Cu(100) than Au(111).	102
[C ₈ C ₁ Im][PF ₆]	Ag(111)	445	405	2	139 ^b 143(4) ¹⁶⁶ 167(18) ⁸⁴	169(4) ¹⁶⁶	8 ²⁴⁹	TP-XPS; WL desorption shifts to < 420 K on 2H-TPP-covered Ag(111).	84, 104-105
	Au(111)	445	405	2				TP-XPS; WL desorption shifts to < 420 K on 2H-TPP-covered Au(111).	84
[C ₈ C ₁ Im][BF ₄]	Au(111)	> 400	> 400	30				TPD; same temperature for multilayer and WL desorption.	253-254
	Cu(111)	> 460	420	-	137(3) ¹⁶⁶	157 ¹³⁷ 162(3) ¹⁶⁶	12 ²⁴⁹	TP-XPS; decomposition of WL before desorption is suggested.	138
[PFBMIm][PF ₆]	Ag(111)	-	390	2	148 ^b	-	-	TP-XPS; cation decomposes in WL > 420 K. WL desorption shifts to < 420 K after replacement by [C ₈ C ₁ Im][PF ₆] at Ag(111) surface.	105
[C ₄ C ₁ Pyrr][Tf ₂ N]	Cu(111)	-	-	-	132(2) ¹²³	152(3) ¹²³ 195(19) ²⁵⁵	-	Anions in contact with Cu surface decompose below 300 K.	97

a: See Fig. 15a; b: Redhead analysis²⁵⁶ with frequency factor $\nu_1 = 10^{16}$ 1/s from literature;¹⁶⁹ TPD: Temperature-programmed desorption; TP-XPS: Temperature-programmed XPS; TP-UPS: Temperature-programmed ultra-violet photoelectron spectroscopy.

The thermal evolution of $[\text{C}_2\text{C}_1\text{Im}][\text{Tf}_2\text{N}]$ on Au(111) was studied via TPD by Hessey and Jones.¹⁶⁹ Compared to the value of 365 K for $[\text{C}_8\text{C}_1\text{Im}][\text{Tf}_2\text{N}]$ on Ag(111) from TP-XPS,¹⁰⁴ they found for $[\text{C}_2\text{C}_1\text{Im}][\text{Tf}_2\text{N}]$ a slightly higher temperature of multilayer desorption of 380 K and a rather broad WL desorption range. Both are likely related to the much higher heating rate of the TPD experiment of 30 K/min¹⁶⁹ compared to the TP-XPS with 2 K/min.^{104, 257-258} The broad range for the WL desorption could also be a sign of decomposition of the IL film on the Au surface.

The temperature of multilayer desorption of $[\text{PFBMIm}][\text{PF}_6]$ of 390 K is close to that of $[\text{C}_8\text{C}_1\text{Im}][\text{PF}_6]$,¹⁰⁵ which indicates that in this specific case the seemingly significant structural variation at the cation of these two ILs – which has a profound effect on the surface composition and enrichment behavior^{105, 259-261} – appears to have only little effect on the multilayer desorption. In contrast to $[\text{C}_8\text{C}_1\text{Im}][\text{PF}_6]$ on Ag(111),⁸⁴ TP-XPS upon heating thin films of $[\text{PFBMIm}][\text{PF}_6]$ on Ag(111) above 420 K reveals signs of decomposition of this IL.¹⁰⁵ Thermal decomposition at temperatures below 500 K was also reported for bulk evaporation experiments on the related IL $[\text{C}_4\text{C}_1\text{Im}][\text{PF}_6]$,²⁶² which indicates that the decomposition of $[\text{PFBMIm}][\text{PF}_6]$ on Ag(111) might also occur in the multilayer independently of any influence by the metallic support. In any case, the findings imply that the adsorption energy of $[\text{PFBMIm}][\text{PF}_6]$ on Ag(111) cannot be deduced simply from TP-XPS because of the decomposition of the IL.¹⁰⁵

Although the multilayer desorption of $[\text{C}_8\text{C}_1\text{Im}][\text{PF}_6]$ partly overlaps with the desorption of $[\text{PFBMIm}][\text{PF}_6]$, the latter can be desorbed intact within the multilayer desorption range from mixed thin films with $[\text{C}_8\text{C}_1\text{Im}][\text{PF}_6]$ on Ag(111), leaving a WL of $[\text{C}_8\text{C}_1\text{Im}][\text{PF}_6]$ behind, as sketched in Figure 16a.¹⁰⁵ In a similar fashion, it is possible to desorb $[\text{C}_8\text{C}_1\text{Im}][\text{Tf}_2\text{N}]$ selectively and entirely from mixed films with $[\text{C}_8\text{C}_1\text{Im}][\text{PF}_6]$ in the temperature range of multilayer desorption, see Figure 16b.¹⁰⁴ In both cases, these multilayer desorption characteristics are enabled by the selective replacement of the respective IL by $[\text{C}_8\text{C}_1\text{Im}][\text{PF}_6]$ at the IL/Ag(111) interface and the surface enrichment of $[\text{PFBMIm}]^+$ cations and $[\text{Tf}_2\text{N}]^-$ anions in the respective mixtures (see Chapter 3.5).¹⁰⁴⁻¹⁰⁵ In effect, it demonstrates that layers of $[\text{PFBMIm}][\text{PF}_6]$ and $[\text{C}_8\text{C}_1\text{Im}][\text{Tf}_2\text{N}]$, respectively, can be destabilized by postdeposition of $[\text{C}_8\text{C}_1\text{Im}][\text{PF}_6]$ which opens new routes for selectively removing specific ions or undesired components at IL/support interfaces.¹⁰⁴⁻¹⁰⁵ In principle, this procedure of sequential deposition and selective desorption should further allow for an

on-surface metathesis of ILs with varying ion combinations that are not directly accessible by PVD (as for example alkyl imidazolium halides¹⁶⁴⁻¹⁶⁵).

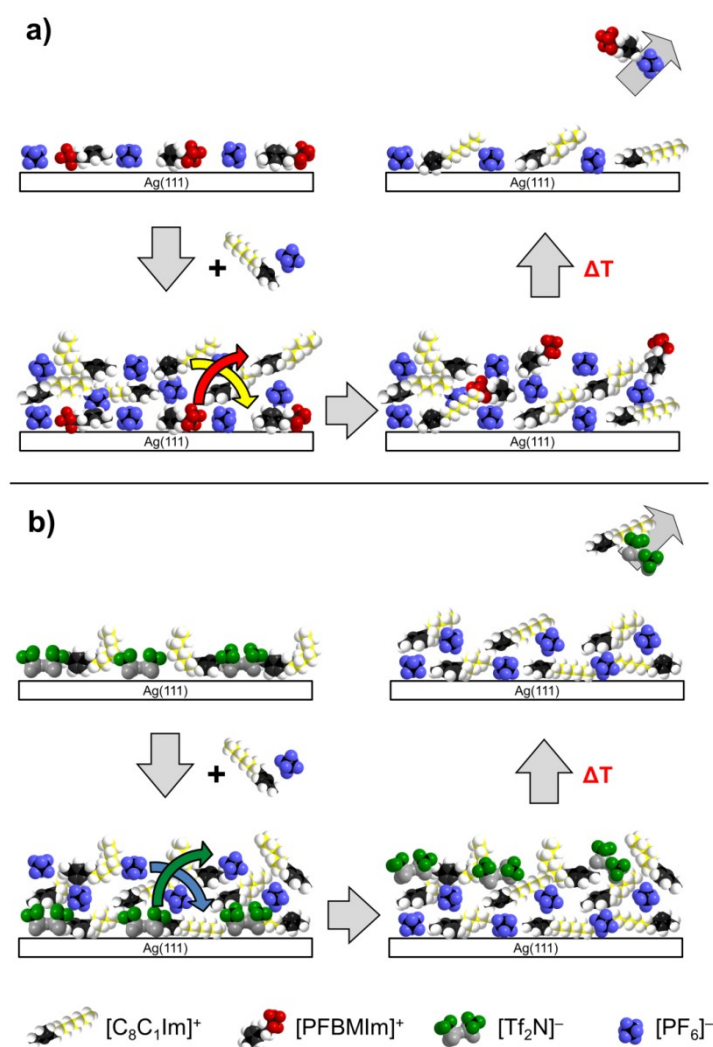


Figure 16: Scheme of selective replacement at the IL/metal interface and subsequent desorption of a) $[\text{PF}_6\text{Im}][\text{PF}_6]$ and b) $[\text{C}_8\text{C}_1\text{Im}][\text{Tf}_2\text{N}]$ after postdeposition of $[\text{C}_8\text{C}_1\text{Im}][\text{PF}_6]$. Adapted in part from¹⁰⁴⁻¹⁰⁵ under license CC BY 4.0.

As mentioned above, $[\text{C}_8\text{C}_1\text{Im}][\text{PF}_6]$ desorbs from $\text{Ag}(111)$ and $\text{Au}(111)$ in two steps with multilayer desorption at 405 K and WL desorption at 445 K.^{84, 104-105} If the metal surface is, however, covered by one closed layer of the porphyrin 2H-TPP (see Table 1), the entire IL film desorbs at 405 K, uncovering the porphyrin monolayer below.⁸⁴ The 2H-TPP layer acts as a spacer between $[\text{C}_8\text{C}_1\text{Im}][\text{PF}_6]$ and the metals and effectively inhibits the specific interaction of the ions with the metal, leading to a pseudo-multilayer behavior of the $[\text{C}_8\text{C}_1\text{Im}][\text{PF}_6]$ WL on 2H-TPP.⁸⁴

Hessey and Jones¹⁶⁹ studied the desorption of acetone from a layer of $[\text{C}_2\text{C}_1\text{Im}][\text{Tf}_2\text{N}]$ on $\text{Au}(111)$ compared to the desorption of acetone directly from $\text{Au}(111)$. They observed

effectively no change in the desorption temperature (125 K) of acetone on Au(111) compared to the acetone/IL/Au(111) system. In this example, however, the acetone seems to show no strong adsorption to the Au(111) surface in the first place, as multilayers and monolayer desorb basically at the same temperature.¹⁶⁹

3.5 Ion Exchange at the IL/Solid Interface [P2, P3]

In light of complex IL systems, composed of more than one type of ion pairs, and the effect of the immediate presence of a metal surface on the film structure, this chapter deals with phenomena that occur when ultrathin layers of two different ILs are successively deposited on the Ag(111) surface. The results from temperature-dependent ARXPS demonstrate that already well below RT ion exchange processes can occur at the IL/metal interface.¹⁰⁴⁻¹⁰⁵

3.5.1 Anion Exchange

For the two ILs $[C_8C_1Im][Tf_2N]$ and $[C_8C_1Im][PF_6]$ with the same cation but two different anions, the different chemical environments of the F_{Tf_2N} and F_{PF_6} fluorine atoms result in distinct chemical shifts of the respective F 1s binding energies in XPS. This allows for a direct comparison of the relative occurrence of the respective anion in the bulk (0° emission) and at the surface (80°) of the IL films in the spectra in Figure 17. Changes in signal intensity by varying the surface sensitivity in ARXPS directly reflect surface enrichment or depletion of one of the anions.¹⁰⁴⁻¹⁰⁵

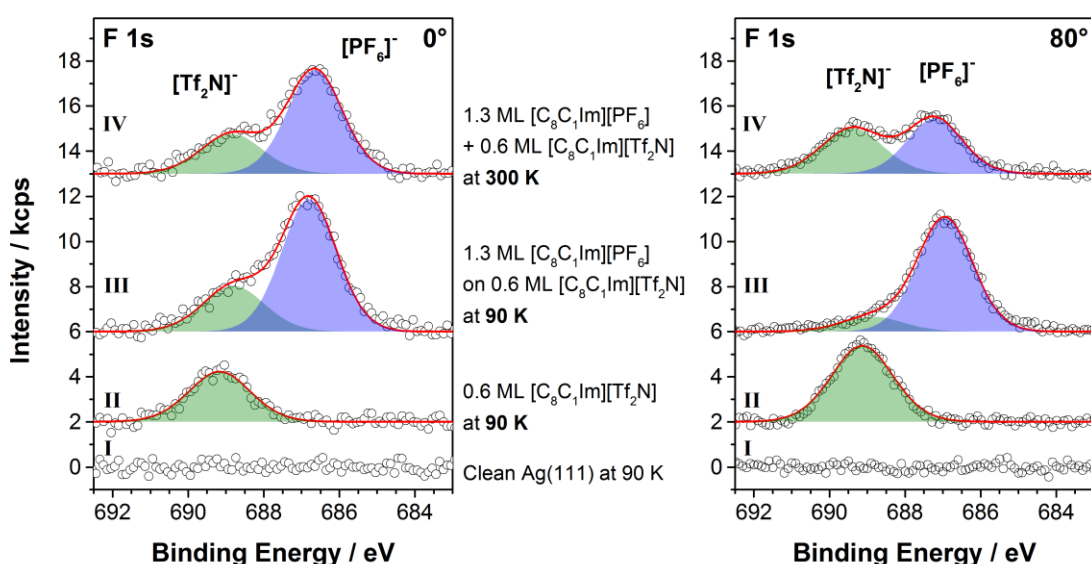


Figure 17: F 1s spectra in 0° and 80° emission for the clean Ag(111) crystal (I), after deposition of a WL of $[C_8C_1Im][Tf_2N]$ at 90 K (II), after deposition of 1.3 ML of $[C_8C_1Im][PF_6]$ on top of the $[C_8C_1Im][Tf_2N]$ WL at 90 K (III) and after heating the resulting composite IL film to 300 K (IV). Reprinted from ¹⁰⁴ under license CC BY 4.0.

First, the equivalent of a WL of $[\text{C}_8\text{C}_1\text{Im}][\text{Tf}_2\text{N}]$ was deposited on $\text{Ag}(111)$ at a temperature of 90 K (see sketch in Figure 18) resulting in one signal in the F 1s spectra in Figure 17-II. At this low temperature, STM¹⁴⁵ and ARXPS¹⁰⁴ indicate the formation of flat uniform films with crystalline and amorphous condensed phases, all with an overall checkerboard arrangement of alternating anions and cations.

In a second step, 1.3 ML of $[\text{C}_8\text{C}_1\text{Im}][\text{PF}_6]$ were deposited on top of the WL of $[\text{C}_8\text{C}_1\text{Im}][\text{Tf}_2\text{N}]$ at 90 K, resulting in a strong attenuation of the $\text{F}_{\text{Tf}_2\text{N}}$ signal at 80° in Figure 17-III, as $[\text{C}_8\text{C}_1\text{Im}][\text{PF}_6]$ homogeneously covers the underlying $[\text{C}_8\text{C}_1\text{Im}][\text{Tf}_2\text{N}]$ layer. As sketched in Figure 18-III, no exchange of anions occurs at this point.¹⁰⁴

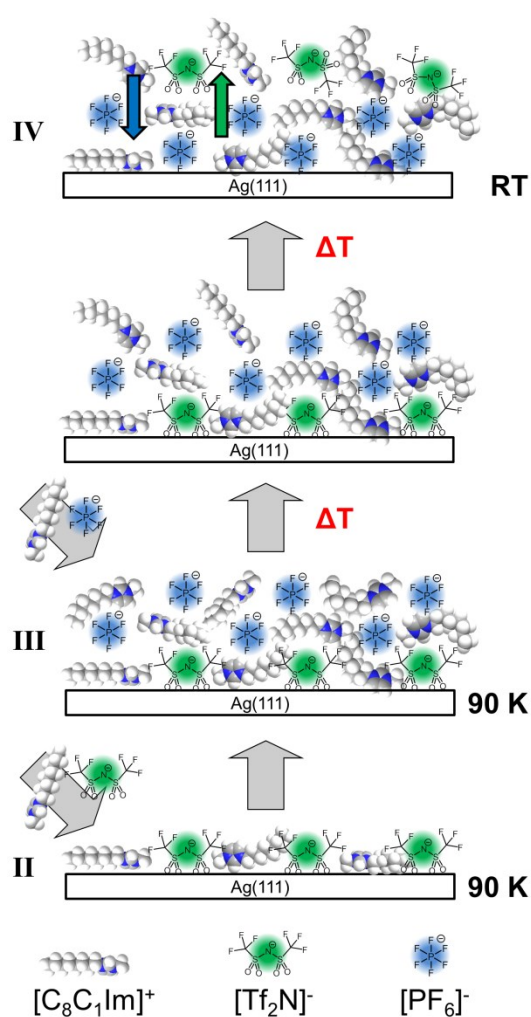


Figure 18: Scheme for the heating experiment after the deposition of $[\text{C}_8\text{C}_1\text{Im}][\text{PF}_6]$ on top of a WL of $[\text{C}_8\text{C}_1\text{Im}][\text{Tf}_2\text{N}]$ on $\text{Ag}(111)$ at 90 K. The Roman numerals refer to the spectra in Figure 17. Adapted from¹⁰⁴ under license CC BY 4.0.

This IL bilayer was then heated to RT. The RT spectra in Figure 17-IV clearly show that $[\text{Tf}_2\text{N}]^-$ anions resurface. The quantitative analysis of F 1s spectra from TP-XPS in the surface sensitive emission angle of 80° is shown in Figure 19. Initially, there are no notable

changes in the $[\text{PF}_6]^-$ and $[\text{Tf}_2\text{N}]^-$ peak intensities. Above 140 K, the $[\text{PF}_6]^-$ signal (blue) begins to decrease, while the $[\text{Tf}_2\text{N}]^-$ signal (green) remains constant up to 170 K. This behavior is attributed to a reorganization within the uppermost layer, such that the octyl chains enrich at the IL/vacuum interface and attenuate the $[\text{PF}_6]^-$ signal at 80° as sketched in Figure 18 (see also Chapter 3.5.2).¹⁰⁴ Unaffected by this reorientation at the outer surface, the $[\text{Tf}_2\text{N}]^-$ anions remain at the IL/Ag(111) interface. Between 170 and 220 K, the exchange of the anions at the IL/Ag(111) interface occurs, as the $[\text{Tf}_2\text{N}]^-$ signal increases while the $[\text{PF}_6]^-$ signal continues to decrease.¹⁰⁴ The glass transition temperatures of bulk $[\text{C}_8\text{C}_1\text{Im}][\text{Tf}_2\text{N}]$ and $[\text{C}_8\text{C}_1\text{Im}][\text{PF}_6]$ (around 185 K^{109, 117, 125, 127} and 190 K,^{2, 124, 130} respectively) correspond well to this temperature range for the anion exchange.¹⁰⁴

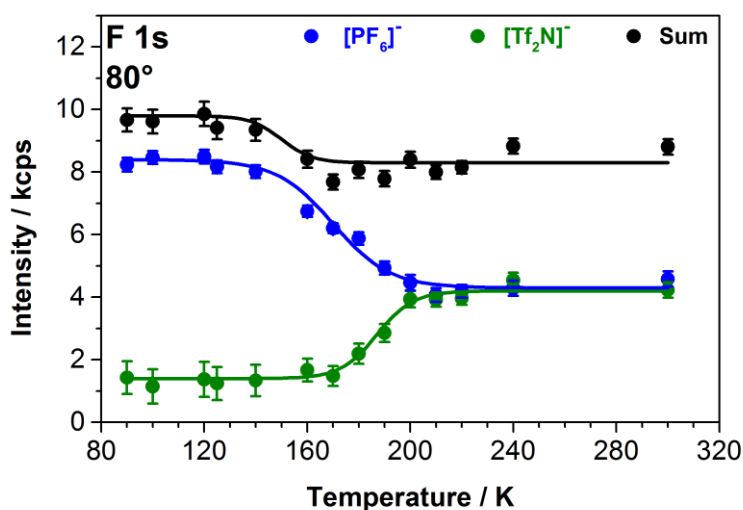


Figure 19: Intensities of the respective F 1s signals of the $[\text{PF}_6]^-$ and $[\text{Tf}_2\text{N}]^-$ anions from TP-XPS in 80° emission as a function of the sample temperature upon heating from 90 K to RT. Reprinted with permission from¹⁰⁴ under license CC BY 4.0.

Two driving forces are proposed to be cooperatively responsible for the replacement of $[\text{C}_8\text{C}_1\text{Im}][\text{Tf}_2\text{N}]$ by $[\text{C}_8\text{C}_1\text{Im}][\text{PF}_6]$ at the IL/Ag(111) interface and the enrichment of $[\text{Tf}_2\text{N}]^-$ at the IL/vacuum interface. As deduced from the desorption temperatures of the neat ILs on Ag(111) (see Chapter 3.4), the adsorption energy of $[\text{C}_8\text{C}_1\text{Im}][\text{PF}_6]$ is considerably larger than that of $[\text{C}_8\text{C}_1\text{Im}][\text{Tf}_2\text{N}]$. Further, the preferential enrichment of $[\text{Tf}_2\text{N}]^-$ at the IL/vacuum interface is favored because of the lower surface tension of $[\text{C}_8\text{C}_1\text{Im}][\text{Tf}_2\text{N}]$ compared to $[\text{C}_8\text{C}_1\text{Im}][\text{PF}_6]$ (see Table 1).^{8, 104}

3.5.2 Cation Exchange

Complementary to the anion exchange discussed above, the exchange of two cations at the IL/Ag(111) interface was studied on the example of $[\text{PFBMIm}][\text{PF}_6]$ and $[\text{C}_8\text{C}_1\text{Im}][\text{PF}_6]$.

Again taking advantage of the different chemical environments of the five F_{CFx} atoms in the side chain of the $[PFBMIm]^+$ cation and six F_{PF6} atoms in the $[PF_6]^-$ anion, the resulting distinct F 1s binding energies (F_{CFx} at 689.1 eV, F_{PF6} at 686.9 eV) allow for a direct comparison of the relative occurrence in the bulk (0° emission) and at the vacuum interface (80°) of the ultrathin films.¹⁰⁵

For the detailed investigation of the dynamics of the cation exchange process, first a WL of $[PFBMIm][PF_6]$, and in a second step 1.0 ML of $[C_8C_1Im][PF_6]$ were deposited at 82 K on Ag(111). ARXPS shows that $[C_8C_1Im][PF_6]$ covers the WL of $[PFBMIm][PF_6]$ and no ion exchange occurs at the IL/Ag(111) interface due to the lack of mobility at this low temperature.¹⁰⁵ Upon heating this layered film at a rate of 2 K/min from 82 K to RT, the thermal evolution of the F 1s and C 1s signals related to cations and anions was measured in 80° emission *in situ*. The result of the quantitative analysis of the individual C 1s (C_{alkyl} and C_{hetero}) and F 1s (F_{CFx} and F_{PF6}) signals is shown in Figure 20.

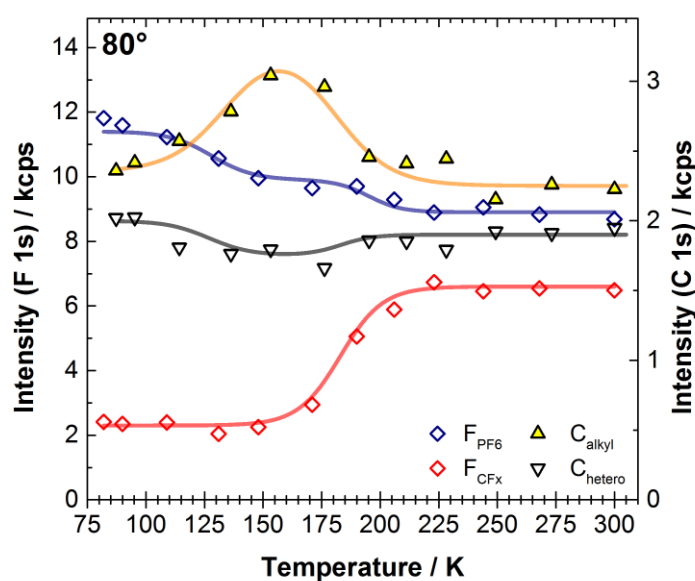


Figure 20: Thermal evolution of the respective F 1s and C 1s signals in 80° upon heating of the layered IL film to RT after the deposition of 1.0 ML of $[C_8C_1Im][PF_6]$ on top of a WL of $[PFBMIm][PF_6]$ on Ag(111) at 82 K. Heating rate 2 K/min. Reprinted with permission from¹⁰⁵ under license CC BY 4.0.

Upon heating, a decrease of the F_{PF6} signal (blue) is observed initially, while simultaneously, the C_{alkyl} signal (yellow) increases until 150 K. These changes are attributed to the enrichment of the alkyl chains at the IL/vacuum interface, which – as already mentioned in Chapter 3.5.1 – leads to the attenuation of the $[PF_6]^-$ ions below. The alkyl enrichment by reorientation is limited to the IL/vacuum interface and there is no change of the

F_{CFx} peak intensity (red) of the $[\text{PFBMIm}]^+$ cations at the IL/Ag(111) interface. Between 160 and 220 K, the cations at the IL/Ag(111) interface exchange, followed by the enrichment of the pentafluorobutyl side chains of $[\text{PFBMIm}][\text{PF}_6]$ at the vacuum interface at the expense of $[\text{C}_8\text{C}_1\text{Im}]^+$ cations, as the F_{CFx} signal increases and the C_{alkyl} signal decreases.¹⁰⁵

The temperature range of the cation exchange corresponds well to the glass transition temperature of 190 K for bulk $[\text{C}_8\text{C}_1\text{Im}][\text{PF}_6]$,^{2, 124} which is in line with previous observations that the bulk glass transition is in good agreement with temperature-programmed phase changes in thin IL films on Ag(111).^{104, 145} While bulk $[\text{PFBMIm}][\text{PF}_6]$ has a melting temperature of 339 K, the $[\text{PFBMIm}]^+$ cations within the mixed thin film become mobile already at a much lower temperature.¹⁰⁵ This indicates that the mobility of the IL on top essentially determines the temperature at which the exchange at the IL/metal interface can occur.

In line with the study of the anion exchange,¹⁰⁴ two main driving forces are suggested to be cooperatively responsible for the cation exchange at the IL/metal interface: A lower surface tension of $[\text{PFBMIm}][\text{PF}_6]$ due to its fluorinated chain,²⁶³⁻²⁶⁵ favoring its enrichment at the IL/vacuum interface, and a larger adsorption energy of $[\text{C}_8\text{C}_1\text{Im}][\text{PF}_6]$ on Ag(111) compared to $[\text{PFBMIm}][\text{PF}_6]$ (see also Chapter 3.4).¹⁰⁵

3.6 Replacement of IL by Porphyrins at Metal Interfaces [P4]

In analogy to the above mentioned examples of molecular exchange and preferential adsorption after sequential deposition of two different ILs on Ag(111),¹⁰⁴⁻¹⁰⁵ studies of organic bilayers on metals involving porphyrins and related aromatic molecules also reported exchange processes.^{224-225, 228, 266-271} These works highlight the importance of the strength of the organic-metal interaction and how it relates to the stability and arrangement in stacked multilayer architectures.^{224-225, 235, 266, 270, 272-276} Synergies between the molecular classes of porphyrins and ILs were realized for catalysis⁸⁶ and dye-sensitized solar cell⁴⁷⁻⁴⁸ technologies. So far, the potential of these pioneering works has only been touched at the surface. In such applications, the function, performance and stability of the organic thin films are strongly determined by the properties of the interface to the support.^{11, 48, 64, 67-71, 86} This chapter covers temperature-dependent changes in the bilayer film structure of the IL $[\text{C}_8\text{C}_1\text{Im}][\text{PF}_6]$ and 5,10,15,20-tetraphenylporphyrin (2H-TPP, see Table 1) at Ag(111) and Au(111) surfaces, depicted in Figure 21.⁸⁴

After deposition of 2H-TPP on top of a frozen film of $[\text{C}_8\text{C}_1\text{Im}][\text{PF}_6]$ at 84 K, the 2H-TPP layer covers the IL film below. Heating this bilayer film subsequently to RT, a

reorganization of the film arrangement at about 240 K was determined by TP-XPS.⁸⁴ All intensities in Figure 22 remain mostly constant until the F_{PF_6} signal increases in one step by almost 70%. The C_{alkyl} signal of the $[\text{C}_8\text{C}_1\text{Im}]^+$ cation increases simultaneously by more than 100%, while the porphyrin-related C 1s contribution decreases to 40%. This behavior indicates the exchange of the IL molecules by the 2H-TPP molecules at the Ag(111) interface and the concomitant enrichment of $[\text{C}_8\text{C}_1\text{Im}][\text{PF}_6]$ at the IL/vacuum interface. Bilayers of $[\text{C}_8\text{C}_1\text{Im}][\text{PF}_6]$ and 2H-TPP on Au(111) show effectively the same behavior.⁸⁴

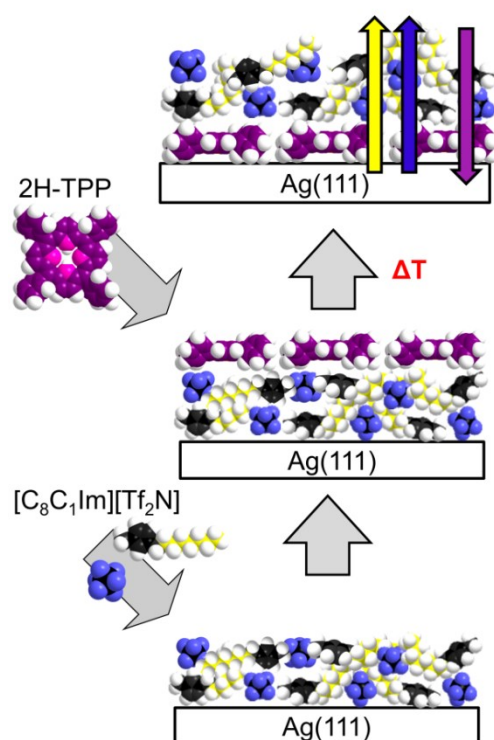


Figure 21: Scheme of the film structure in the heating experiment after the deposition of a monolayer of 2H-TPP onto 1 ML of $[\text{C}_8\text{C}_1\text{Im}][\text{PF}_6]$ on Ag(111) at 84 K. Adapted with permission from⁸⁴ under license CC BY 4.0.

In the temperature-programmed exchange studies in bilayered IL films with $[\text{C}_8\text{C}_1\text{Im}][\text{PF}_6]$ initially at the vacuum interface,¹⁰⁴⁻¹⁰⁵ the onsets of diffusion were slightly below the glass transition of about 190 K reported for bulk $[\text{C}_8\text{C}_1\text{Im}][\text{PF}_6]$.^{2, 124} The exchange of $[\text{C}_8\text{C}_1\text{Im}][\text{PF}_6]$ by 2H-TPP at the Ag(111) surface occurs at a temperature that is about 50 K higher, which indicates that this exchange process is determined rather by the properties of the porphyrin layer at the vacuum interface than the IL layer below as $[\text{C}_8\text{C}_1\text{Im}][\text{PF}_6]$ should already be liquid at a lower temperature. The delay of the exchange process to considerably higher temperatures could result from a change in mobility of $[\text{C}_8\text{C}_1\text{Im}][\text{PF}_6]$ due to the confinement of the IL film under the 2H-TPP layer,^{84, 277} which itself is likely

stabilized laterally by strong phenyl-phenyl bonds.^{84, 177-178, 219, 227, 229, 236-242, 278} In fact, Thussing *et al.* also reported in studies of the thermal stability of organic bilayers a high stability of the 2D-network of the top layer molecules due to strong intermolecular bonding, limiting the mobility of the molecules at the metal surface below.²²⁴⁻²²⁵ Note, in contrast to the pure IL systems (Chapter 3.5), the IL film confined under the 2H-TPP layer shows no sign of molecular reorientations (*i.e.* alkyl chain enrichment) prior to the actual molecular exchange.

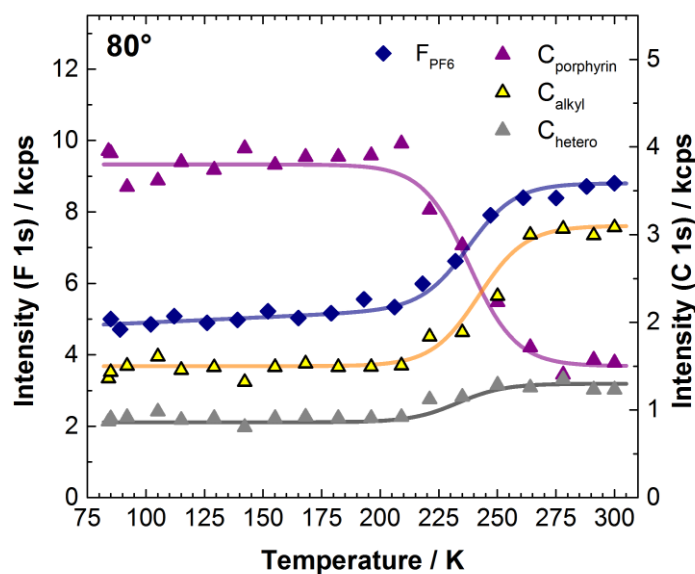


Figure 22: Thermal evolution of F 1s and C 1s spectra measured in 80° during heating after deposition of a monolayer of 2H-TPP on top of 1 ML of [C₈C₁Im][PF₆] on Ag(111) at 84 K. Heating rate: 2 K/min. Reprinted with permission from⁸⁴ under license CC BY 4.0.

As the exchange process is most likely driven by the larger adsorption energy of 2H-TPP at the metal surfaces compared to the IL,⁸⁴ it is also possible that the shift of the transition to higher temperature could be the result of a higher activation energy for the replacement of the IL by the porphyrin at the metal interface compared to the IL/IL films on Ag(111).¹⁰⁴⁻¹⁰⁵

This molecular-level UHV study on the replacement of the IL at the IL/metal interface after postdeposition of porphyrins helps understanding processes at liquid/solid interfaces in general, as it could be considered a general case of preferential adsorption of large molecules on surfaces from solutions. Compared to the deposition from the gas phase, the deposition from a liquid phase follows very different mechanisms and the resulting structures of the organic layer on the surface could be different.^{84, 279}

Replacement effects of this kind are further related to stability concerns in IL-based catalysts. One example could be the poisoning of a SCILL system, where the adsorption of large molecular reactants might block the reactive sites on the surface irreversibly and would lower the catalytic activity over time, similar to poisoning of Pt catalysts by sulfur or other nonreactive species.^{66, 280-283} Another example would concern SILP systems based on metalloporphyrin derivatives as catalytic centers.⁸⁶ It would cause major challenges if the complexes preferentially adsorb to the support surface and thus deplete from the liquid phase. The catalytic system would lose the characteristic homogeneous nature of the catalyst and possibly diminish its reactivity/selectivity. From an even more general point of view, the observed exchange is also relevant for the stability of organic-organic heterostructures on solid supports. If a porphyrin-based electronic device is prepared at one temperature but used at higher temperatures, the increased mobility of the molecules could change the intended structure of the layered film stack.

4. Summary

Thin films of ionic liquids (ILs) on high surface area solid supports are not only the key ingredient to effective SCILL and SILP catalysis but further show increasing potential for widespread use in other fields. For these thin IL film applications, the function, performance and stability of the system are strongly determined by the interface properties. In this context, the molecular-level ARXPS studies on model systems in ultra-high vacuum (UHV) in the present study highlight fundamental aspects of wetting and film growth of various ILs on single-crystalline Ag(111) and Au(111) supports, and of the structure and composition of the IL/support and IL/vacuum interfaces of pure and mixed IL films.

The IL thin film growth on metal surfaces (Chapter 3.1, [P1, P2, P3, P4]) was studied on the example of four imidazolium-based ILs. The variations in molecular structure (with or without alkyl substituent or partially fluorinated side chain) and composition (different counter ions, $[\text{Tf}_2\text{N}]^-$ or $[\text{PF}_6]^-$) allow for the derivation of certain structure-property relationships regarding the points raised above. In agreement with literature, the formation of a closed wetting layer (WL) on metal surfaces appears to be one general similarity for ILs, but the intermolecular structure and molecular orientation at the interfaces seem to be determined predominantly by the composition of the IL and less by the nature of the support. In the present state, however, the variety of systems is still limited to a hand full of popular representatives. As homogeneous wetting is a crucial requirement for many applications, the results of this thesis provide an important basis for the deeper understanding of film morphologies in the later stages of thin film growth.

Time-dependent changes in the growth of IL films (Chapter 3.2, [P1]) were studied on the example of $[\text{C}_1\text{C}_1\text{Im}][\text{Tf}_2\text{N}]$ on Ag(111). This IL forms initially very pronounced 3D islands on a WL which then slowly spread towards a more 2D structure over the course of the measurement. $[\text{C}_2\text{C}_1\text{Im}][\text{Tf}_2\text{N}]$ on Au(110) was reported to behave similarly. As films of $[\text{C}_8\text{C}_1\text{Im}][\text{Tf}_2\text{N}]$, in contrast, reveal no such time-dependent behavior, the observed morphology changes appear to be related to the length of the alkyl substituents at the cationic imidazolium head group.

The growth and desorption of 2H-TPP on Ag(111) and Au(111) (Chapter 3.3, [P4]) were characterized by ARXPS. As parameters like charge carrier mobility and device efficiency strongly depend on the molecular arrangement and orientation, the structure and stability of multilayer porphyrins is of utmost importance for applications in organic electronic devices. Information on porphyrin multilayers on metal substrates – in general – as well as

their thermal behavior is, however, scarce. The results of the present work indicate Stranski-Krastanov-like growth for 2H-TPP on both metals, with 2D growth up to two closed molecular layers and the formation of 3D islands on top of this bilayer. The thermal stability of 2H-TPP multilayers on the metal surfaces was monitored through the thermal evolution of XPS signals. On both surfaces, 2H-TPP multilayers desorb at the same temperature of about 450 K while the monolayer remains stable on the surface up to at least 500 K. At temperatures above 525 K, the molecules in the 2H-TPP monolayer may be subject to decomposition.

The desorption of ILs from metal surfaces (Chapter 3.4, [P2, P3, P4]) plays a pivotal role for thin IL film applications at high temperature, despite their commonly high thermal stability and very low vapor pressures. By means of temperature-programmed XPS, the desorption of pure and mixed films of ILs from Ag(111) and Au(111) was studied. While the difference in the length of the alkyl chain between $[C_1C_1Im][Tf_2N]$ and $[C_8C_1Im][Tf_2N]$ leads to a considerably lower multilayer desorption temperature of the former compared to the latter, the two ILs have similar desorption temperatures of the remaining IL WL on Ag(111). The different anion in $[C_8C_1Im][PF_6]$ results in both, higher multilayer and WL desorption temperatures compared to $[C_8C_1Im][Tf_2N]$. The stronger adsorption to the metal is likely related to the smaller ion size and more localized charge. The similar WL desorption temperatures of $[C_8C_1Im][PF_6]$ on Ag(111) and Au(111) indicate comparable binding energies for the IL on both metals. Bilayer films of $[C_8C_1Im][PF_6]$ on 2H-TPP-covered Ag(111) and Au(111) are stable up to above 100 °C, but the direct interaction of the IL with the metal surface is inhibited and the IL film desorbs entirely in the temperature range of multilayer desorption. In a similar way, it is also possible to selectively desorb one IL from mixed IL films. The thorough discussion of the results for IL desorption of this thesis with respect to literature studies provides a vantage point for obtaining a more comprehensive picture of the material properties at elevated temperatures.

Ion exchange at the IL/solid interface (Chapter 3.5, [P2, P3]) and preferential enrichment of ions at the vacuum interface were observed after the sequential deposition of ultrathin films of two different ILs on Ag(111). After IL deposition at temperatures around 90 K, the exchange processes occur upon heating to room temperature. The exact temperatures at which the exchange occurs appears to be related to the bulk glass transition temperature of the IL on top. Two driving forces are suggested to be responsible for the replacement at IL/solid interfaces, a lower surface tension of the mixed thin film and a higher adsorption energy of one of

the ILs. The results highlight how the interface compositions of thin multi-component IL films depend on the combination of ions and how they can be controlled via temperature.

The replacement of IL by porphyrins at metal interfaces (Chapter 3.6, [P4]) was studied in light of the increasing interest in organic-organic multicomponent heterostructures on metals. When the 2H-TPP is deposited on top of $[\text{C}_8\text{C}_1\text{Im}][\text{PF}_6]$ at temperatures below 90 K, the porphyrin molecules adsorb on top of the IL film at first, but replace the IL at the IL/metal interfaces upon heating above 240 K. This exchange process appears to be driven by the higher adsorption energy of 2H-TPP on the Ag(111) and Au(111) surfaces compared to the IL. Such molecular-level UHV studies on the replacement of ILs by large organic molecules at IL/metal interfaces help understanding processes at liquid/solid interfaces in general. In comparison to the deposition from the gas phase, the deposition from a liquid phase follows very different mechanisms and the resulting structures of the organic layer on the surface could be different.

5. Kurzfassung der Arbeit

In Form dünner Filme auf porösen Trägermaterialien sind Ionische Flüssigkeiten (engl. *Ionic Liquids*, ILs) wesentlicher Bestandteil leistungsfähiger SCILL (*Solid Catalyst with Ionic Liquid Layer*) und SILP (*Supported Ionic Liquid Phase*) Katalysatorsysteme. Für diese und zahlreiche weitere Anwendungsgebiete dünner IL-Filme sind insbesondere die Grenzflächeneigenschaften für die Funktionalität, Leistungsfähigkeit und Stabilität der jeweiligen Systeme von besonderer Bedeutung. Die Untersuchungen der vorliegenden Arbeit im Ultrahochvakuum mittels winkelaufgelöster Röntgenphotoelektronenspektroskopie (engl. *Angle-Resolved X-ray Photoelectron Spectroscopy*, ARXPS) an Modellsystemen tragen in diesem Zusammenhang vor allem zum grundlegenden Verständnis des Benetzungs- und Wachstumsverhaltens von ILs auf Metalloberflächen sowie der Struktur und Zusammensetzung der Grenzflächen IL/Metall und IL/Vakuum bei. Die Ergebnisse dieser Arbeit wurden eingehend unter Berücksichtigung früherer Erkenntnisse aus der Fachliteratur diskutiert.

Das Wachstum ultradünner IL-Filme auf Metalloberflächen (Kapitel 3.1, [P1, P2, P3, P4]) wurde für vier Imidazolium-ILs auf einkristallinem Ag(111) und Au(111) untersucht. Die Variation der Molekülstruktur des Kations (mit und ohne Alkylsubstituenten sowie mit partiell fluorierter Seitenkette) und der jeweiligen Gegenionen ($[\text{Tf}_2\text{N}]^-$ und $[\text{PF}_6]^-$) ermöglicht hierbei die Ableitung belastbarer Struktur-Eigenschafts-Beziehungen für die untersuchten Systeme. Zusammenfassend lässt sich sagen, dass für ILs auf Metalloberflächen generell die Ausbildung einer geschlossenen molekularen Benetzungslage (engl. *Wetting Layer*, WL) beobachtet wird. Molekulare Vorzugsorientierungen und supramolekulare Anordnungen innerhalb dieses WLs scheinen bevorzugt durch die jeweilige IL bestimmt zu werden und lassen kaum Abhängigkeiten von der Art der Metalloberfläche erkennen; allerdings liegt erst eine geringe Anzahl an Systemen mit aussagekräftigen Studien vor. Da ein gleichmäßiges Benetzungsverhalten eine wesentliche Voraussetzung für viele Anwendungen darstellt, bilden die vorliegenden Untersuchungen eine wichtige Grundlage für ein vertieftes Verständnis der molekularen Zusammenhänge des Filmwachstums.

Zeitabhängige Änderungen beim Wachstum von IL-Filmen (Kapitel 3.2, [P1]) wurden an $[\text{C}_1\text{C}_1\text{Im}][\text{Tf}_2\text{N}]$ auf Ag(111) untersucht. Nach Abscheidung aus der Gasphase bildet diese IL zu Beginn ausgeprägte dreidimensionale Inseln auf einem WL aus. Diese Inselstruktur ändert sich im Laufe zeitabhängiger Messungen langsam hin zu einer flacheren Filmmorphologie. Während ähnliche Beobachtungen bereits zuvor in der Literatur für $[\text{C}_2\text{C}_1\text{Im}][\text{Tf}_2\text{N}]$ auf Au(110) beschrieben wurden, zeigt $[\text{C}_8\text{C}_1\text{Im}][\text{Tf}_2\text{N}]$ kein derartiges zeitabhängiges Verhalten.

Die Unterschiede in der Molekülstruktur der drei genannten ILs deuten auf einen Einfluss der Kettenlänge der Alkylsubstituenten am Imidazolium-Kation auf dieses zeitabhängige Benetzungsverhalten hin.

Das Wachstum und Desorptionsverhalten des Porphyrins 2H-TPP auf Ag(111) und Au(111) (Kapitel 3.3, [P4]) wurde in dieser Arbeit ebenfalls mittels ARXPS untersucht. Bei elektronischen Bauteilen, die auf organischen Dünnschichtmaterialien basieren, hängt die Effizienz und Mobilität von Ladungsträgern stark von der Anordnung und Orientierung der Moleküle an den Grenzflächen und innerhalb der Schichten ab. Umfassende Kenntnis der Struktur und Stabilität von Porphyrin-Multilagen sind daher unabdingbar für deren erfolgreichen Einsatz in funktionalen Mehrschichtsystemen. Detaillierte Informationen zum Multilagenwachstum von Porphyrinen auf Metalloberflächen sowie zur thermischen Stabilität fanden in bisherigen Untersuchungen jedoch wenig Beachtung. Die Ergebnisse der vorliegenden Arbeit deuten für beide Metalloberflächen auf ein zweidimensionales Wachstum des Porphyrins 2H-TPP bis zur Vollendung der zweiten Moleküllage hin. Auf dieser Porphyrin-Doppellage wachsen im weiteren Verlauf dreidimensionale Inseln (Stranski-Krastanow-Wachstum). Die thermische Stabilität der 2H-TPP-Multilagen wurde durch temperaturprogrammierte (TP-)XPS-Messungen charakterisiert. Auf beiden Metalloberflächen desorbieren die Multilagen bei ungefähr 450 K, während die Porphyrinmoleküle in der Monolage bis 500 K stabil sind. Oberhalb von 525 K können Zersetzungreaktionen auftreten.

Die Desorption von ILs von Metalloberflächen (Kapitel 3.4, [P2, P3, P4]) spielt eine entscheidende Rolle für die Einsatztemperaturgrenzen von ILs in Dünnschichtanwendungen. Obwohl ILs in der Regel eine hohe thermische Stabilität aufweisen, kann der – bei Raumtemperatur typischerweise extrem niedrige und dadurch meist vernachlässigbare – Dampfdruck von ILs bei erhöhter Temperatur eine Berücksichtigung des Desorptionsverhaltens erforderlich machen. In dieser Arbeit wurde mittels TP-XPS-Messungen die Desorption von ILs und IL-Mischungen auf Einflüsse der molekularen Zusammensetzung der IL und der Art des Substratmaterials hin untersucht. Während die unterschiedliche Länge der Alkylsubstituenten zu einer deutlich niedrigeren Multilagen-Desorptionstemperatur von $[C_1C_1Im][Tf_2N]$ im Vergleich zu $[C_8C_1Im][Tf_2N]$ führt, zeigt die jeweils verbleibende Benetzungslage auf Ag(111) für beide ILs die gleiche Desorptionstemperatur. Das Verhalten der Multilagen ist im Einklang mit makroskopischen Untersuchungen des Dampfdrucks der beiden ILs. Für die Adsorption auf der Metalloberfläche scheint der ionische Charakter der ILs den Einfluss durch die unterschiedlichen Substituenten zu dominieren. Bei einer Variation

des Gegenions verschiebt sich für $[\text{C}_8\text{C}_1\text{Im}][\text{PF}_6]$ im Vergleich zu $[\text{C}_8\text{C}_1\text{Im}][\text{Tf}_2\text{N}]$ sowohl für Multilagen als auch für die Benetzungslage auf Ag(111) die Desorption zu höheren Temperaturen. Dies deutet auf eine stärkere Adsorption von $[\text{C}_8\text{C}_1\text{Im}][\text{PF}_6]$ hin, welche wahrscheinlich auf der geringeren Größe und dadurch stärker lokalisierten Ladung beruht. Die Desorptionstemperaturen für die Benetzungslage von $[\text{C}_8\text{C}_1\text{Im}][\text{PF}_6]$ auf Ag(111) und Au(111) liegen sehr nahe beieinander, was auf ähnliche Adsorptionsenergien auf beiden Metalloberflächen hinweist. Komplexere Schichtsysteme in Form von $[\text{C}_8\text{C}_1\text{Im}][\text{PF}_6]$ -Multilagen auf einer 2H-TPP-Monolage auf Ag(111) bzw. Au(111) sind stabil bis über 100°C , jedoch wird die direkte Wechselwirkung der IL mit der Metalloberfläche durch die Porphyrinschicht verhindert, sodass in diesem Fall $[\text{C}_8\text{C}_1\text{Im}][\text{PF}_6]$ komplett im Bereich der Multilagensorption desorbiert. In Analogie dazu ist es ebenfalls möglich, eine IL aus einem gemischten IL-Film selektiv zu desorbieren. Die Ergebnisse dieser Arbeit zum Desorptionsverhalten von ILs wurden ausführlich mit in der Fachliteratur verfügbarer Studien verglichen und liefern einen tragfähigen Ausgangspunkt für eine umfassende weitere Klassifizierung dieser Materialeigenschaften.

Ionenaustauschphänomene an der IL/Metall-Grenzfläche (Kapitel 3.5, [P2, P3]) und bevorzugte Anreicherung von Ionen an der IL/Vakuum-Grenzfläche wurden nach der aufeinander folgenden Abscheidung von zwei verschiedenen ILs auf Ag(111) beobachtet. Nach der Abscheidung der IL-Filme bei niedrigen Temperaturen um 90 K treten die Austauschprozesse beim Heizen bereits unterhalb von RT auf. Die Ergebnisse der untersuchten Systeme deuten darauf hin, dass die Übergangstemperaturen für den Ionenaustausch nahe der Glasübergangstemperatur der jeweils oberen IL liegen. Zwei Triebkräfte für den Ionen-Austausch an der IL/Metall-Grenzfläche wurden identifiziert: Einerseits führt eine niedrigere Oberflächenspannung einer der ILs zur bevorzugten Anreicherung an der IL/Vakuum-Grenzfläche, während andererseits die höhere Adsorptionsenergie einer IL zur selektiven Adsorption auf der Metalloberfläche führt. Die Ergebnisse zeigen anschaulich, wie die Grenzflächenzusammensetzung in komplexen IL-Filmen variabler Mischungszusammensetzung zum einen von der jeweiligen Kombination der Ionen und zum anderen von der Temperatur abhängen kann.

Der Austausch von IL durch Porphyrine an Metalloberflächen (Kapitel 3.6, [P4]) wurde im Hinblick auf das wachsende Interesse an organischen Multikomponenten-Heterostrukturen auf Metalloberflächen untersucht. Das Porphyrin 2H-TPP wurde hierfür bei Temperaturen unterhalb von 90 K auf einen dünnen $[\text{C}_8\text{C}_1\text{Im}][\text{PF}_6]$ -Film auf den Ag(111)- und

Au(111)-Oberflächen abgeschieden. Die Porphyrinmoleküle adsorbieren dabei zunächst auf dem IL-Film. Wird das System über 240 K erwärmt, ersetzt 2H-TPP die IL an der IL/Metall-Grenzfläche. Dieser Austausch geht vermutlich auf die wesentlich höhere Adsorptionsenergie des 2H-TPP im Vergleich zu $[\text{C}_8\text{C}_1\text{Im}][\text{PF}_6]$ auf den beiden Metalloberflächen zurück. Die vorliegende Untersuchung zeigt auf molekularer Ebene wie ILs durch andere organische Moleküle an der IL/Metall-Grenzfläche verdrängt werden können und hilft dadurch beim allgemeinen Verständnis von Prozessen an flüssig/fest-Grenzflächen. Darüber hinaus folgt die Abscheidung aus der Gasphase im Vergleich zur Abscheidung aus der flüssigen Phase sehr unterschiedlichen Mechanismen und kann als Resultat zu wesentlich anderen Strukturen innerhalb der organischen Adsorbatschicht auf der Metalloberfläche führen.

6. References

1. Welton, T., Room-Temperature Ionic Liquids. Solvents for Synthesis and Catalysis. *Chem. Rev.* **1999**, *99* (8), 2071-2084.
2. Huddleston, J. G.; Visser, A. E.; Reichert, W. M.; Willauer, H. D.; Broker, G. A.; Rogers, R. D., Characterization and comparison of hydrophilic and hydrophobic room temperature ionic liquids incorporating the imidazolium cation. *Green Chem.* **2001**, *3* (4), 156-164.
3. Wasserscheid, P.; Welton, T., *Ionic Liquids in Synthesis*. Wiley VCH: Weinheim, 2007.
4. Binnemans, K., Ionic Liquid Crystals. *Chem. Rev.* **2005**, *105* (11), 4148-4204.
5. Cremer, T.; Kolbeck, C.; Lovelock, K. R. J.; Paape, N.; Wölfel, R.; Schulz, P. S.; Wasserscheid, P.; Weber, H.; Thar, J.; Kirchner, B.; Maier, F.; Steinrück, H.-P., Towards a Molecular Understanding of Cation–Anion Interactions—Probing the Electronic Structure of Imidazolium Ionic Liquids by NMR Spectroscopy, X-ray Photoelectron Spectroscopy and Theoretical Calculations. *Chemistry – A European Journal* **2010**, *16* (30), 9018-9033.
6. Maier, F.; Cremer, T.; Kolbeck, C.; Lovelock, K. R. J.; Paape, N.; Schulz, P. S.; Wasserscheid, P.; Steinrück, H.-P., Insights into the surface composition and enrichment effects of ionic liquids and ionic liquid mixtures. *Phys. Chem. Chem. Phys.* **2010**, *12* (8), 1905-1915.
7. Lovelock, K. R. J.; Villar-Garcia, I. J.; Maier, F.; Steinrück, H. P.; Licence, P., Photoelectron spectroscopy of ionic liquid-based interfaces. *Chem. Rev.* **2010**, *110* (9), 5158-5190.
8. Kolbeck, C.; Lehmann, J.; Lovelock, K. R. J.; Cremer, T.; Paape, N.; Wasserscheid, P.; Fröba, A. P.; Maier, F.; Steinrück, H.-P., Density and Surface Tension of Ionic Liquids. *J. Phys. Chem. B* **2010**, *114* (51), 17025-17036.
9. Hallett, J. P.; Welton, T., Room-Temperature Ionic Liquids: Solvents for Synthesis and Catalysis. 2. *Chem. Rev.* **2011**, *111* (5), 3508-3576.
10. Hayes, R.; Warr, G. G.; Atkin, R., Structure and Nanostructure in Ionic Liquids. *Chem. Rev.* **2015**, *115* (13), 6357-6426.
11. Steinrück, H.-P.; Wasserscheid, P., Ionic Liquids in Catalysis. *Catal. Lett.* **2015**, *145* (1), 380-397.
12. Wang, R.-T.; Lee, G.-H.; Lai, C. K., Effect of counter ions on the mesogenic ionic N-phenylpyridiniums. *CrystEngComm* **2018**, *20* (18), 2593-2607.
13. Esperança, J. M. S. S.; Tariq, M.; Pereiro, A. B.; Araújo, J. M. M.; Seddon, K. R.; Rebelo, L. P. N., Anomalous and Not-So-Common Behavior in Common Ionic Liquids and Ionic Liquid-Containing Systems. *Frontiers in Chemistry* **2019**, *7* (450).
14. Seddon, K. R., A taste of the future. *Nature Materials* **2003**, *2* (6), 363-365.
15. Plechkova, N. V.; Seddon, K. R., Applications of ionic liquids in the chemical industry. *Chem. Soc. Rev.* **2008**, *37* (1), 123-150.
16. Pinilla, C.; Del Pópolo, M. G.; Lynden-Bell, R. M.; Kohanoff, J., Structure and Dynamics of a Confined Ionic Liquid. Topics of Relevance to Dye-Sensitized Solar Cells. *J. Phys. Chem. B* **2005**, *109* (38), 17922-17927.
17. Silvester, D. S., Recent advances in the use of ionic liquids for electrochemical sensing. *Analyst* **2011**, *136* (23), 4871-4882.
18. Vatamanu, J.; Borodin, O.; Smith, G. D., Molecular Simulations of the Electric Double Layer Structure, Differential Capacitance, and Charging Kinetics for N-Methyl-N-propylpyrrolidinium Bis(fluorosulfonyl)imide at Graphite Electrodes. *J. Phys. Chem. B* **2011**, *115* (12), 3073-3084.
19. Goossens, K.; Lava, K.; Bielawski, C. W.; Binnemans, K., Ionic Liquid Crystals: Versatile Materials. *Chem. Rev.* **2016**, *116* (8), 4643-4807.

20. Zhou, F.; Liang, Y.; Liu, W., Ionic liquid lubricants: designed chemistry for engineering applications. *Chem. Soc. Rev.* **2009**, *38* (9), 2590-2599.
21. Cooper, P. K.; Wear, C. J.; Li, H.; Atkin, R., Ionic Liquid Lubrication of Stainless Steel: Friction is Inversely Correlated with Interfacial Liquid Nanostructure. *ACS Sustainable Chem. Eng.* **2017**, *5* (12), 11737-11743.
22. Cooper, P. K.; Staddon, J.; Zhang, S.; Aman, Z. M.; Atkin, R.; Li, H., Nano- and Macroscale Study of the Lubrication of Titania Using Pure and Diluted Ionic Liquids. *Frontiers in Chemistry* **2019**, *7* (287).
23. Riisager, A.; Fehrmann, R.; Haumann, M.; Wasserscheid, P., Supported ionic liquids: versatile reaction and separation media. *Top. Catal.* **2006**, *40* (1), 91-102.
24. Maier, F., Capture of Carbon Dioxide at the Gas-Liquid Interface Elucidated by Surface Science Approaches. *Angew. Chem. Int. Ed.* **2011**, *50* (43), 10133-10134.
25. Niedermaier, I.; Bahlmann, M.; Papp, C.; Kolbeck, C.; Wei, W.; Krick Calderón, S.; Grabau, M.; Schulz, P. S.; Wasserscheid, P.; Steinrück, H.-P.; Maier, F., Carbon Dioxide Capture by an Amine Functionalized Ionic Liquid: Fundamental Differences of Surface and Bulk Behavior. *J. Am. Chem. Soc.* **2014**, *136* (1), 436-441.
26. Chen, S.; Sun, Y.; Chao, J.; Cheng, L.; Chen, Y.; Liu, J., Dispersive liquid-liquid microextraction of silver nanoparticles in water using ionic liquid 1-octyl-3-methylimidazolium hexafluorophosphate. *J. Environ. Sci.* **2016**, *41*, 211-217.
27. Odugbesi, G. A.; Nan, H.; Soltani, M.; Davis, J. H.; Anderson, J. L., Ultra-high thermal stability perarylated ionic liquids as gas chromatographic stationary phases for the selective separation of polyaromatic hydrocarbons and polychlorinated biphenyls. *J. Chromatogr. A* **2019**, *1604*, 460466.
28. Anderson, J. L.; Armstrong, D. W., Immobilized Ionic Liquids as High-Selectivity/High-Temperature/High-Stability Gas Chromatography Stationary Phases. *Anal. Chem.* **2005**, *77* (19), 6453-6462.
29. Armstrong, D. W.; He, L.; Liu, Y.-S., Examination of Ionic Liquids and Their Interaction with Molecules, When Used as Stationary Phases in Gas Chromatography. *Anal. Chem.* **1999**, *71* (17), 3873-3876.
30. Johnston, M.; Lee, J.-J.; Chottiner, G. S.; Miller, B.; Tsuda, T.; Hussey, C. L.; Scherson, D. A., Electrochemistry in Ultrahigh Vacuum: Underpotential Deposition of Al on Polycrystalline W and Au from Room Temperature AlCl₃/1-Ethyl-3-methylimidazolium Chloride Melts. *J. Phys. Chem. B* **2005**, *109* (22), 11296-11300.
31. Endres, F.; Zein El Abedin, S., Air and water stable ionic liquids in physical chemistry. *Phys. Chem. Chem. Phys.* **2006**, *8* (18), 2101-2116.
32. Hapiot, P.; Lagrost, C., Electrochemical Reactivity in Room-Temperature Ionic Liquids. *Chem. Rev.* **2008**, *108* (7), 2238-2264.
33. Souda, R., Matrix effects on secondary ion emission from a room-temperature ionic liquid, 1-ethyl-3-methylimidazolium bis[trifluoromethanesulfonyl]imide. *J. Chem. Phys.* **2009**, *130* (24), 244707.
34. Souda, R., Phase Transition of 1-Ethyl-3-Methylimidazolium Bis(trifluoromethylsulfonyl)imide Thin Films on Highly Oriented Pyrolytic Graphite. *J. Phys. Chem. B* **2009**, *113* (39), 12973-12977.
35. Endres, F.; Hofft, O.; Borisenko, N.; Gasparotto, L. H.; Prowald, A.; Al-Salman, R.; Carstens, T.; Atkin, R.; Bund, A.; Zein El Abedin, S., Do solvation layers of ionic liquids influence electrochemical reactions? *Phys. Chem. Chem. Phys.* **2010**, *12* (8), 1724-1732.
36. Weingarh, D.; Foelske-Schmitz, A.; Wokaun, A.; Kötz, R., In situ electrochemical XPS study of the Pt/[EMIM][BF₄] system. *Electrochem. Commun.* **2011**, *13* (6), 619-622.

37. Reyna-González, J. M.; Reyes-López, J. C.; Aguilar-Martínez, M., Silver and silver–copper electrodeposition from a pyridinium-based ionic liquid. *Electrochim. Acta* **2013**, *94*, 344-352.
38. Elbourne, A.; McDonald, S.; Voichovsky, K.; Endres, F.; Warr, G. G.; Atkin, R., Nanostructure of the Ionic Liquid–Graphite Stern Layer. *ACS Nano* **2015**, *9* (7), 7608-7620.
39. Buchner, F.; Forster-Tonigold, K.; Bozorgchenani, M.; Gross, A.; Behm, R. J., Interaction of a Self-Assembled Ionic Liquid Layer with Graphite(0001): A Combined Experimental and Theoretical Study. *The Journal of Physical Chemistry Letters* **2016**, *7* (2), 226-233.
40. Carstens, T.; Lahiri, A.; Borisenko, N.; Endres, F., [Py1,4]FSI-NaFSI-Based Ionic Liquid Electrolyte for Sodium Batteries: Na⁺ Solvation and Interfacial Nanostructure on Au(111). *J. Phys. Chem. C* **2016**, *120* (27), 14736-14741.
41. Liu, Z.; Cui, T.; Lu, T.; Shapouri Ghazvini, M.; Endres, F., Anion Effects on the Solid/Ionic Liquid Interface and the Electrodeposition of Zinc. *J. Phys. Chem. C* **2016**, *120* (36), 20224-20231.
42. Iwahashi, T.; Miwa, Y.; Zhou, W.; Sakai, Y.; Yamagata, M.; Ishikawa, M.; Kim, D.; Ouchi, Y., IV-SFG studies on the effect of Li⁺ in extending the electrochemical window at the Pt[[C2mim]][FSA] interface. *Electrochem. Commun.* **2016**, *72*, 54-58.
43. Berger, C. A.; Arkhipova, M.; Maas, G.; Jacob, T., Dysprosium electrodeposition from a hexaalkylguanidinium-based ionic liquid. *Nanoscale* **2016**, *8* (29), 13997-14003.
44. Buchner, F.; Forster-Tonigold, K.; Kim, J.; Adler, C.; Bansmann, J.; Groß, A.; Behm, R. J., Experimental and Computational Study on the Interaction of an Ionic Liquid Monolayer with Lithium on Pristine and Lithiated Graphite. *J. Phys. Chem. C* **2018**, *122* (33), 18968-18981.
45. Borisenko, N.; Lahiri, A.; Pulletikurthi, G.; Cui, T.; Carstens, T.; Zahlbach, J.; Atkin, R.; Endres, F., The Au(111)/IL interfacial nanostructure in the presence of precursors and its influence on the electrodeposition process. *Faraday Discuss.* **2018**, *206* (0), 459-473.
46. Hoffmann, V.; Pulletikurthi, G.; Carstens, T.; Lahiri, A.; Borodin, A.; Schammer, M.; Horstmann, B.; Latz, A.; Endres, F., Influence of a silver salt on the nanostructure of a Au(111)/ionic liquid interface: an atomic force microscopy study and theoretical concepts. *Phys. Chem. Chem. Phys.* **2018**, *20* (7), 4760-4771.
47. Armel, V.; Pringle, J. M.; Forsyth, M.; MacFarlane, D. R.; Officer, D. L.; Wagner, P., Ionic liquid electrolyte porphyrin dye sensitised solar cells. *Chem. Commun.* **2010**, *46* (18), 3146-3148.
48. MacFarlane, D. R.; Tachikawa, N.; Forsyth, M.; Pringle, J. M.; Howlett, P. C.; Elliott, G. D.; Davis, J. H.; Watanabe, M.; Simon, P.; Angell, C. A., Energy applications of ionic liquids. *Energy & Environmental Science* **2014**, *7* (1), 232-250.
49. Brooke, R.; Fabretto, M.; Krasowska, M.; Talemi, P.; Pering, S.; Murphy, P. J.; Evans, D., Organic energy devices from ionic liquids and conducting polymers. *Journal of Materials Chemistry C* **2016**, *4* (7), 1550-1556.
50. Kernchen, U.; Etzold, B.; Korth, W.; Jess, A., Solid Catalyst with Ionic Liquid Layer (SCILL) – A New Concept to Improve Selectivity Illustrated by Hydrogenation of Cyclooctadiene. *Chemical Engineering & Technology* **2007**, *30* (8), 985-994.
51. Mehnert, C. P.; Mozeleski, E. J.; Cook, R. A., Supported ionic liquid catalysis investigated for hydrogenation reactions. *Chem. Commun.* **2002**, (24), 3010-3011.
52. Riisager, A.; Fehrmann, R.; Flicker, S.; van Hal, R.; Haumann, M.; Wasserscheid, P., Very Stable and Highly Regioselective Supported Ionic-Liquid-Phase (SILP)

- Catalysis: Continuous-Flow Fixed-Bed Hydroformylation of Propene. *Angew. Chem. Int. Ed.* **2005**, *44* (5), 815-819.
53. Wasserscheid, P.; Keim, W., Ionic Liquids—New “Solutions” for Transition Metal Catalysis. *Angew. Chem. Int. Ed.* **2000**, *39* (21), 3772-3789.
 54. Huang, J.; Jiang, T.; Gao, H.; Han, B.; Liu, Z.; Wu, W.; Chang, Y.; Zhao, G., Pd Nanoparticles Immobilized on Molecular Sieves by Ionic Liquids: Heterogeneous Catalysts for Solvent-Free Hydrogenation. *Angew. Chem. Int. Ed.* **2004**, *43* (11), 1397-1399.
 55. Hagiwara, H.; Sugawara, Y.; Isobe, K.; Hoshi, T.; Suzuki, T., Immobilization of Pd(OAc)₂ in Ionic Liquid on Silica: Application to Sustainable Mizoroki–Heck Reaction. *Org. Lett.* **2004**, *6* (14), 2325-2328.
 56. Breitenlechner, S.; Fleck, M.; Müller, T. E.; Suppan, A., Solid catalysts on the basis of supported ionic liquids and their use in hydroamination reactions. *J. Mol. Catal. A: Chem.* **2004**, *214* (1), 175-179.
 57. Riisager, A.; Fehrmann, R.; Haumann, M.; Gorle, B. S. K.; Wasserscheid, P., Stability and Kinetic Studies of Supported Ionic Liquid Phase Catalysts for Hydroformylation of Propene. *Industrial & Engineering Chemistry Research* **2005**, *44* (26), 9853-9859.
 58. Yamaguchi, K.; Yoshida, C.; Uchida, S.; Mizuno, N., Peroxotungstate Immobilized on Ionic Liquid-Modified Silica as a Heterogeneous Epoxidation Catalyst with Hydrogen Peroxide. *J. Am. Chem. Soc.* **2005**, *127* (2), 530-531.
 59. Yang, Y.; Deng, C.; Yuan, Y., Characterization and hydroformylation performance of mesoporous MCM-41-supported water-soluble Rh complex dissolved in ionic liquids. *J. Catal.* **2005**, *232* (1), 108-116.
 60. Steffan, M.; Lucas, M.; Brandner, A.; Wollny, M.; Oldenburg, N.; Claus, P., Selective Hydrogenation of Citral in an Organic Solvent, in a Ionic Liquid, and in Substance. *Chemical Engineering & Technology* **2007**, *30* (4), 481-486.
 61. Virtanen, P.; Salmi, T.; Mikkola, J.-P., Kinetics of Cinnamaldehyde Hydrogenation by Supported Ionic Liquid Catalysts (SILCA). *Industrial & Engineering Chemistry Research* **2009**, *48* (23), 10335-10342.
 62. Virtanen, P.; Salmi, T. O.; Mikkola, J.-P., Supported Ionic Liquid Catalysts (SILCA) for Preparation of Organic Chemicals. *Top. Catal.* **2010**, *53* (15), 1096-1103.
 63. Haumann, M.; Schönweiz, A.; Breitzke, H.; Buntkowsky, G.; Werner, S.; Szesni, N., Solid-State NMR Investigations of Supported Ionic Liquid Phase Water-Gas Shift Catalysts: Ionic Liquid Film Distribution vs. Catalyst Performance. *Chemical Engineering & Technology* **2012**, *35* (8), 1421-1426.
 64. Heinze, M. T.; Zill, J. C.; Matysik, J.; Einicke, W. D.; Gläser, R.; Stark, A., Solid–ionic liquid interfaces: pore filling revisited. *Phys. Chem. Chem. Phys.* **2014**, *16* (44), 24359-24372.
 65. Miller, S. F.; Friedrich, H. B.; Holzapfel, C. W., The Effects of SCILL Catalyst Modification on the Competitive Hydrogenation of 1-Octyne and 1,7-Octadiene versus 1-Octene. *ChemCatChem* **2012**, *4* (9), 1337-1344.
 66. Zhang, G.-R.; Munoz, M.; Etzold, B. J. M., Accelerating Oxygen-Reduction Catalysts through Preventing Poisoning with Non-Reactive Species by Using Hydrophobic Ionic Liquids. *Angew. Chem. Int. Ed.* **2016**, *55* (6), 2257-2261.
 67. Castner Jr, E. W.; Wishart, J. F., Spotlight on ionic liquids. *J. Chem. Phys.* **2010**, *132* (12), 120901.
 68. Steinrück, H.-P.; Libuda, J.; Wasserscheid, P.; Cremer, T.; Kolbeck, C.; Laurin, M.; Maier, F.; Sobota, M.; Schulz, P. S.; Stark, M., Surface Science and Model Catalysis with Ionic Liquid-Modified Materials. *Adv. Mater.* **2011**, *23* (22-23), 2571-2587.

69. Steinrück, H.-P., Recent developments in the study of ionic liquid interfaces using X-ray photoelectron spectroscopy and potential future directions. *Phys. Chem. Chem. Phys.* **2012**, *14* (15), 5010-5029.
70. Schernich, S.; Laurin, M.; Lykhach, Y.; Tsud, N.; Sobota, M.; Skála, T.; Prince, K. C.; Taccardi, N.; Wagner, V.; Steinrück, H.-P.; Matolín, V.; Wasserscheid, P.; Libuda, J., Interactions of Imidazolium-Based Ionic Liquids with Oxide Surfaces Controlled by Alkyl Chain Functionalization. *ChemPhysChem* **2013**, *14* (16), 3673-3677.
71. Schernich, S.; Laurin, M.; Lykhach, Y.; Steinrück, H.-P.; Tsud, N.; Skála, T.; Prince, K. C.; Taccardi, N.; Matolín, V.; Wasserscheid, P.; Libuda, J., Functionalization of Oxide Surfaces through Reaction with 1,3-Dialkylimidazolium Ionic Liquids. *The Journal of Physical Chemistry Letters* **2013**, *4* (1), 30-35.
72. Smith, E. F.; Villar Garcia, I. J.; Briggs, D.; Licence, P., Ionic liquids in vacuo; solution-phase X-ray photoelectron spectroscopy. *Chem. Commun.* **2005**, (45), 5633-5635.
73. Steinrück, H.-P., Surface science goes liquid ! *Surf. Sci.* **2010**, *604* (5-6), 481-484.
74. Butler, A. R.; Williams, D. L. H., The physiological role of nitric oxide. *Chem. Soc. Rev.* **1993**, *22* (4), 233-241.
75. Ford, P. C.; Bourassa, J.; Miranda, K.; Lee, B.; Lorkovic, I.; Boggs, S.; Kudo, S.; Laverman, L., Photochemistry of metal nitrosyl complexes. Delivery of nitric oxide to biological targets. *Coord. Chem. Rev.* **1998**, *171*, 185-202.
76. Forrest, S. R., Ultrathin Organic Films Grown by Organic Molecular Beam Deposition and Related Techniques. *Chem. Rev.* **1997**, *97* (6), 1793-1896.
77. Paolesse, R.; Di Natale, C.; Campo Dall'Orto, V.; Macagnano, A.; Angelaccio, A.; Motta, N.; Sgarlata, A.; Hurst, J.; Rezzano, I.; Mascini, M.; D'Amico, A., Porphyrin thin films coated quartz crystal microbalances prepared by electropolymerization technique. *Thin Solid Films* **1999**, *354* (1), 245-250.
78. Drain, C. M., Self-organization of self-assembled photonic materials into functional devices: Photo-switched conductors. *Proceedings of the National Academy of Sciences* **2002**, *99* (8), 5178.
79. Auwärter, W.; Weber-Bargioni, A.; Riemann, A.; Schiffrin, A.; Gröning, O.; Fasel, R.; Barth, J. V., Self-assembly and conformation of tetrapyrrolyl-porphyrin molecules on Ag(111). *J. Chem. Phys.* **2006**, *124* (19), 194708.
80. Saito, S.; Osuka, A., Expanded Porphyrins: Intriguing Structures, Electronic Properties, and Reactivities. *Angew. Chem. Int. Ed.* **2011**, *50* (19), 4342-4373.
81. Zucca, P.; Neves, C. M.; Simoes, M. M.; Neves Mda, G.; Cocco, G.; Sanjust, E., Immobilized Lignin Peroxidase-Like Metalloporphyrins as Reusable Catalysts in Oxidative Bleaching of Industrial Dyes. *Molecules* **2016**, *21* (7).
82. Ruggieri, C.; Rangan, S.; Bartynski, R. A.; Galoppini, E., Zinc(II) Tetraphenylporphyrin on Ag(100) and Ag(111): Multilayer Desorption and Dehydrogenation. *J. Phys. Chem. C* **2016**, *120* (14), 7575-7585.
83. Thompson, S. J.; Brennan, M. R.; Lee, S. Y.; Dong, G., Synthesis and applications of rhodium porphyrin complexes. *Chem. Soc. Rev.* **2018**, *47* (3), 929-981.
84. Lexow, M.; Massicot, S.; Maier, F.; Steinrück, H.-P., Stability and Exchange Processes in Ionic Liquid/Porphyrin Composite Films on Metal Surfaces. *J. Phys. Chem. C* **2019**, *123*, 29708-29721.
85. Yokoyama, T.; Yokoyama, S.; Kamikado, T.; Mashiko, S., Nonplanar adsorption and orientational ordering of porphyrin molecules on Au(111). *J. Chem. Phys.* **2001**, *115* (8), 3814-3818.
86. Dees, A.; Jux, N.; Tröppner, O.; Dürr, K.; Lippert, R.; Schmid, M.; Küstner, B.; Schlücker, S.; Steinrück, H.-P.; Gottfried, J. M.; Ivanović-Burmazović, I., Reactions

- of Superoxide with Iron Porphyrins in the Bulk and the Near-Surface Region of Ionic Liquids. *Inorg. Chem.* **2015**, *54* (14), 6862-6872.
87. Jiang, Y.; Yang, S.; Li, S.; Liu, W., Aromatic molecules on low-index coinage metal surfaces: Many-body dispersion effects. *Sci. Rep.* **2016**, *6* (1).
 88. Mehnert, C. P.; Cook, R. A.; Dispenziere, N. C.; Afeworki, M., Supported Ionic Liquid Catalysis – A New Concept for Homogeneous Hydroformylation Catalysis. *J. Am. Chem. Soc.* **2002**, *124* (44), 12932-12933.
 89. Wagstaffe, M.; Jackman, M. J.; Syres, K. L.; Generalov, A.; Thomas, A. G., Ionic Liquid Ordering at an Oxide Surface. *ChemPhysChem* **2016**, *17* (21), 3430-3434.
 90. Silvester Debbie, S.; Compton Richard, G., Electrochemistry in Room Temperature Ionic Liquids: A Review and Some Possible Applications. In *Z. Phys. Chem.*, 2006; Vol. 220, p 1247.
 91. Earle, M. J.; Esperanca, J. M. S. S.; Gilea, M. A.; Canongia Lopes, J. N.; Rebelo, L. P. N.; Magee, J. W.; Seddon, K. R.; Widegren, J. A., The distillation and volatility of ionic liquids. *Nature* **2006**, *439* (7078), 831-834.
 92. Souda, R., Glass–Liquid Transition, Crystallization, and Melting of a Room Temperature Ionic Liquid: Thin Films of 1-Ethyl-3-methylimidazolium Bis[trifluoromethanesulfonyl]imide Studied with TOF-SIMS. *J. Phys. Chem. B* **2008**, *112* (48), 15349-15354.
 93. Cremer, T.; Killian, M.; Gottfried, J. M.; Paape, N.; Wasserscheid, P.; Maier, F.; Steinrück, H.-P., Physical Vapor Deposition of [EMIM][Tf2N]: A New Approach to the Modification of Surface Properties with Ultrathin Ionic Liquid Films. *ChemPhysChem* **2008**, *9* (15), 2185-2190.
 94. Cremer, T.; Stark, M.; Deyko, A.; Steinrück, H.-P.; Maier, F., Liquid/Solid Interface of Ultrathin Ionic Liquid Films: [C1C1Im][Tf2N] and [C8C1Im][Tf2N] on Au(111). *Langmuir* **2011**, *27* (7), 3662-3671.
 95. Cremer, T. Ionic Liquid Bulk and Interface Properties: Electronic Interaction, Molecular Orientation and Growth Characteristics. Dissertation, Friedrich-Alexander-Universität Erlangen-Nürnberg, 2012.
 96. Uhl, B.; Cremer, T.; Roos, M.; Maier, F.; Steinrück, H.-P.; Behm, R. J., At the ionic liquid|metal interface: structure formation and temperature dependent behavior of an ionic liquid adlayer on Au(111). *Phys. Chem. Chem. Phys.* **2013**, *15* (40), 17295-17302.
 97. Uhl, B.; Buchner, F.; Gabler, S.; Bozorgchenani, M.; Behm, R. J., Adsorption and reaction of sub-monolayer films of an ionic liquid on Cu(111). *Chem. Commun.* **2014**, *50* (62), 8601-8604.
 98. Deyko, A.; Cremer, T.; Rietzler, F.; Perkin, S.; Crowhurst, L.; Welton, T.; Steinrück, H.-P.; Maier, F., Interfacial Behavior of Thin Ionic Liquid Films on Mica. *J. Phys. Chem. C* **2013**, *117* (10), 5101-5111.
 99. Rietzler, F.; Nagengast, J.; Steinrück, H.-P.; Maier, F., Interface of Ionic Liquids and Carbon: Ultrathin [C1C1Im][Tf2N] Films on Graphite and Graphene. *J. Phys. Chem. C* **2015**, *119* (50), 28068-28076.
 100. Rietzler, F. Interfaces of Ionic Liquids and of Liquid Metals Studied by X-Ray Photoelectron Spectroscopy. Dissertation, Friedrich-Alexander-Universität Erlangen-Nürnberg, 2016.
 101. Rietzler, F.; May, B.; Steinrück, H.-P.; Maier, F., Switching adsorption and growth behavior of ultrathin [C2C1Im][OTf] films on Au(111) by Pd deposition. *Phys. Chem. Chem. Phys.* **2016**, *18* (36), 25143-25150.
 102. Biedron, A. B.; Garfunkel, E. L.; Castner Jr, E. W.; Rangan, S., Ionic liquid ultrathin films at the surface of Cu(100) and Au(111). *J. Chem. Phys.* **2017**, *146* (5), 054704.

103. Lexow, M.; Talwar, T.; Heller, B. S. J.; May, B.; Bhui, R. G.; Maier, F.; Steinrück, H.-P., Time-dependent changes in the growth of ultrathin ionic liquid films on Ag(111). *Phys. Chem. Chem. Phys.* **2018**, *20* (18), 12929-12938.
104. Lexow, M.; Heller, B. S. J.; Maier, F.; Steinrück, H.-P., Anion Exchange at the Liquid/Solid Interface of Ultrathin Ionic Liquid Films on Ag(111). *ChemPhysChem* **2018**, *19*, 2978-2984.
105. Lexow, M.; Heller, B. S. J.; Partl, G.; Bhui, R. G.; Maier, F.; Steinrück, H.-P., Cation Exchange at the Interfaces of Ultrathin Films of Fluorous Ionic Liquids on Ag(111). *Langmuir* **2019**, *35* (2), 398-495.
106. Lovelock, K. R. J.; Kolbeck, C.; Cremer, T.; Paape, N.; Schulz, P. S.; Wasserscheid, P.; Maier, F.; Steinrück, H. P., Influence of Different Substituents on the Surface Composition of Ionic Liquids Studied Using ARXPS. *J. Phys. Chem. B* **2009**, *113* (9), 2854-2864.
107. Heller, B.; Kolbeck, C.; Niedermaier, I.; Dommer, S.; Schatz, J.; Hunt, P.; Maier, F.; Steinrück, H.-P., Surface enrichment in equimolar mixtures of non-functionalized and functionalized imidazolium-based ionic liquids. *ChemPhysChem* **2018**, *19* (14), 1733-1745.
108. Bonhôte, P.; Dias, A.-P.; Papageorgiou, N.; Kalyanasundaram, K.; Grätzel, M., Hydrophobic, Highly Conductive Ambient-Temperature Molten Salts. *Inorg. Chem.* **1996**, *35* (5), 1168-1178.
109. Tokuda, H.; Hayamizu, K.; Ishii, K.; Susan, M. A. B. H.; Watanabe, M., Physicochemical Properties and Structures of Room Temperature Ionic Liquids. 2. Variation of Alkyl Chain Length in Imidazolium Cation. *J. Phys. Chem. B* **2005**, *109* (13), 6103-6110.
110. Cremer, T.; Wibmer, L.; Krick Calderón, S.; Deyko, A.; Maier, F.; Steinrück, H.-P., Interfaces of ionic liquids and transition metal surfaces-adsorption, growth, and thermal reactions of ultrathin [C1C1Im][Tf2N] films on metallic and oxidised Ni(111) surfaces. *Phys. Chem. Chem. Phys.* **2012**, *14* (15), 5153-5163.
111. MacFarlane, D. R.; Meakin, P.; Amini, N.; Forsyth, M., Structural studies of ambient temperature plastic crystal ion conductors. *J. Phys.: Condens. Matter* **2001**, *13* (36), 8257-8267.
112. Every, H.; Bishop, A. G.; Forsyth, M.; MacFarlane, D. R., Ion diffusion in molten salt mixtures. *Electrochim. Acta* **2000**, *45* (8), 1279-1284.
113. Fredlake, C. P.; Crosthwaite, J. M.; Hert, D. G.; Aki, S. N. V. K.; Brennecke, J. F., Thermophysical Properties of Imidazolium-Based Ionic Liquids. *Journal of Chemical & Engineering Data* **2004**, *49* (4), 954-964.
114. Dzyuba, S. V.; Bartsch, R. A., Influence of Structural Variations in 1-Alkyl(aralkyl)-3-Methylimidazolium Hexafluorophosphates and Bis(trifluoromethylsulfonyl)imides on Physical Properties of the Ionic Liquids. *ChemPhysChem* **2002**, *3* (2), 161-166.
115. Krossing, I.; Slattery, J. M.; Dagueuet, C.; Dyson, P. J.; Oleinikova, A.; Weingärtner, H., Why Are Ionic Liquids Liquid? A Simple Explanation Based on Lattice and Solvation Energies. *J. Am. Chem. Soc.* **2006**, *128* (41), 13427-13434.
116. Appetecchi, G. B.; Montanino, M.; Carewska, M.; Moreno, M.; Alessandrini, F.; Passerini, S., Chemical-physical properties of bis(perfluoroalkylsulfonyl)imide-based ionic liquids. *Electrochim. Acta* **2011**, *56* (3), 1300-1307.
117. Paulechka, Y. U.; Blokhin, A. V.; Kabo, G. J.; Strechan, A. A., Thermodynamic properties and polymorphism of 1-alkyl-3-methylimidazolium bis(triflamides). *The Journal of Chemical Thermodynamics* **2007**, *39* (6), 866-877.
118. Cichowska-Kopczynska, I.; Joskowska, M.; Debski, B.; Luczak, J.; Aranowski, R., Influence of Ionic Liquid Structure on Supported Ionic Liquid Membranes

- Effectiveness in Carbon Dioxide/Methane Separation. *Journal of Chemistry* **2013**, *2013*, 980689.
119. Fröba, A. P.; Kremer, H.; Leipertz, A., Density, Refractive Index, Interfacial Tension, and Viscosity of Ionic Liquids [EMIM][EtSO₄], [EMIM][NTf₂], [EMIM][N(CN)₂], and [OMA][NTf₂] in Dependence on Temperature at Atmospheric Pressure. *J. Phys. Chem. B* **2008**, *112* (39), 12420-12430.
 120. Martino, W.; de la Mora, J. F.; Yoshida, Y.; Saito, G.; Wilkes, J., Surface tension measurements of highly conducting ionic liquids. *Green Chem.* **2006**, *8* (4), 390-397.
 121. Smoll, E. J.; Tesa-Serrate, M. A.; Purcell, S. M.; D'Andrea, L.; Bruce, D. W.; Slattery, J. M.; Costen, M. L.; Minton, T. K.; McKendrick, K. G., Determining the composition of the vacuum-liquid interface in ionic-liquid mixtures. *Faraday Discuss.* **2018**, *206* (0), 497-522.
 122. Kilaru, P.; Baker, G. A.; Scovazzo, P., Density and Surface Tension Measurements of Imidazolium-, Quaternary Phosphonium-, and Ammonium-Based Room-Temperature Ionic Liquids: Data and Correlations. *Journal of Chemical & Engineering Data* **2007**, *52* (6), 2306-2314.
 123. Deyko, A.; Lovelock, K. R. J.; Corfield, J.-A.; Taylor, A. W.; Gooden, P. N.; Villar-Garcia, I. J.; Licence, P.; Jones, R. G.; Krasovskiy, V. G.; Chernikova, E. A.; Kustov, L. M., Measuring and predicting [capital Delta]vaph₂₉₈ values of ionic liquids. *Phys. Chem. Chem. Phys.* **2009**, *11* (38), 8544-8555.
 124. Sippel, P.; Lunkenheimer, P.; Krohns, S.; Thoms, E.; Loidl, A., Importance of liquid fragility for energy applications of ionic liquids. *Sci. Rep.* **2015**, *5*, 13922.
 125. Papaiconomou, N.; Yakelis, N.; Salminen, J.; Bergman, R.; Prausnitz, J. M., Synthesis and Properties of Seven Ionic Liquids Containing 1-Methyl-3-octylimidazolium or 1-Butyl-4-methylpyridinium Cations. *Journal of Chemical & Engineering Data* **2006**, *51* (4), 1389-1393.
 126. Tokuda, H.; Hayamizu, K.; Ishii, K.; Susan, M. A. B. H.; Watanabe, M., Physicochemical Properties and Structures of Room Temperature Ionic Liquids. 1. Variation of Anionic Species. *J. Phys. Chem. B* **2004**, *108* (42), 16593-16600.
 127. Kulkarni, P. S.; Branco, L. C.; Crespo, J. G.; Nunes, M. C.; Raymundo, A.; Afonso, C. A. M., Comparison of Physicochemical Properties of New Ionic Liquids Based on Imidazolium, Quaternary Ammonium, and Guanidinium Cations. *Chemistry – A European Journal* **2007**, *13* (30), 8478-8488.
 128. Zaitsau, D. H.; Kabo, G. J.; Strechan, A. A.; Paulechka, Y. U.; Tschersich, A.; Verevkin, S. P.; Heintz, A., Experimental Vapor Pressures of 1-Alkyl-3-methylimidazolium Bis(trifluoromethylsulfonyl)imides and a Correlation Scheme for Estimation of Vaporization Enthalpies of Ionic Liquids. *J. Phys. Chem. A* **2006**, *110* (22), 7303-7306.
 129. Luo, H.; Dai, S.; Bonnesen, P. V., Solvent Extraction of Sr²⁺ and Cs⁺ Based on Room-Temperature Ionic Liquids Containing Monoaza-Substituted Crown Ethers. *Anal. Chem.* **2004**, *76* (10), 2773-2779.
 130. Law, G.; Watson, P. R., Surface Tension Measurements of N-Alkylimidazolium Ionic Liquids. *Langmuir* **2001**, *17* (20), 6138-6141.
 131. Branco, L. C.; Rosa, J. N.; Moura Ramos, J. J.; Afonso, C. A. M., Preparation and Characterization of New Room Temperature Ionic Liquids. *Chemistry – A European Journal* **2002**, *8* (16), 3671-3677.
 132. Rietzler, F.; Piermaier, M.; Deyko, A.; Steinrück, H.-P.; Maier, F., Electrospray Ionization Deposition of Ultrathin Ionic Liquid Films: [C₈C₁Im]Cl and [C₈C₁Im][Tf₂N] on Au(111). *Langmuir* **2014**, *30* (4), 1063-1071.
 133. Montalbán, M. G.; Bolívar, C. L.; Díaz Baños, F. G.; Villora, G., Effect of Temperature, Anion, and Alkyl Chain Length on the Density and Refractive Index of

- 1-Alkyl-3-methylimidazolium-Based Ionic Liquids. *Journal of Chemical & Engineering Data* **2015**, *60* (7), 1986-1996.
134. Suarez, P. A. Z.; Einloft, S.; Dullius, J. E. L.; de Souza, R. F.; Dupont, J., Synthesis and physical-chemical properties of ionic liquids based on 1-n-butyl-3-methylimidazolium cation. *J. Chim. Phys.* **1998**, *95* (7), 1626-1639.
135. Gu, Z.; Brennecke, J. F., Volume Expansivities and Isothermal Compressibilities of Imidazolium and Pyridinium-Based Ionic Liquids. *Journal of Chemical & Engineering Data* **2002**, *47* (2), 339-345.
136. Leys, J.; Wübbenhorst, M.; Preethy Menon, C.; Rajesh, R.; Thoen, J.; Glorieux, C.; Nockemann, P.; Thijs, B.; Binnemans, K.; Longuemart, S., Temperature dependence of the electrical conductivity of imidazolium ionic liquids. *J. Chem. Phys.* **2008**, *128* (6), 064509.
137. Deyko, A.; Hessey, S. G.; Licence, P.; Chernikova, E. A.; Krasovskiy, V. G.; Kustov, L. M.; Jones, R. G., The enthalpies of vaporisation of ionic liquids: new measurements and predictions. *Phys. Chem. Chem. Phys.* **2012**, *14* (9), 3181-3193.
138. Syres, K. L.; Jones, R. G., Adsorption, Desorption, and Reaction of 1-Octyl-3-methylimidazolium Tetrafluoroborate, [C8C1Im][BF₄], Ionic Liquid Multilayers on Cu(111). *Langmuir* **2015**, *31* (36), 9799-9808.
139. Arce, A.; Rodil, E.; Soto, A., Physical and Excess Properties for Binary Mixtures of 1-Methyl-3-Octylimidazolium Tetrafluoroborate, [Omim][BF₄], Ionic Liquid with Different Alcohols. *J. Solution Chem.* **2006**, *35* (1), 63-78.
140. Stefan, C. S.; Lemordant, D.; Biensan, P.; Siret, C.; Claude-Montigny, B., Thermal stability and crystallization of N-alkyl-N-alkyl'-pyrrolidinium imides. *J. Therm. Anal. Calorim.* **2010**, *102* (2), 685-693.
141. Fletcher, S. I.; Sillars, F. B.; Hudson, N. E.; Hall, P. J., Physical Properties of Selected Ionic Liquids for Use as Electrolytes and Other Industrial Applications. *Journal of Chemical & Engineering Data* **2010**, *55* (2), 778-782.
142. Hamor, M. J.; Hamor, T. A.; Hoard, J. L., The Structure of Crystalline Tetraphenylporphine. The Stereochemical Nature of the Porphine Skeleton. *J. Am. Chem. Soc.* **1964**, *86* (10), 1938-1942.
143. Silvers, S. J.; Tulinsky, A., The crystal and molecular structure of triclinic tetraphenylporphyrin. *J. Am. Chem. Soc.* **1967**, *89* (13), 3331-3337.
144. Buchner, F.; Forster-Tonigold, K.; Uhl, B.; Alwast, D.; Wagner, N.; Farkhondeh, H.; Groß, A.; Behm, R. J., Toward the Microscopic Identification of Anions and Cations at the Ionic Liquid|Ag(111) Interface: A Combined Experimental and Theoretical Investigation. *ACS Nano* **2013**, *7* (9), 7773-7784.
145. Uhl, B.; Huang, H.; Alwast, D.; Buchner, F.; Behm, R. J., Interaction of ionic liquids with noble metal surfaces: structure formation and stability of [OMIM][TFSA] and [EMIM][TFSA] on Au(111) and Ag(111). *Phys. Chem. Chem. Phys.* **2015**, *17* (37), 23816-23832.
146. Foulston, R.; Gangopadhyay, S.; Chiutu, C.; Moriarty, P.; Jones, R. G., Mono- and multi-layer adsorption of an ionic liquid on Au(110). *Phys. Chem. Chem. Phys.* **2012**, *14* (17), 6054-6066.
147. Rebelo, L. P. N.; Canongia Lopes, J. N.; Esperança, J. M. S. S.; Filipe, E., On the Critical Temperature, Normal Boiling Point, and Vapor Pressure of Ionic Liquids. *J. Phys. Chem. B* **2005**, *109* (13), 6040-6043.
148. Gottfried, J. M., Surface chemistry of porphyrins and phthalocyanines. *Surf. Sci. Rep.* **2015**, *70* (3), 259-379.
149. Wittstock, A.; Neumann, B.; Schaefer, A.; Dumbuya, K.; Kübel, C.; Biener, M. M.; Zielasek, V.; Steinrück, H.-P.; Gottfried, J. M.; Biener, J.; Hamza, A.; Bäumer, M.,

- Nanoporous Au: An Unsupported Pure Gold Catalyst? *J. Phys. Chem. C* **2009**, *113* (14), 5593-5600.
150. Xu, B.; Siler, C. G. F.; Madix, R. J.; Friend, C. M., Ag/Au Mixed Sites Promote Oxidative Coupling of Methanol on the Alloy Surface. *Chemistry - A European Journal* **2014**, *20* (16), 4646-4652.
 151. Hertz, H., Ueber einen Einfluss des ultravioletten Lichtes auf die elektrische Entladung. *Annalen der Physik* **1887**, *267* (8), 983-1000.
 152. Hallwachs, W., Ueber den Einfluss des Lichtes auf electrostatisch geladene Körper. *Annalen der Physik* **1888**, *269* (2), 301-312.
 153. Einstein, A., Über einen die Erzeugung und Verwandlung des Lichtes betreffenden heuristischen Gesichtspunkt. *Annalen der Physik* **1905**, *322* (6), 132-148.
 154. Tanuma, S.; Powell, C. J.; Penn, D. R., Calculations of electron inelastic mean free paths. *Surf. Interface Anal.* **2005**, *37* (1), 1-14.
 155. Seah, M. P.; Dench, W. A., Quantitative electron spectroscopy of surfaces: A standard data base for electron inelastic mean free paths in solids. *Surf. Interface Anal.* **1979**, *1* (1), 2-11.
 156. Probst, M. Photoelektronenspektroskopische Untersuchungen an reaktiven Übergangsmetallschichten auf MoO₃- und Si-Substraten. Dissertation, Friedrich-Alexander-Universität Erlangen-Nürnberg, Erlangen, 2003.
 157. Shirley, D. A., High-Resolution X-Ray Photoemission Spectrum of the Valence Bands of Gold. *Phys. Rev. B* **1972**, *5* (12), 4709-4714.
 158. Bates, C. W.; Wertheim, G. K.; Buchanan, D. N. E., Nature of the 3.8 eV plasmon in x-ray photoemission from silver. *Phys. Lett. A* **1979**, *72* (2), 178-180.
 159. Leiro, J.; Minni, E.; Suoninen, E., Study of plasmon structure in XPS spectra of silver and gold. *J. Phys. F: Met. Phys.* **1983**, *13* (1), 215.
 160. Mårtensson, N.; Nyholm, R.; Johansson, B., New observation of two-hole core-level satellites in copper, silver, and gold. *Phys. Rev. B* **1984**, *29* (8), 4800-4802.
 161. Schmid, M.; Kaftan, A.; Steinrück, H.-P.; Gottfried, J. M., The electronic structure of cobalt(II) phthalocyanine adsorbed on Ag(111). *Surf. Sci.* **2012**, *606* (11), 945-949.
 162. Uhl, B.; Hekmatfar, M.; Buchner, F.; Behm, R. J., Interaction of the ionic liquid [BMP][TFSA] with rutile TiO₂(110) and coadsorbed lithium. *Phys. Chem. Chem. Phys.* **2016**, *18* (9), 6618-6636.
 163. Buchner, F.; Forster-Tonigold, K.; Kim, J.; Bansmann, J.; Groß, A.; Behm, R. J., Interaction between Li, Ultrathin Adsorbed Ionic Liquid Films, and CoO(111) Thin Films: A Model Study of the Solid|Electrolyte Interphase Formation. *Chem. Mater.* **2019**, *31* (15), 5537-5549.
 164. Chan, B.; Chang, N.; Grimmett, M., The synthesis and thermolysis of imidazole quaternary salts. *Aust. J. Chem.* **1977**, *30* (9), 2005-2013.
 165. Lovelock, K. R. J.; Armstrong, J. P.; Licence, P.; Jones, R. G., Vaporisation and thermal decomposition of dialkylimidazolium halide ion ionic liquids. *Phys. Chem. Chem. Phys.* **2014**, *16* (4), 1339-1353.
 166. Armstrong, J. P.; Hurst, C.; Jones, R. G.; Licence, P.; Lovelock, K. R. J.; Satterley, C. J.; Villar-Garcia, I. J., Vapourisation of ionic liquids. *Phys. Chem. Chem. Phys.* **2007**, *9* (8), 982-990.
 167. Leal, J. P.; Esperança, J. M. S. S.; Minas da Piedade, M. E.; Canongia Lopes, J. N.; Rebelo, L. P. N.; Seddon, K. R., The Nature of Ionic Liquids in the Gas Phase. *J. Phys. Chem. A* **2007**, *111* (28), 6176-6182.
 168. Akai, N.; Parazs, D.; Kawai, A.; Shibuya, K., Cryogenic Neon Matrix-isolation FTIR Spectroscopy of Evaporated Ionic Liquids: Geometrical Structure of Cation–Anion 1:1 Pair in the Gas Phase. *J. Phys. Chem. B* **2009**, *113* (14), 4756-4762.

169. Hessey, S. G.; Jones, R. G., On the evaporation, bonding, and adsorbate capture of an ionic liquid on Au(111). *Chem. Sci.* **2013**, *4* (6), 2519-2529.
170. Horike, S.; Ayano, M.; Tsuno, M.; Fukushima, T.; Koshiba, Y.; Misaki, M.; Ishida, K., Thermodynamics of ionic liquid evaporation under vacuum. *Phys. Chem. Chem. Phys.* **2018**, *20* (33), 21262-21268.
171. Argile, C.; Rhead, G. E., Adsorbed layer and thin film growth modes monitored by Auger electron spectroscopy. *Surf. Sci. Rep.* **1989**, *10* (6), 277-356.
172. Tanuma, S.; Powell, C. J.; Penn, D. R., Calculations of electron inelastic mean free paths. V. Data for 14 organic compounds over the 50–2000 eV range. *Surf. Interface Anal.* **1994**, *21* (3), 165-176.
173. Bluhm, H., 4 - X-ray photoelectron spectroscopy (XPS) for in situ characterization of thin film growth. In *In Situ Characterization of Thin Film Growth*, Koster, G.; Rijnders, G., Eds. Woodhead Publishing: 2011; pp 75-98.
174. Deyko, A.; Bajus, S.; Rietzler, F.; Bösmann, A.; Wasserscheid, P.; Steinrück, H.-P.; Maier, F., Interface Properties and Physicochemical Characterization of the Low-Temperature Molten Salt Li/K/Cs Acetate. *J. Phys. Chem. C* **2013**, *117* (44), 22939-22946.
175. Morgado, P.; Lewis, J. B.; Laginhas, C. M. C.; Martins, L. F. G.; McCabe, C.; Blas, F. J.; Filipe, E. J. M., Systems Involving Hydrogenated and Fluorinated Chains: Volumetric Properties of Perfluoroalkanes and Perfluoroalkylalkane Surfactants. *J. Phys. Chem. B* **2011**, *115* (50), 15013-15023.
176. Lukaszcyk, T.; Flechtner, K.; Merte, L. R.; Jux, N.; Maier, F.; Gottfried, J. M.; Steinrück, H.-P., Interaction of Cobalt(II) Tetraarylporphyrins with a Ag(111) Surface Studied with Photoelectron Spectroscopy. *J. Phys. Chem. C* **2007**, *111* (7), 3090-3098.
177. Buchner, F.; Kellner, I.; Hieringer, W.; Görling, A.; Steinrück, H.-P.; Marbach, H., Ordering aspects and intramolecular conformation of tetraphenylporphyrins on Ag(111). *Phys. Chem. Chem. Phys.* **2010**, *12* (40), 13082-13090.
178. Di Santo, G.; Blankenburg, S.; Castellarin-Cudia, C.; Fanetti, M.; Borghetti, P.; Sangaletti, L.; Floreano, L.; Verdini, A.; Magnano, E.; Bondino, F.; Pignedoli, C. A.; Nguyen, M. T.; Gaspari, R.; Passerone, D.; Goldoni, A., Supramolecular Engineering through Temperature-Induced Chemical Modification of 2H-Tetraphenylporphyrin on Ag(111): Flat Phenyl Conformation and Possible Dehydrogenation Reactions. *Chemistry - A European Journal* **2011**, *17* (51), 14354-14359.
179. Taguchi, R.; Machida, H.; Sato, Y.; Smith, R. L., High-Pressure Densities of 1-Alkyl-3-methylimidazolium Hexafluorophosphates and 1-Alkyl-3-methylimidazolium Tetrafluoroborates at Temperatures from (313 to 473) K and at Pressures up to 200 MPa. *Journal of Chemical & Engineering Data* **2009**, *54* (1), 22-27.
180. Zafarani-Moattar, M. T.; Majdan-Cegincara, R., Viscosity, Density, Speed of Sound, and Refractive Index of Binary Mixtures of Organic Solvent + Ionic Liquid, 1-Butyl-3-methylimidazolium Hexafluorophosphate at 298.15 K. *Journal of Chemical & Engineering Data* **2007**, *52* (6), 2359-2364.
181. Klomfar, J.; Součková, M.; Pátek, J., Low Temperature Densities from (218 to 364) K and up to 50 MPa in Pressure and Surface Tension for Trihexyl(tetradecyl)phosphonium Bis(trifluoromethylsulfonyl)imide and Dicyanamide and 1-Hexyl-3-methylimidazolium Hexafluorophosphate. *Journal of Chemical & Engineering Data* **2014**, *59* (7), 2263-2274.
182. Rocha, M. A. A.; Ribeiro, F. M. S.; Ferreira, A. I. M. C. L.; Coutinho, J. A. P.; Santos, L. M. N. B. F., Thermophysical properties of [CN-1C1im][PF6] ionic liquids. *J. Mol. Liq.* **2013**, *188*, 196-202.
183. Mitlin, V. S., Dewetting Conditions for Ionic Liquid Films: Novel Features of the Stability Diagram. *J. Colloid Interface Sci.* **1995**, *170* (1), 65-70.

184. Liu, Y.; Zhang, Y.; Wu, G.; Hu, J., Coexistence of Liquid and Solid Phases of Bmim-PF6 Ionic Liquid on Mica Surfaces at Room Temperature. *J. Am. Chem. Soc.* **2006**, *128* (23), 7456-7457.
185. Bovio, S.; Podestà, A.; Lenardi, C.; Milani, P., Evidence of Extended Solidlike Layering in [Bmim][NTf2] Ionic Liquid Thin Films at Room-Temperature. *J. Phys. Chem. B* **2009**, *113* (19), 6600-6603.
186. Zhang, F.-C.; Sha, M.-L.; Ren, X.-P.; Wu, G.-Z.; JunHu; Zhang, Y., Morphology and Wettability of [Bmim] [PF6] Ionic Liquid on HOPG Substrate. *Chinese Physics Letters* **2010**, *27* (8), 086101.
187. Beattie, D. A.; Espinosa-Marzal, R. M.; Ho, T. T. M.; Popescu, M. N.; Ralston, J.; Richard, C. J. E.; Sellapperumage, P. M. F.; Krasowska, M., Molecularly-Thin Precursor Films of Imidazolium-Based Ionic Liquids on Mica. *J. Phys. Chem. C* **2013**, *117* (45), 23676-23684.
188. Gong, X.; Frankert, S.; Wang, Y.; Li, L., Thickness-dependent molecular arrangement and topography of ultrathin ionic liquid films on a silica surface. *Chem. Commun.* **2013**, *49* (71), 7803-7805.
189. Delcheva, I.; Ralston, J.; Beattie, D. A.; Krasowska, M., Static and dynamic wetting behaviour of ionic liquids. *Adv. Colloid Interface Sci.* **2015**, *222*, 162-171.
190. Gong, X.; Li, L., Understanding the wettability of nanometer-thick room temperature ionic liquids (RTILs) on solid surfaces. *Chin. Chem. Lett.* **2017**, *28* (11), 2045-2052.
191. Gong, X.; Wang, B.; Li, L., Spreading of Nanodroplets of Ionic Liquids on the Mica Surface. *ACS Omega* **2018**, *3* (12), 16398-16402.
192. Delcheva, I.; Beattie, D. A.; Ralston, J.; Krasowska, M., Dynamic wetting of imidazolium-based ionic liquids on gold and glass. *Phys. Chem. Chem. Phys.* **2018**, *20* (3), 2084-2093.
193. Panhwar, G. M.; Mysyk, R.; Rojo, T.; Shaikhutdinov, S.; Bondarchuk, O., Electrowetting of Ionic Liquid on Graphite: Probing via in Situ Electrochemical X-ray Photoelectron Spectroscopy. *Langmuir* **2018**, *34* (48), 14528-14536.
194. Bittner, R. W.; Bica, K.; Hoffmann, H., Fluorine-free, liquid-repellent surfaces made from ionic liquid-infused nanostructured silicon. *Monatshefte für Chemie - Chemical Monthly* **2017**, *148* (1), 167-177.
195. Mo, Y.; Wan, Y.; Chau, A.; Huang, F., Graphene/Ionic Liquid Composite Films and Ion Exchange. *Sci. Rep.* **2014**, *4*, 5466.
196. Malali, S.; Foroutan, M., Study of Wetting Behavior of BMIM+/PF6- Ionic Liquid on TiO2 (110) Surface by Molecular Dynamics Simulation. *J. Phys. Chem. C* **2017**, *121* (21), 11226-11233.
197. Bordes, E.; Douce, L.; Quitevis, E. L.; Pádua, A. A. H.; Costa Gomes, M., Ionic liquids at the surface of graphite: Wettability and structure. *J. Chem. Phys.* **2018**, *148* (19), 193840.
198. Uhl, B.; Buchner, F.; Alwast, D.; Wagner, N.; Behm, R. J., Adsorption of the ionic liquid [BMP][TFSA] on Au(111) and Ag(111): substrate effects on the structure formation investigated by STM. *Beilstein Journal of Nanotechnology* **2013**, *4*, 903-918.
199. Sobota, M.; Nikiforidis, I.; Hieringer, W.; Paape, N.; Happel, M.; Steinrück, H.-P.; Görling, A.; Wasserscheid, P.; Laurin, M.; Libuda, J., Toward Ionic-Liquid-Based Model Catalysis: Growth, Orientation, Conformation, and Interaction Mechanism of the [Tf2N]- Anion in [BMIM][Tf2N] Thin Films on a Well-Ordered Alumina Surface. *Langmuir* **2010**, *26* (10), 7199-7207.
200. Xu, T.; Waehler, T.; Vecchiotti, J.; Bonivardi, A.; Bauer, T.; Schwegler, J.; Schulz, P. S.; Wasserscheid, P.; Libuda, J., Interaction of Ester-Functionalized Ionic Liquids with

- Atomically-Defined Cobalt Oxides Surfaces: Adsorption, Reaction and Thermal Stability. *ChemPhysChem* **2017**, *18* (23), 3443-3453.
201. Xu, T.; Waehler, T.; Vecchiotti, J.; Bonivardi, A.; Bauer, T.; Schwegler, J.; Schulz, P. S.; Wasserscheid, P.; Libuda, J., Gluing Ionic Liquids to Oxide Surfaces: Chemical Anchoring of Functionalized Ionic Liquids by Vapor Deposition onto Cobalt(II) Oxide. *Angew. Chem.* **2017**, *129* (31), 9200-9204.
 202. Schernich, S.; Kostyshyn, D.; Wagner, V.; Taccardi, N.; Laurin, M.; Wasserscheid, P.; Libuda, J., Interactions Between the Room-Temperature Ionic Liquid [C2C1Im][OTf] and Pd(111), Well-Ordered Al₂O₃, and Supported Pd Model Catalysts from IR Spectroscopy. *J. Phys. Chem. C* **2014**, *118* (6), 3188-3193.
 203. Schernich, S.; Wagner, V.; Taccardi, N.; Wasserscheid, P.; Laurin, M.; Libuda, J., Interface Controls Spontaneous Crystallization in Thin Films of the Ionic Liquid [C2C1Im][OTf] on Atomically Clean Pd(111). *Langmuir* **2014**, *30* (23), 6846-6851.
 204. Bauer, T.; Mehl, S.; Brummel, O.; Pohako-Esko, K.; Wasserscheid, P.; Libuda, J., Ligand Effects at Ionic Liquid-Modified Interfaces: Coadsorption of [C2C1Im][OTf] and CO on Pd(111). *J. Phys. Chem. C* **2016**, *120* (8), 4453-4465.
 205. Mehl, S.; Bauer, T.; Brummel, O.; Pohako-Esko, K.; Schulz, P.; Wasserscheid, P.; Libuda, J., Ionic-Liquid-Modified Hybrid Materials Prepared by Physical Vapor Codeposition: Cobalt and Cobalt Oxide Nanoparticles in [C1C2Im][OTf] Monitored by In Situ IR Spectroscopy. *Langmuir* **2016**, *32* (34), 8613-8622.
 206. Waldmann, T.; Huang, H. H.; Hoster, H. E.; Höfft, O.; Endres, F.; Behm, R. J., Imaging an Ionic Liquid Adlayer by Scanning Tunneling Microscopy at the Solid|Vacuum Interface. *ChemPhysChem* **2011**, *12* (14), 2565-2567.
 207. Morino, Y.; Kanai, Y.; Imanishi, A.; Yokota, Y.; Fukui, K.-i., Fabrication of ionic liquid ultrathin film by sequential deposition. *Japanese Journal of Applied Physics* **2014**, *53* (5S1), 05FY01.
 208. Kaisei, K.; Kobayashi, K.; Matsushige, K.; Yamada, H., Fabrication of ionic liquid thin film by nano-inkjet printing method using atomic force microscope cantilever tip. *Ultramicroscopy* **2010**, *110* (6), 733-736.
 209. Stranski, I. N.; Krastanow, L., Zur Theorie der orientierten Ausscheidung von Ionenkristallen aufeinander. *Monatshefte für Chemie und verwandte Teile anderer Wissenschaften* **1937**, *71* (1), 351-364.
 210. Brochard-Wyart, F.; Di Meglio, J. M.; Quere, D.; De Gennes, P. G., Spreading of nonvolatile liquids in a continuum picture. *Langmuir* **1991**, *7* (2), 335-338.
 211. Costa, J. C. S.; Coelho, A. F. S. M. G.; Mendes, A.; Santos, L. M. N. B. F., Nucleation and growth of microdroplets of ionic liquids deposited by physical vapor method onto different surfaces. *Appl. Surf. Sci.* **2018**, *428*, 242-249.
 212. Venables, J. A.; Spiller, G. D. T.; Hanbucken, M., Nucleation and growth of thin films. *Rep. Prog. Phys.* **1984**, *47* (4), 399.
 213. Gyure, M. F.; Ratsch, C.; Merriman, B.; Caflisch, R. E.; Osher, S.; Zinck, J. J.; Vvedensky, D. D., Level-set methods for the simulation of epitaxial phenomena. *Physical Review E* **1998**, *58* (6), R6927-R6930.
 214. Chen, S.; Merriman, B.; Kang, M.; Caflisch, R. E.; Ratsch, C.; Cheng, L.-T.; Gyure, M.; Fedkiw, R. P.; Anderson, C.; Osher, S., A Level Set Method for Thin Film Epitaxial Growth. *Journal of Computational Physics* **2001**, *167* (2), 475-500.
 215. Ratsch, C.; Gyure, M. F.; Caflisch, R. E.; Gibou, F.; Petersen, M.; Kang, M.; Garcia, J.; Vvedensky, D. D., Level-set method for island dynamics in epitaxial growth. *Phys. Rev. B* **2002**, *65* (19), 195403.
 216. Ratsch, C.; Venables, J. A., Nucleation theory and the early stages of thin film growth. *Journal of Vacuum Science & Technology A: Vacuum, Surfaces, and Films* **2003**, *21* (5), S96-S109.

217. Liu, M.; Shao, Y.; Wu, Q., Charge reduction in ions in the ionic liquid 1-ethyl-2,3-dimethylimidazolium bis(trifluoromethanesulfonyl)imide on the Au(111) surface. *Theor. Chem. Acc.* **2020**, *139* (2), 24.
218. Zhang, Z.; Lagally, M. G., Atomistic Processes in the Early Stages of Thin-Film Growth. *Science* **1997**, *276* (5311), 377.
219. Rojas, G.; Chen, X.; Kunkel, D.; Bode, M.; Enders, A., Temperature Dependence of Metal–Organic Heteroepitaxy. *Langmuir* **2011**, *27* (23), 14267-14271.
220. Checcoli, P.; Conte, G.; Salvatori, S.; Paolesse, R.; Bolognesi, A.; Berliocchi, M.; Brunetti, F.; D’Amico, A.; Di Carlo, A.; Lugli, P., Tetra-phenyl porphyrin based thin film transistors. *Synth. Met.* **2003**, *138* (1), 261-266.
221. Chen, M.; Feng, X.; Zhang, L.; Ju, H.; Xu, Q.; Zhu, J.; Gottfried, J. M.; Ibrahim, K.; Qian, H.; Wang, J., Direct Synthesis of Nickel(II) Tetraphenylporphyrin and Its Interaction with a Au(111) Surface: A Comprehensive Study. *J. Phys. Chem. C* **2010**, *114* (21), 9908-9916.
222. Brédas, J. L.; Calbert, J. P.; da Silva Filho, D. A.; Cornil, J., Organic semiconductors: A theoretical characterization of the basic parameters governing charge transport. *Proceedings of the National Academy of Sciences* **2002**, *99* (9), 5804-5809.
223. Karl, N., Charge carrier transport in organic semiconductors. *Synth. Met.* **2003**, *133-134*, 649-657.
224. Thussing, S.; Jakob, P., Thermal Stability and Interlayer Exchange Processes in Heterolayers of CuPc and PTCDA on Ag(111). *J. Phys. Chem. C* **2017**, *121* (25), 13680-13691.
225. Thussing, S.; Fernández, L.; Jakob, P., Thermal stability and interlayer exchange processes in heterolayers of TiOPc and PTCDA on Ag(111). *J. Phys.: Condens. Matter* **2019**, *31* (13), 134002.
226. Shubina, T. E.; Marbach, H.; Flechtner, K.; Kretschmann, A.; Jux, N.; Buchner, F.; Steinrück, H.-P.; Clark, T.; Gottfried, J. M., Principle and Mechanism of Direct Porphyrin Metalation: Joint Experimental and Theoretical Investigation. *J. Am. Chem. Soc.* **2007**, *129* (30), 9476-9483.
227. Rojas, G.; Chen, X.; Bravo, C.; Kim, J.-H.; Kim, J.-S.; Xiao, J.; Dowben, P. A.; Gao, Y.; Zeng, X. C.; Choe, W.; Enders, A., Self-Assembly and Properties of Nonmetalated Tetraphenyl-Porphyrin on Metal Substrates. *J. Phys. Chem. C* **2010**, *114* (20), 9408-9415.
228. Zhang, X.-L.; Chen, L.-G.; Lv, P.; Gao, H.-Y.; Wei, S.-J.; Dong, Z.-C.; Hou, J. G., Fluorescence decay of quasimonolayered porphyrins near a metal surface separated by short-chain alkanethiols. *Appl. Phys. Lett.* **2008**, *92* (22), 223118.
229. Brede, J.; Linares, M.; Kuck, S.; Schwöbel, J.; Scarfato, A.; Chang, S.-H.; Hoffmann, G.; Wiesendanger, R.; Lensen, R.; Kouwer, P. H. J.; Hoogboom, J.; Rowan, A. E.; Bröring, M.; Funk, M.; Stafström, S.; Zerbetto, F.; Lazzaroni, R., Dynamics of molecular self-ordering in tetraphenyl porphyrin monolayers on metallic substrates. *Nanotechnology* **2009**, *20* (27), 275602.
230. Narioka, S.; Ishii, H.; Ouchi, Y.; Yokoyama, T.; Ohta, T.; Seki, K., XANES Spectroscopic Studies of Evaporated Porphyrin Films: Molecular Orientation and Electronic Structure. *The Journal of Physical Chemistry* **1995**, *99* (4), 1332-1337.
231. Polzonetti, G.; Carravetta, V.; Iucci, G.; Ferri, A.; Paolucci, G.; Goldoni, A.; Parent, P.; Laffon, C.; Russo, M. V., Electronic structure of platinum complex/Zn-porphyrinato assembled macrosystems, related precursors and model molecules, as probed by X-ray absorption spectroscopy (NEXAFS): theory and experiment. *Chem. Phys.* **2004**, *296* (1), 87-100.

232. Wang, S. D.; Dong, X.; Lee, C. S.; Lee, S. T., Orderly Growth of Copper Phthalocyanine on Highly Oriented Pyrolytic Graphite (HOPG) at High Substrate Temperatures. *J. Phys. Chem. B* **2004**, *108* (5), 1529-1532.
233. Cudia, C. C.; Vilmercati, P.; Larciprete, R.; Cepek, C.; Zampieri, G.; Sangaletti, L.; Pagliara, S.; Verdini, A.; Cossaro, A.; Floreano, L.; Morgante, A.; Petaccia, L.; Lizzit, S.; Battocchio, C.; Polzonetti, G.; Goldoni, A., Electronic structure and molecular orientation of a Zn-tetra-phenyl porphyrin multilayer on Si(111). *Surf. Sci.* **2006**, *600* (18), 4013-4017.
234. Stock, T. J. Z.; Nogami, J., Copper phthalocyanine thin films on Cu(111): Sub-monolayer to multi-layer. *Surf. Sci.* **2015**, *637-638*, 132-139.
235. He, Y.; Kröger, J.; Wang, Y., Organic Multilayer Films Studied by Scanning Tunneling Microscopy. *ChemPhysChem* **2017**, *18* (5), 429-450.
236. Rojas, G.; Simpson, S.; Chen, X.; Kunkel, D. A.; Nitz, J.; Xiao, J.; Dowben, P. A.; Zurek, E.; Enders, A., Surface state engineering of molecule–molecule interactions. *Phys. Chem. Chem. Phys.* **2012**, *14* (14), 4971-4976.
237. Comanici, K.; Buchner, F.; Flechtner, K.; Lukasczyk, T.; Gottfried, J. M.; Steinrück, H.-P.; Marbach, H., Understanding the Contrast Mechanism in Scanning Tunneling Microscopy (STM) Images of an Intermixed Tetrphenylporphyrin Layer on Ag(111). *Langmuir* **2008**, *24* (5), 1897-1901.
238. Buchner, F.; Flechtner, K.; Bai, Y.; Zillner, E.; Kellner, I.; Steinrück, H.-P.; Marbach, H.; Gottfried, J. M., Coordination of Iron Atoms by Tetrphenylporphyrin Monolayers and Multilayers on Ag(111) and Formation of Iron-Tetrphenylporphyrin. *J. Phys. Chem. C* **2008**, *112* (39), 15458-15465.
239. Buchner, F.; Warnick, K.-G.; Wölfle, T.; Görling, A.; Steinrück, H.-P.; Hieringer, W.; Marbach, H., Chemical Fingerprints of Large Organic Molecules in Scanning Tunneling Microscopy: Imaging Adsorbate–Substrate Coupling of Metalloporphyrins. *J. Phys. Chem. C* **2009**, *113* (37), 16450-16457.
240. Di Santo, G.; Castellarin-Cudia, C.; Fanetti, M.; Taleatu, B.; Borghetti, P.; Sangaletti, L.; Floreano, L.; Magnano, E.; Bondino, F.; Goldoni, A., Conformational Adaptation and Electronic Structure of 2H-Tetrphenylporphyrin on Ag(111) during Fe Metalation. *J. Phys. Chem. C* **2011**, *115* (10), 4155-4162.
241. Di Santo, G.; Sfiligoj, C.; Castellarin-Cudia, C.; Verdini, A.; Cossaro, A.; Morgante, A.; Floreano, L.; Goldoni, A., Changes of the Molecule–Substrate Interaction upon Metal Inclusion into a Porphyrin. *Chemistry - A European Journal* **2012**, *18* (40), 12619-12623.
242. Seufert, K.; Auwärter, W.; García de Abajo, F. J.; Ecija, D.; Vijayaraghavan, S.; Joshi, S.; Barth, J. V., Controlled Interaction of Surface Quantum-Well Electronic States. *Nano Lett.* **2013**, *13* (12), 6130-6135.
243. Bauer, E., Phänomenologische Theorie der Kristallabscheidung an Oberflächen. I. In *Zeitschrift für Kristallographie - Crystalline Materials*, 1958; Vol. 110, p 372.
244. Kilian, L.; Umbach, E.; Sokolowski, M., Molecular beam epitaxy of organic films investigated by high resolution low energy electron diffraction (SPA-LEED): 3,4,9,10-perylenetetracarboxylicacid-dianhydride (PTCDA) on Ag(111). *Surf. Sci.* **2004**, *573* (3), 359-378.
245. Marchetto, H.; Schmidt, T.; Groh, U.; Maier, F. C.; Lévesque, P. L.; Fink, R. H.; Freund, H.-J.; Umbach, E., Direct observation of epitaxial organic film growth: temperature-dependent growth mechanisms and metastability. *Phys. Chem. Chem. Phys.* **2015**, *17* (43), 29150-29160.
246. Schmidt, T.; Marchetto, H.; Groh, U.; Fink, R. H.; Freund, H.-J.; Umbach, E., Influence of Substrate Bonding and Surface Morphology on Dynamic Organic Layer

- Growth: Perylenetetracarboxylic Dianhydride on Au(111). *Langmuir* **2018**, *34* (19), 5444-5453.
247. Schmidt, T.; Marchetto, H.; Groh, U.; Fink, R. H.; Umbach, E., Complex Monolayer Growth Dynamics of a Highly Symmetric Molecule: NTCDA on Ag(111). *J. Phys. Chem. C* **2019**, *123* (13), 8244-8255.
248. Habenschaden, E.; Küppers, J., Evaluation of flash desorption spectra. *Surf. Sci.* **1984**, *138* (1), L147-L150.
249. Zaitsau, D. H.; Yermalayeu, A. V.; Emel'yanenko, V. N.; Verevkin, S. P., Thermodynamics of Imidazolium-Based Ionic Liquids Containing the Trifluoromethanesulfonate Anion. *Chemical Engineering & Technology* **2018**, *41* (8), 1604-1612.
250. Verevkin, S. P.; Zaitsau, D. H.; Emel'yanenko, V. N.; Yermalayeu, A. V.; Schick, C.; Liu, H.; Maginn, E. J.; Bulut, S.; Krossing, I.; Kalb, R., Making Sense of Enthalpy of Vaporization Trends for Ionic Liquids: New Experimental and Simulation Data Show a Simple Linear Relationship and Help Reconcile Previous Data. *J. Phys. Chem. B* **2013**, *117* (21), 6473-6486.
251. Zaitsau, D. H.; Yermalayeu, A. V.; Schubert, T. J. S.; Verevkin, S. P., Alkyl-imidazolium tetrafluoroborates: Vapor pressure, thermodynamics of vaporization, and enthalpies of formation. *J. Mol. Liq.* **2017**, *242* (Supplement C), 951-957.
252. Zaitsau, D. H.; Yermalayeu, A. V.; Emel'yanenko, V. N.; Butler, S.; Schubert, T.; Verevkin, S. P., Thermodynamics of Imidazolium-Based Ionic Liquids Containing PF₆ Anions. *J. Phys. Chem. B* **2016**, *120* (32), 7949-7957.
253. Buckley, M. Ionic liquids interacting with small molecules and a gold (110) surface. PhD thesis, University of Nottingham, UK, 2016.
254. Buckley, M.; Syres, Karen L.; Jones, R. G., Interactions and stabilisation of acetone, sulfur dioxide and water with 1-octyl-3-methylimidazolium tetrafluoroborate [OMIM][BF₄] at low temperatures. *Faraday Discuss.* **2018**, *206* (0), 475-495.
255. Chambreau, S. D.; Vaghjiani, G. L.; To, A.; Koh, C.; Strasser, D.; Kostko, O.; Leone, S. R., Heats of Vaporization of Room Temperature Ionic Liquids by Tunable Vacuum Ultraviolet Photoionization. *J. Phys. Chem. B* **2010**, *114* (3), 1361-1367.
256. Redhead, P. A., Thermal desorption of gases. *Vacuum* **1962**, *12* (4), 203-211.
257. Falconer, J. L.; Madix, R. J., Flash desorption activation energies: DCOOH decomposition and CO desorption from Ni (110). *Surf. Sci.* **1975**, *48* (2), 393-405.
258. Meyers, J. M.; Gellman, A. J., Effect of substituents on the phenyl coupling reaction on Cu(111). *Surf. Sci.* **1995**, *337* (1), 40-50.
259. Heller, B. S. J.; Lexow, M.; Greco, F.; Shin, S.; Partl, G.; Maier, F.; Steinrück, H.-P., Temperature-dependent surface enrichment effects in binary mixtures of fluorinated and non-fluorinated ionic liquids. *Chemistry – A European Journal* **2019**, *26*, 1117-1126.
260. Heller, B. S. J.; Paap, U.; Maier, F.; Steinrück, H.-P., Pronounced surface enrichment of fluorinated ionic liquids in binary mixtures with methoxy-functionalized ionic liquids. *J. Mol. Liq.* **2020**, *305*, 112783.
261. Nakajima, K.; Lísal, M.; Kimura, K., Surfaces of Ionic Liquids. In *Surface and Interface Science*, Wandelt, K., Ed. Wiley-VCH: 2020; Vol. 7, pp 351-389.
262. Zaitsau, D. H.; Paulechka, Y. U.; Kabo, G. J., The Kinetics of Thermal Decomposition of 1-Butyl-3-methylimidazolium Hexafluorophosphate. *J. Phys. Chem. A* **2006**, *110* (41), 11602-11604.
263. Luís, A.; Shimizu, K.; Araújo, J. M. M.; Carvalho, P. J.; Lopes-da-Silva, J. A.; Canongia Lopes, J. N.; Rebelo, L. P. N.; Coutinho, J. A. P.; Freire, M. G.; Pereira, A. B., Influence of Nanosegregation on the Surface Tension of Fluorinated Ionic Liquids. *Langmuir* **2016**, *32* (24), 6130-6139.

264. Tariq, M.; Freire, M. G.; Saramago, B.; Coutinho, J. A. P.; Lopes, J. N. C.; Rebelo, L. P. N., Surface tension of ionic liquids and ionic liquid solutions. *Chem. Soc. Rev.* **2012**, *41* (2), 829-868.
265. Merrigan, T. L.; Bates, E. D.; Dorman, S. C.; Davis Jr, J. H., New fluorosurfactant ionic liquids function as surfactants in conventional room-temperature ionic liquids. *Chem. Commun.* **2000**, (20), 2051-2052.
266. Offord, D. A.; Sachs, S. B.; Ennis, M. S.; Eberspacher, T. A.; Griffin, J. H.; Chidsey, C. E. D.; Collman, J. P., Synthesis and Properties of Metalloporphyrin Monolayers and Stacked Multilayers Bound to an Electrode via Site Specific Axial Ligation to a Self-Assembled Monolayer. *J. Am. Chem. Soc.* **1998**, *120* (18), 4478-4487.
267. Zhang, Z.; Hou, S.; Zhu, Z.; Liu, Z., Preparation and Characterization of a Porphyrin Self-Assembled Monolayer with a Controlled Orientation on Gold. *Langmuir* **2000**, *16* (2), 537-540.
268. Zhang, Z.; Imae, T.; Sato, H.; Watanabe, A.; Ozaki, Y., Surface-Enhanced Raman Scattering and Surface-Enhanced Infrared Absorption Spectroscopic Studies of a Metalloporphyrin Monolayer Film Formed on Pyridine Self-Assembled Monolayer-Modified Gold. *Langmuir* **2001**, *17* (15), 4564-4568.
269. Gallego, J. M.; Ecija, D.; Martín, N.; Otero, R.; Miranda, R., An STM study of molecular exchange processes in organic thin film growth. *Chem. Commun.* **2014**, *50* (69), 9954-9957.
270. Wang, Q.; Franco-Cañellas, A.; Ji, P.; Bürker, C.; Wang, R.-B.; Broch, K.; Thakur, P. K.; Lee, T.-L.; Zhang, H.; Gerlach, A.; Chi, L.; Duhm, S.; Schreiber, F., Bilayer Formation vs Molecular Exchange in Organic Heterostructures: Strong Impact of Subtle Changes in Molecular Structure. *J. Phys. Chem. C* **2018**, *122* (17), 9480-9490.
271. Deimel, P. S.; Feulner, P.; Barth, J. V.; Allegretti, F., Spatial decoupling of macrocyclic metal-organic complexes from a metal support: a 4-fluorothiophenol self-assembled monolayer as a thermally removable spacer. *Phys. Chem. Chem. Phys.* **2019**, *21* (21), 10992-11003.
272. Kanjilal, A.; Ottaviano, L.; Di Castro, V.; Beccari, M.; Betti, M. G.; Mariani, C., Pentacene Grown on Self-Assembled Monolayer: Adsorption Energy, Interface Dipole, and Electronic Properties. *J. Phys. Chem. C* **2007**, *111* (1), 286-293.
273. Wei, Y.; Reutt-Robey, J. E., Directed Organization of C70 Kagome Lattice by Titanyl Phthalocyanine Monolayer Template. *J. Am. Chem. Soc.* **2011**, *133* (39), 15232-15235.
274. Skomski, D.; Tait, S. L., Interfacial Organic Layers for Chemical Stability and Crystalline Ordering of Thiophene and Carboxyl Films on a Metal Surface. *J. Phys. Chem. C* **2014**, *118* (3), 1594-1601.
275. Korolkov, V. V.; Baldoni, M.; Watanabe, K.; Taniguchi, T.; Besley, E.; Beton, P. H., Supramolecular heterostructures formed by sequential epitaxial deposition of two-dimensional hydrogen-bonded arrays. *Nature Chemistry* **2017**, *9*, 1191.
276. Buck, M., A step beyond flatland. *Nature Chemistry* **2017**, *9*, 1152.
277. Chen, S.; Wu, G.; Sha, M.; Huang, S., Transition of Ionic Liquid [bmim][PF₆] from Liquid to High-Melting-Point Crystal When Confined in Multiwalled Carbon Nanotubes. *J. Am. Chem. Soc.* **2007**, *129*, 2416-2417.
278. Auwärter, W.; Weber-Bargioni, A.; Brink, S.; Riemann, A.; Schiffrin, A.; Ruben, M.; Barth, J. V., Controlled Metalation of Self-Assembled Porphyrin Nanoarrays in Two Dimensions. *ChemPhysChem* **2007**, *8* (2), 250-254.
279. Kolb, T.; Neuber, C.; Krysak, M.; Ober, C. K.; Schmidt, H.-W., Multicomponent Physical Vapor Deposited Films with Homogeneous Molecular Material Distribution Featuring Improved Resist Sensitivity. *Adv. Funct. Mater.* **2012**, *22* (18), 3865-3873.

280. Happel, M.; Desikusumastuti, A.; Sobota, M.; Laurin, M.; Libuda, J., Impact of Sulfur Poisoning on the NO_x Uptake of a NO_x Storage and Reduction (NSR) Model Catalyst. *J. Phys. Chem. C* **2010**, *114* (10), 4568-4575.
281. Happel, M.; Lykhach, Y.; Tsud, N.; Skála, T.; Prince, K. C.; Matolín, V.; Libuda, J., Mechanism of Sulfur Poisoning and Storage: Adsorption and Reaction of SO₂ with Stoichiometric and Reduced Ceria Films on Cu(111). *J. Phys. Chem. C* **2011**, *115* (40), 19872-19882.
282. Papp, C.; Steinrück, H.-P., In situ high-resolution X-ray photoelectron spectroscopy – Fundamental insights in surface reactions. *Surf. Sci. Rep.* **2013**, *68* (3), 446-487.
283. Bauer, T.; Maisel, S.; Blaumeiser, D.; Vecchiotti, J.; Taccardi, N.; Wasserscheid, P.; Bonivardi, A.; Görling, A.; Libuda, J., Operando DRIFTS and DFT Study of Propane Dehydrogenation over Solid- and Liquid-Supported Ga₂O Catalysts. *ACS Catalysis* **2019**, *9* (4), 2842-2853.

7. Acknowledgements

I would like to express my overwhelming gratitude to Prof. Dr. Hans-Peter Steinrück, for providing an excellent research environment, for his patience, advice, trust and understanding, and for sharing a life-time of experience in UHV surface science with me,

To Dr. Florian Maier, for challenging, mentoring, and inspiring me inside and outside of this project,

To Dr. Andreas Bayer, for very enjoyable conversations and for overseeing and managing all technical aspects of our labs,

To Bernd Kreß and Hans-Peter Bäumler, for all the invaluable and uncomplicated help and support in the lab,

To Susana Kreß and Andrea Meixner-Wolf, for all the help and support with everything outside of the lab,

To the shared workshop of the Chairs of Physical Chemistry,

To Dr. Nicola Taccardi and Dr. Gabriel Partl, for fruitful collaboration,

To all of my colleagues at FAU and especially at PC II,

And last but not least, to my wife, my family and my friends for always being patient with me and for supporting me throughout all challenges!

8. Appendix

8.1 Atomic Sensitivity Factors for XPS

The atomic sensitivity factors (ASFs) that were used for the quantitative analysis of the XPS spectra in this work are provided in Table 4 along with the constraints for fitting the P 2p and S 2p signals, that is, the ratio between the two spin-orbit split components of the core level, the relative full width at half maximum (FWHM) of the two lines, and the separation in binding energy.

Table 4: ASFs and constraints (peak ratio, full width at half maximum (FWHM), peak separation (ΔE_b)) for fitting the two peaks of the 2p core levels, used for the quantitative analysis of XPS data.

Core level	C 1s	F 1s	N 1s	O 1s	P 2p	S 2p
ASF	0.21	1	0.36	0.60	0.31	0.41
Peak ratio (1/2 to 3/2)					1:2	1:2
FWHM					Set equal	Set equal
$\Delta E_b / \text{eV}$					0.90	1.18

8.2 Calculated IL Monolayer Heights

The height h of 1 ML of various ILs as calculated with Eq. 4 is shown in Figure 9. Table 5 provides the corresponding values for the homologous series of $[\text{C}_n\text{C}_1\text{Im}]^+$ cations with $[\text{Tf}_2\text{N}]^-$ and $[\text{PF}_6]^-$ anions.

Table 5: Calculated monolayer height h for ILs of the homologous series of $[\text{C}_n\text{C}_1\text{Im}]\text{X}$ with $[\text{Tf}_2\text{N}]^-$ and $[\text{PF}_6]^-$ anions. The values are based on density data from literature as indicated.

n	$[\text{C}_n\text{C}_1\text{Im}][\text{Tf}_2\text{N}]$	$[\text{C}_n\text{C}_1\text{Im}][\text{PF}_6]$
1	0.74 ⁸	
2	0.75 ^{8, 147}	0.65 ¹⁷⁹
4	0.79 ^{8, 147}	0.70 ^{147, 180, 182}
5		0.72 ¹⁸²
6	0.82 ^{8, 147}	0.74 ^{147, 181-182}
7		0.75 ¹⁸²
8	0.84 ^{8, 128}	0.77 ^{8, 147, 182}
9		0.79 ¹⁸²
10	0.87 ^{8, 147}	0.80 ¹⁴⁷
12	0.89 ⁸	
14	0.92 ¹²⁸	

8.3 Variation of X-Ray Gun Power During Time-Dependent XPS

To investigate a possible influence of X-rays on the IL growth, the time-dependent behavior of $[C_1C_1Im][Tf_2N]$ films after IL PVD on Ag(111) at RT (*cf.* Chapter 3.2) was measured with varying power of the X-ray gun during time-dependent XPS. Figure 24a shows the temporal evolution of the intensity ratio I_d/I_0 of the Ag 3d core level of the supporting Ag(111) for three films of similar thickness (about 1.5 to 2.0 nm nominal thickness) at emission currents between X-ray gun filament and anode of 2 and 20 mA, respectively. This difference in emission current directly results in a variation of the photon flux by a factor of ten (which also means, the signal intensities in XPS are by a factor of ten lower for 2 mA than for 20 mA). For reference, the 0° data from Figure 12a¹⁰³ is included in Figure 23a. Comparing the curves in Figure 23a, the morphology changes in the film are considerably slower for the lower emission current of 2 mA. At 20 mA, the peak intensity levels off after less than 60 min, whereas at 2 mA, the intensity only begins to decrease after this period and seems to level off only after more than 6 hours. The plot of absolute signal intensities in Figure 23b shows how the F 1s signal related to the $[Tf_2N]^-$ anion of the IL increases correspondingly on the same time scales as the Ag 3d signal decreases. Notably, the shapes of the individual XP peaks show no sign of beam damage.

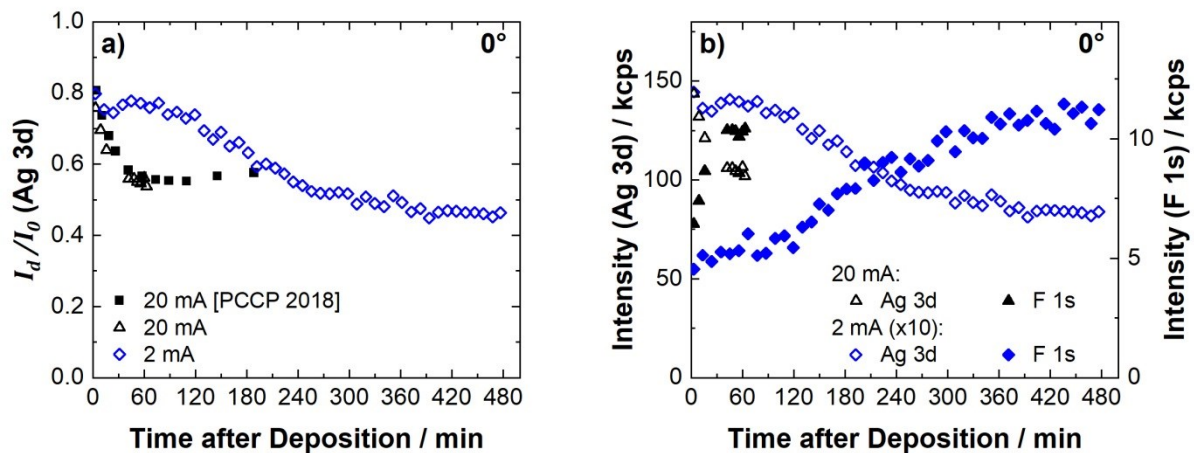


Figure 23: Temporal evolution of the Ag 3d (support) and F 1s (IL) signal intensities from time-dependent ARXPS of the IL films of $[C_1C_1Im][Tf_2N]$ after ending the IL deposition of equivalents of approximately 2 ML on Ag(111) at RT. a) I_d/I_0 (Ag 3d) and b) absolute intensities of Ag 3d and F 1s core levels. The emission current between filament and anode of the X-ray gun was varied between 2 and 20 mA, that is, a variation of the power from 24 to 240 W (at 12 kV). I_d/I_0 (Ag 3d) data for 20 mA (squares in a) adapted from Ref. ¹⁰³. See also Figure 12a.

The time-dependent decrease of the intensity of the Ag 3d signal observed experimentally after ending the deposition indicates the slow transformation of the $[C_1C_1Im][Tf_2N]$ film

towards a flat morphology, as concluded from the stronger signal attenuation of the supporting Ag crystal.¹⁰³ The simultaneous increase in the IL-related F 1s signal intensity supports this assumption. The interpretation provided in Chapter 3.2 was that flat films are thermodynamically more stable than pronounced 3D islands.¹⁰³ In line with a similar study by Foulston *et al.*,¹⁴⁶ the initial 3D islands that form during IL deposition were assumed to be kinetically stabilized and flatten only slowly over time.¹⁰³ The results of Figure 23 indicate that the magnitude of the X-ray photon flux during measurement affects the timescale of the morphology changes as well. The origin of this effect is not clear at the moment. One possibility is that the X-rays induce a small number of defects (too few to be detected in XPS) in the WL or in the form of isolated fragments on top of it which serve as additional nuclei for 2D island formation. Hence, the flattening process described in Chapter 3.2 towards a thermodynamically more stable 2D layer could be accelerated by these nuclei. While local temperature changes due to the varying power of the X-ray source can be ruled out, other possible factors accelerating the transition to 2D islands might be an enhanced emission of ion pairs or ions from the 3D islands due to processes stimulated by X-rays (or secondary electrons), or due to repulsive Coulomb interactions after the photoemission (and subsequent de-excitation processes): As charge neutralization by electron transport from the metal substrate requires some time, the accumulated positive charge in a 3D island could depend on the photon flux.

After deposition of the same amount of $[\text{C}_1\text{C}_1\text{Im}][\text{Tf}_2\text{N}]$ on Ag(111) at 90 K, initially a film thickness of 2.0 nm is determined from XPS. Upon heating to RT, this apparent film thickness decreases from 2.0 to 0.7 nm, indicating changes in the film morphology towards the formation of pronounced 3D islands. Similar morphology changes were observed by Syres and Jones for $[\text{C}_8\text{C}_1\text{Im}][\text{BF}_4]$ on Cu(111) upon heating to RT after deposition at 120 K.¹³⁸ For the initial characterization of the film of $[\text{C}_1\text{C}_1\text{Im}][\text{Tf}_2\text{N}]$ on Ag(111) after deposition at 90 K, the X-ray exposure was limited to 6 min at 20 mA emission current of the X-ray gun. The temporal evolution of the Ag 3d and F 1s signals in Figure 24 from time-dependent XPS after heating to RT shows that the IL then behaves identical compared to a film deposited at RT. The ratio of I_d/I_0 (Figure 24a) as well as the absolute intensity of the Ag 3d core level (Figure 24b) related to the Ag(111) crystal decrease at the same rate for both preparation routes from similar starting to final intensities while the F 1s intensity (Figure 24b) related to the IL anion simultaneously increases.

Time-dependent spreading of IL droplets was also reported in AFM studies on mica.^{187, 191} These experiments were, however, conducted in absence of ionizing radiation and the morphology changes occurred on the time-scale of tens of hours.

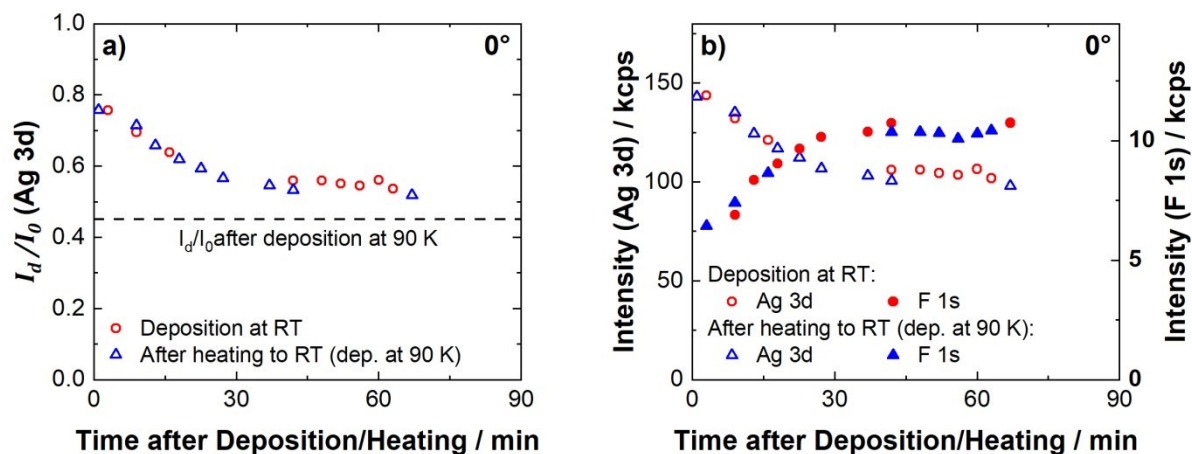
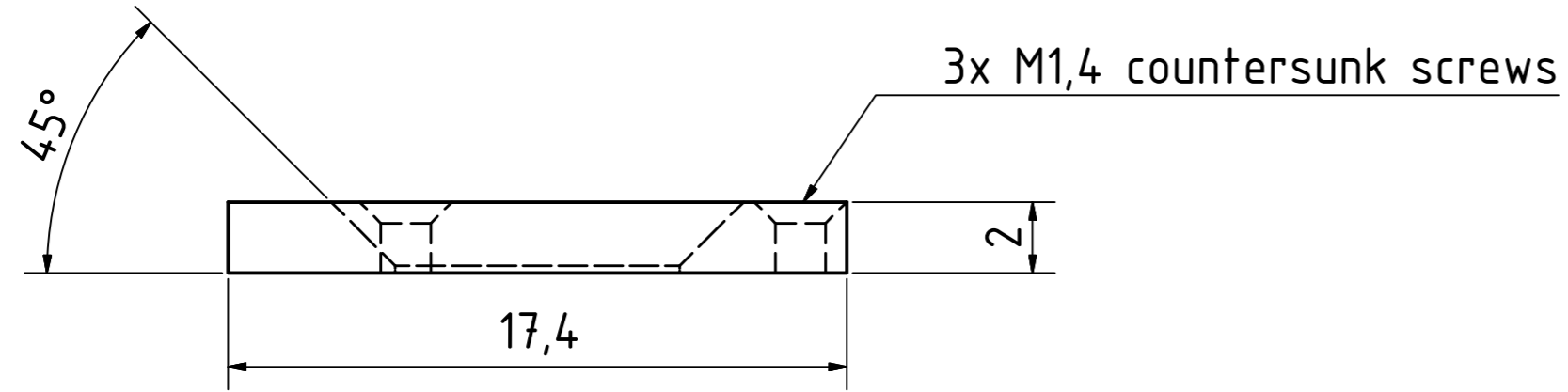


Figure 24: Temporal evolution of the Ag 3d (support) and F 1s (IL) signal intensities from time-dependent XPS (0°) of films of [C₁C₁Im][Tf₂N] after ending the IL deposition on Ag(111) at RT (red circles) and after heating to RT after IL deposition at 90 K (blue triangles). a) I_d/I_0 (Ag 3d) and b) absolute intensities of Ag 3d and F 1s core levels.

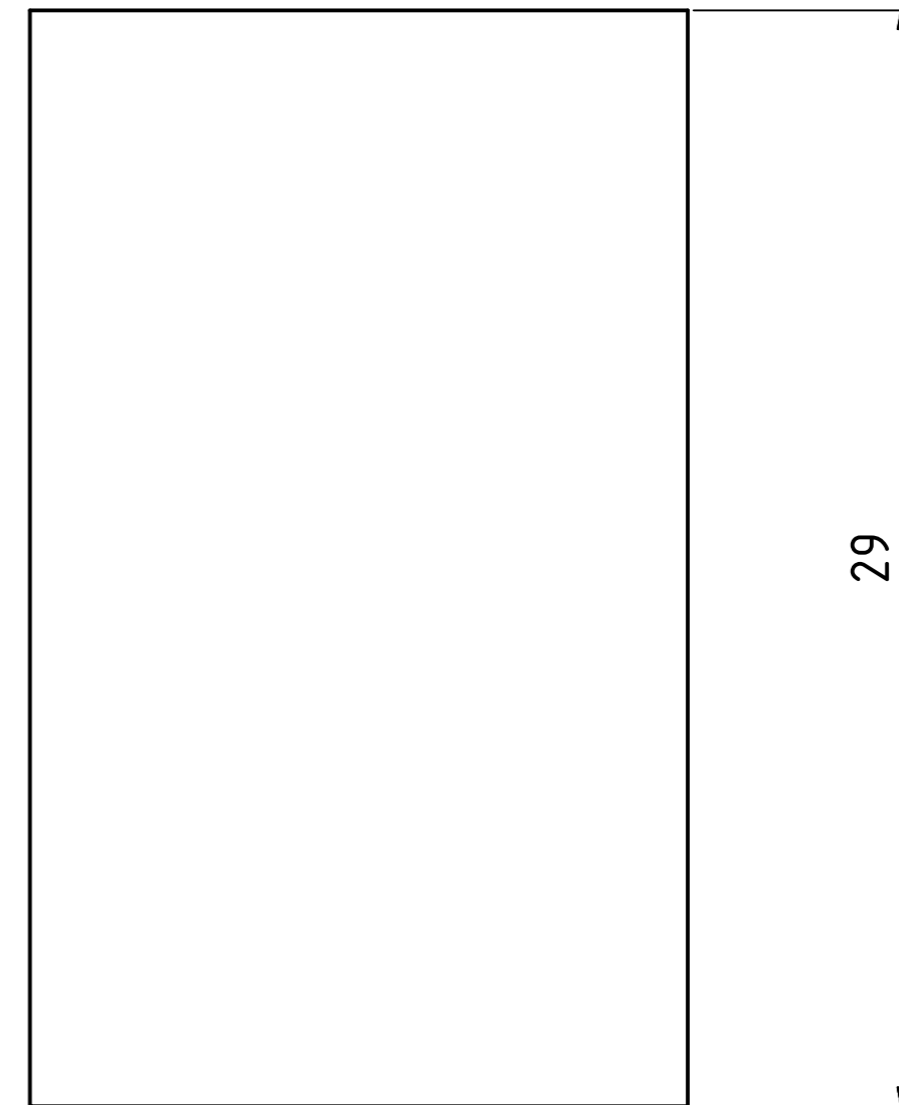
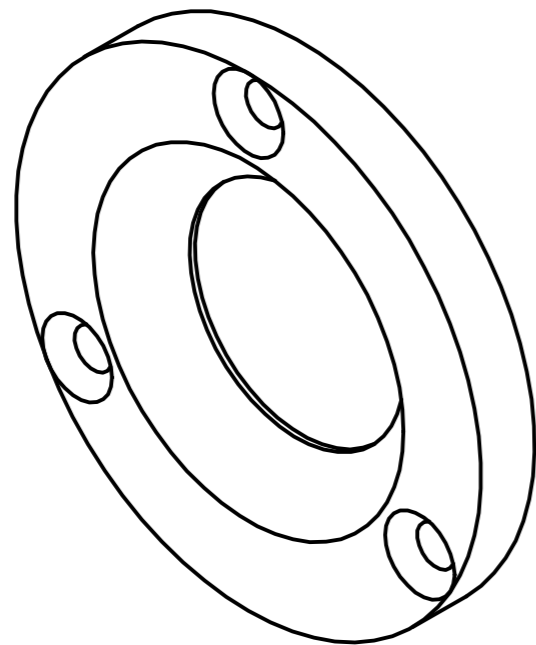
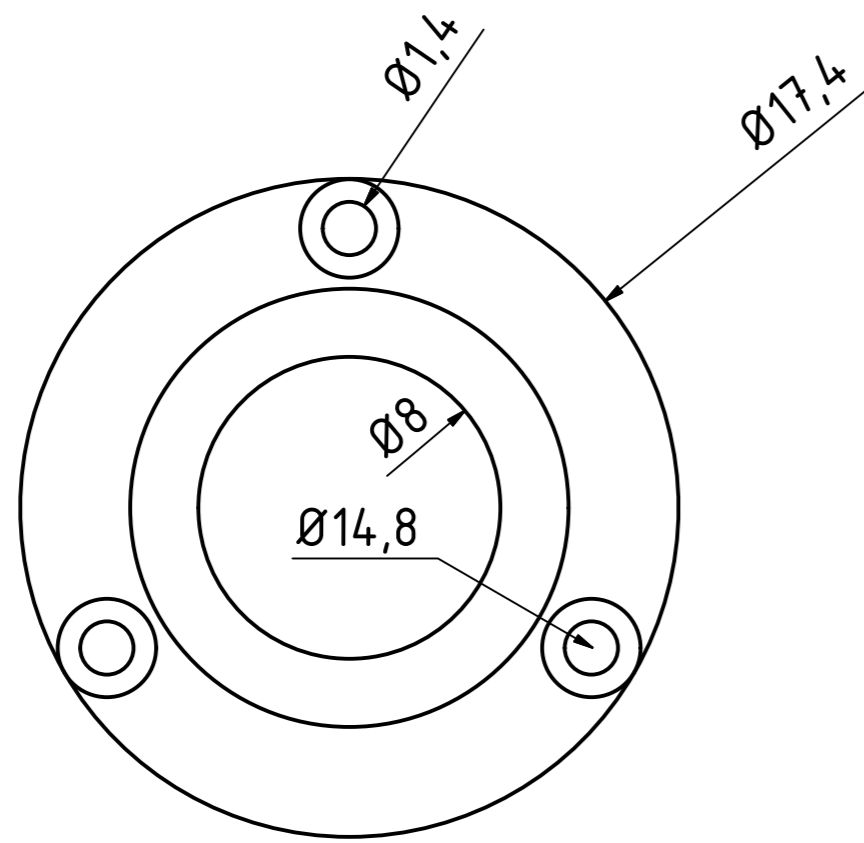
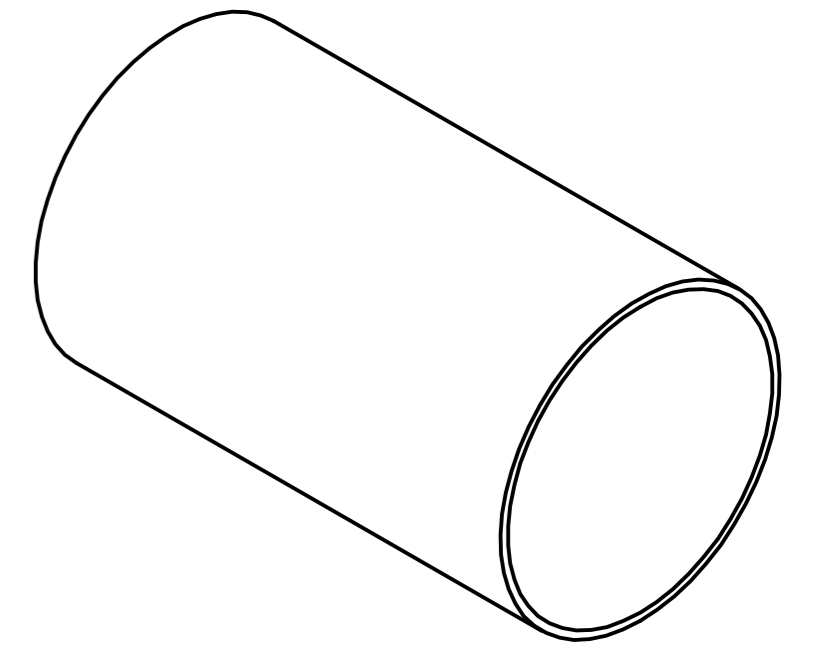
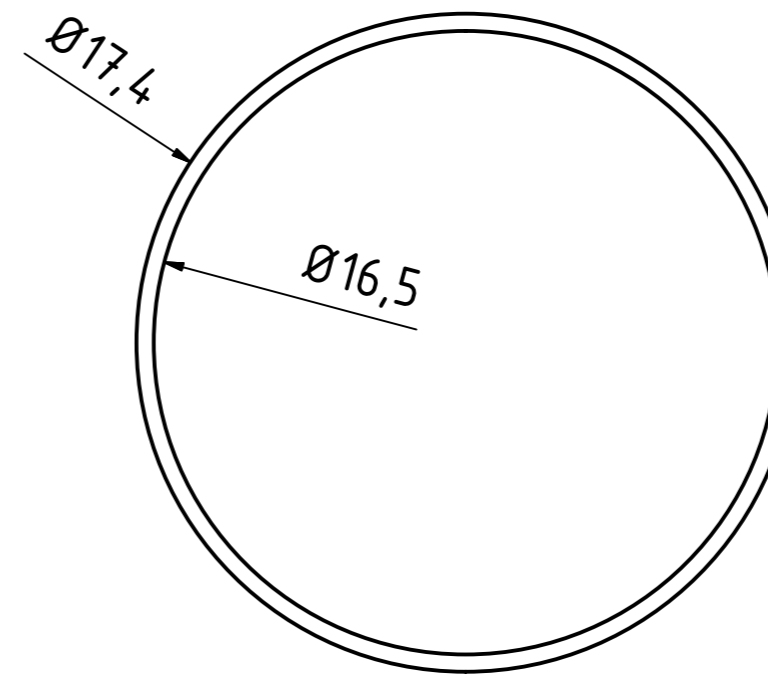
8.4 Technical Drawings of the IL Evaporator Parts

The complete technical drawings of the IL evaporator parts are provided on the following pages.

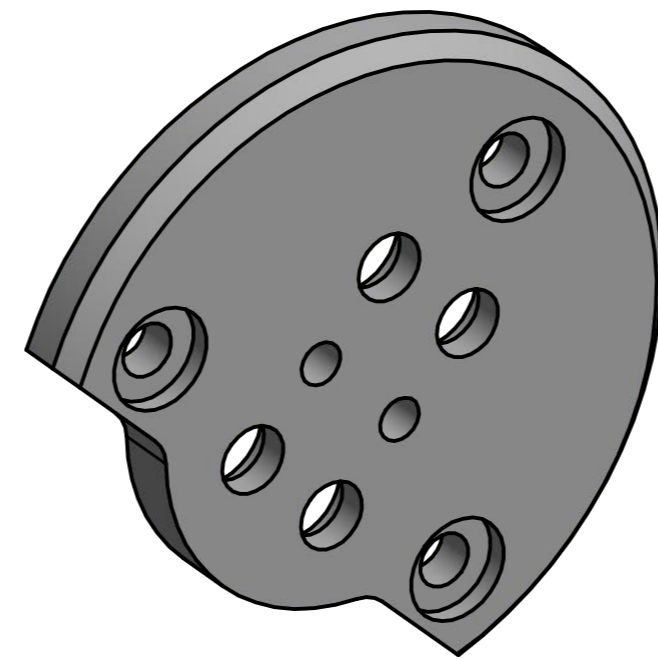
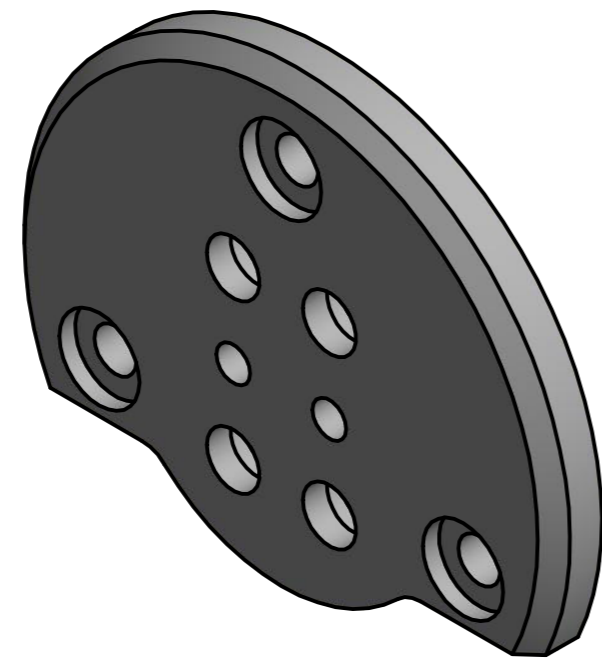
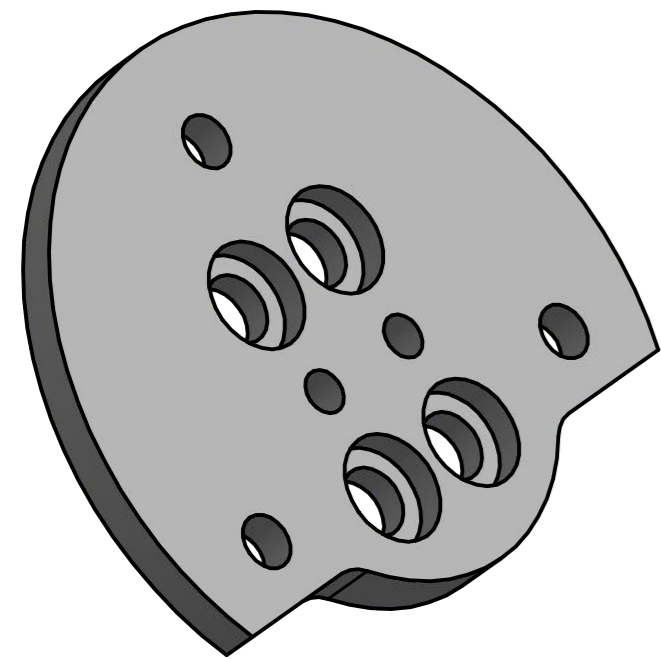
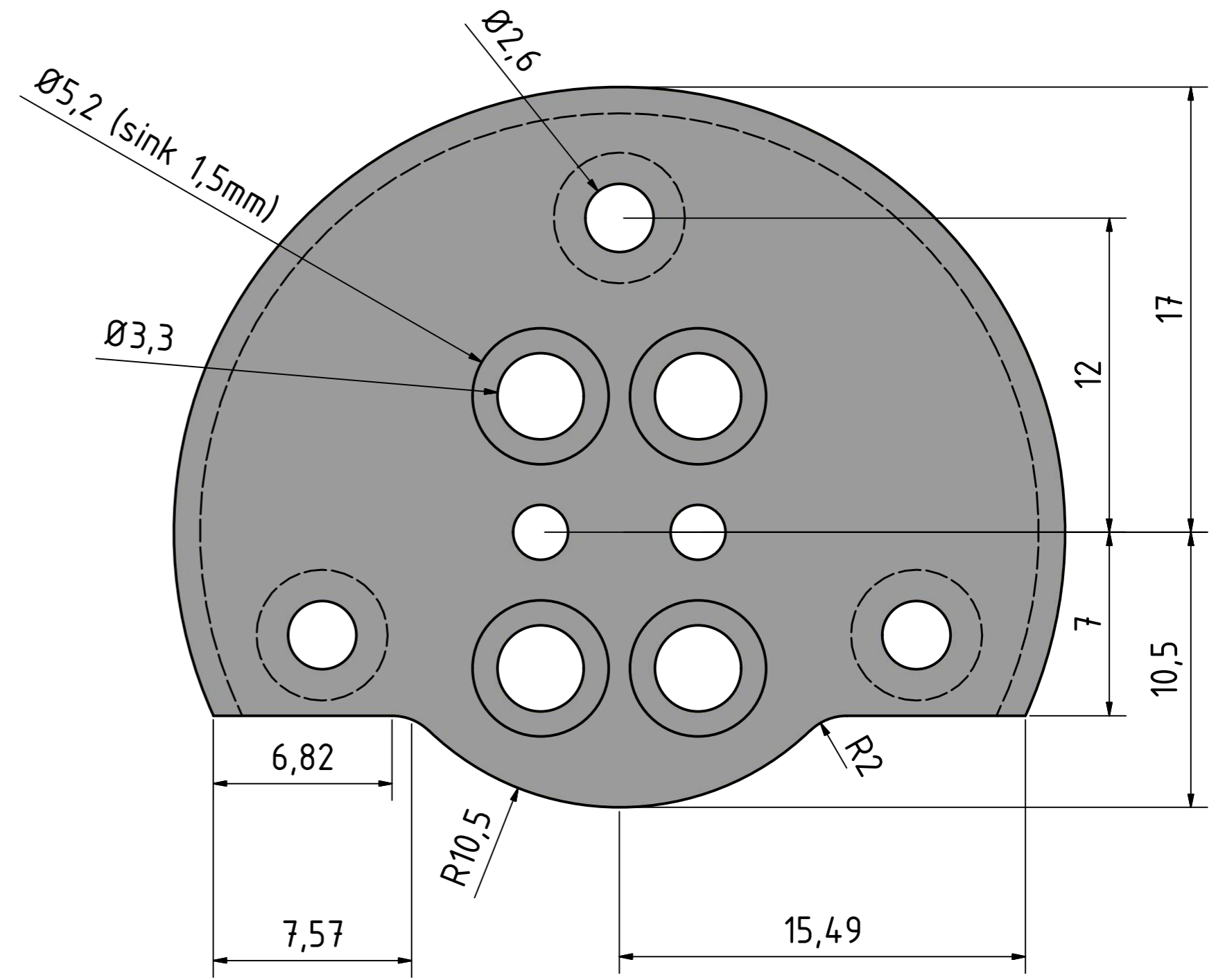
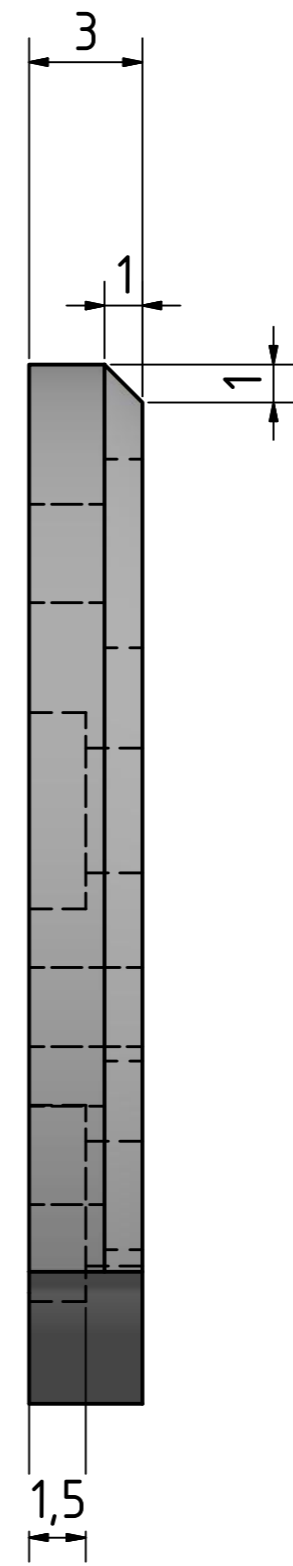
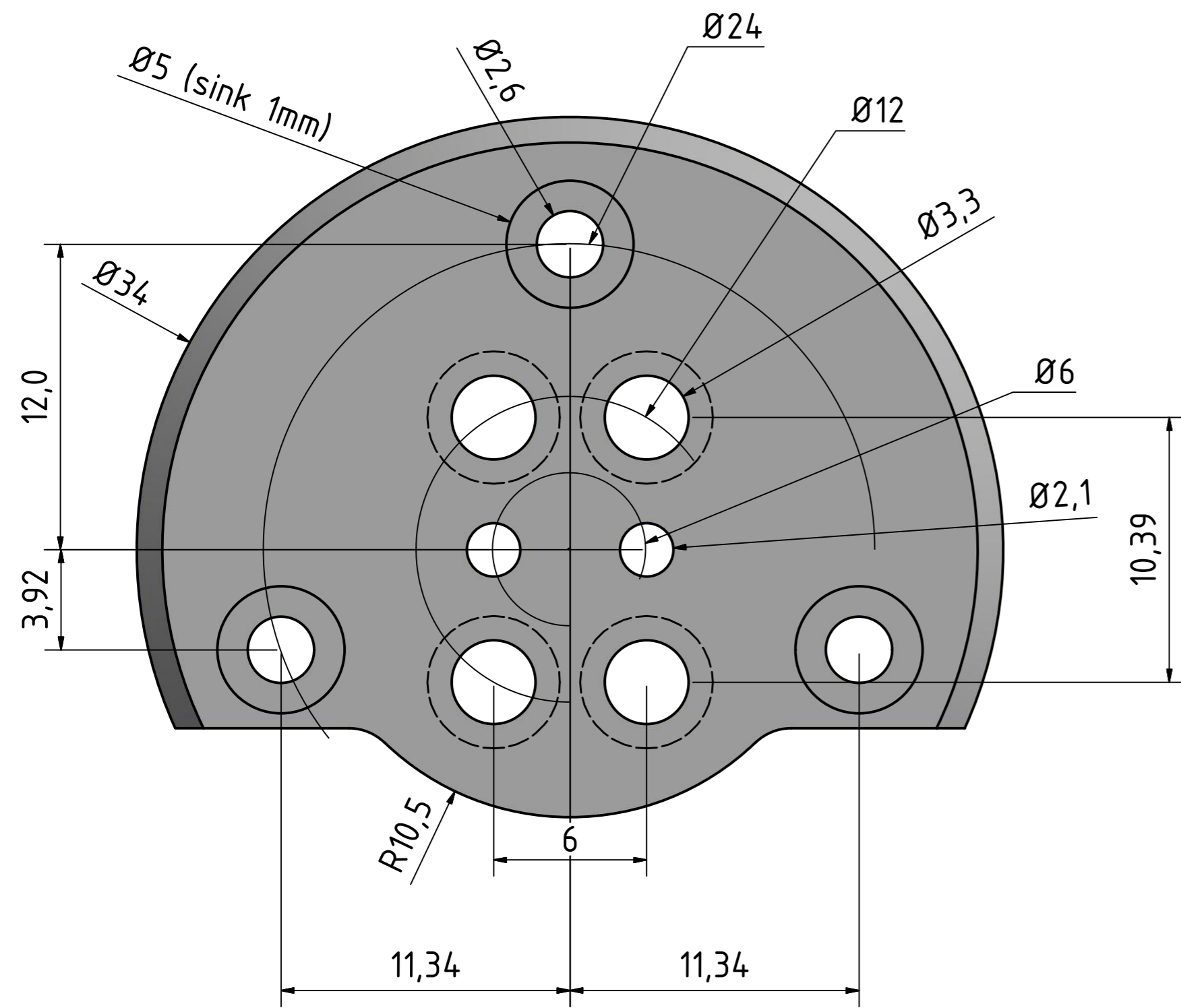
Cu ring



Radiation shield (stainless steel)



Bottom plate (stainless steel)



		Date	Name					
		Drawn	16.06.2016	Kress				
		Checked						
		Standard						
				Bottom plate VA				
						1		
						A2		
State	Changes	Date	Name					

8.5 Technical Drawing of the Single Crystals

The technical drawing in Figure 25 shows the geometry of the Ag(111) and Au(111) single crystals used in this thesis. See also Chapter 2.1.2.

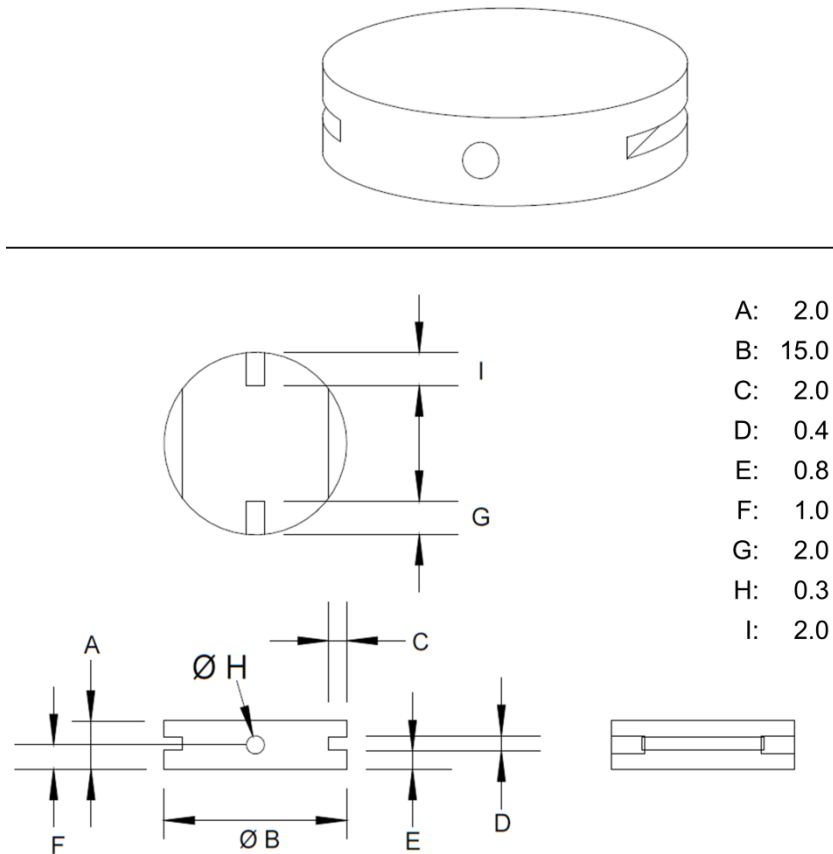
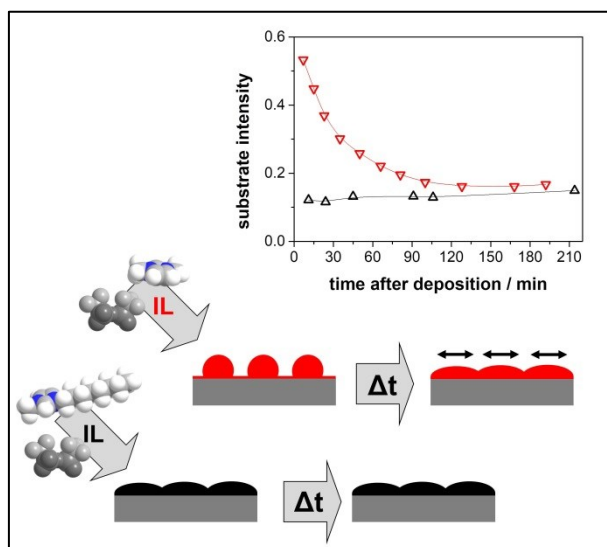


Figure 25: Technical drawing of the single crystals used in this thesis.

8.6 Publications [P1-P4]

The individual publications [P1, P2, P3, P4] are provided on the following pages along with the corresponding Supporting Information.

[P1]

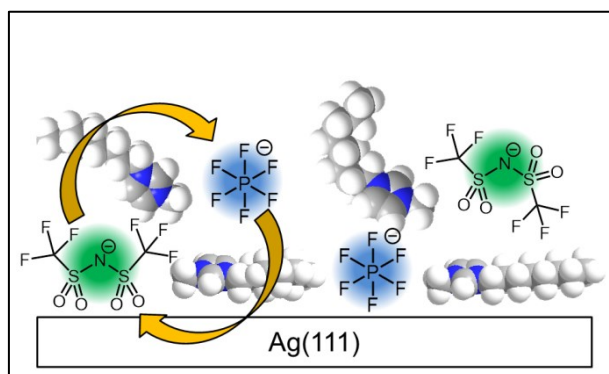


M. Lexow, T. Talwar, B.S.J. Heller, B. May, R.G. Bhuin, F. Maier, H.-P. Steinrück:
Time-dependent changes in the growth of ultrathin ionic liquid films on Ag(111)
Physical Chemistry Chemical Physics, 20, 12929-12938 (2018).

DOI: 10.1039/C8CP01411F

Reprinted under license CC BY-NC 3.0 – Published by the PCCP Owner Societies:
<https://pubs.rsc.org/en/content/articlelanding/2018/CP/C8CP01411F>

[P2]



M. Lexow, B.S.J. Heller, F. Maier, H.-P. Steinrück:

Anion exchange in ultrathin ionic liquid films on Ag(111)

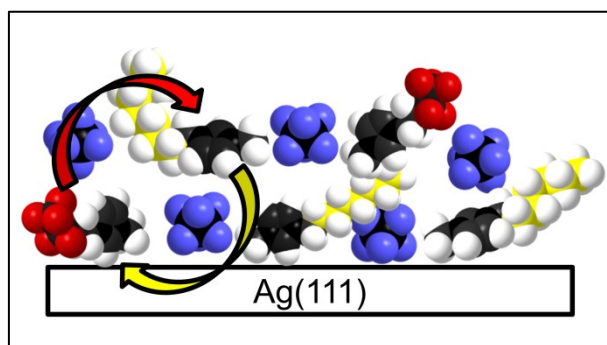
ChemPhysChem, 19, 2978-2984 (2018).

DOI: 10.1002/cphc.201800773

Reprinted under license CC BY 4.0:

<https://onlinelibrary.wiley.com/doi/full/10.1002/cphc.201800773>

[P3]



M. Lexow, B.S.J. Heller, G. Partl, R.G. Bhui, F. Maier, H.-P. Steinrück:

**Cation Exchange at the Interfaces of Ultrathin Films of Fluorous Ionic Liquids
on Ag(111)**

Langmuir, 35, 398-405 (2019).

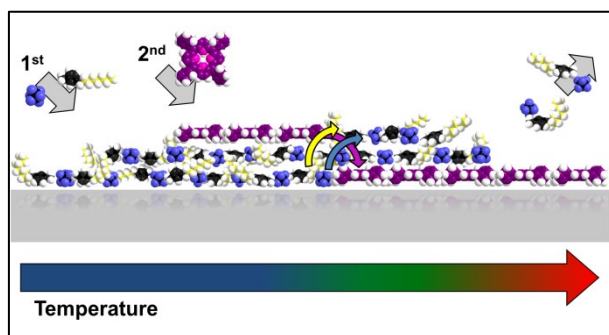
DOI: 10.1021/acs.langmuir.8b03517

Reprinted under license CC BY 4.0:

<https://pubs.acs.org/doi/10.1021/acs.langmuir.8b03517>

Further permissions related to the material excerpted should be directed to the ACS.

[P4]



M. Lexow, S. Massicot, F. Maier, H.-P. Steinrück:

Stability and Exchange Processes in Ionic Liquid/Porphyrin Composite Films on Metal Surfaces

The Journal of Physical Chemistry C, 123, 29708-29721 (2019).

DOI: 10.1021/acs.jpcc.9b08531

Reprinted under license CC BY 4.0:

<https://pubs.acs.org/doi/10.1021/acs.jpcc.9b08531>

Further permissions related to the material excerpted should be directed to the ACS.

Follow your dreams, they know the way.